SYNTHESIS AND CHARACTERIZATION OF ZEOLITE CATALYSTS

A THESIS

SUBMITTED TO THE

SHIVAJI UNIVERSITY, KOLHAPUR

FOR THE DEGREE OF

DOCTOR OF PHILOSOPHY

(IN CHEMISTRY)

UNDER THE FACULTY OF SCIENCE

BY

Miss SHOBHANA VAMAN AWATE

UNDER THE GUIDANCE OF

Dr. PAUL RATNASAMY

CATALYSIS DIVISION

NATIONAL CHEMICAL LABORATORY

PUNE- 411008, INDIA

DECEMBER 1993

CERTIFICATE

Certified that the work incorporated in the thesis, **"SYNTHESIS AND CHARACTERIZATION OF ZEOLITE CATALYSTS"** submitted by **Miss Shobhana Vaman Awate,** M.Sc. was carried out by the candidate at Catalysis Division, National Chemical Laboratory, Pune 411 008, under my supervision for the Degree of Doctor of Philosophy in Chemistry. Such material as has been obtained from other sources has been duly acknowledged in the thesis.

(Dr. Paul Ratnasamy)

Research Guide

ACKNOWLEDGMENTS

I wish to express my deep sense of gratitude to Dr. Paul Ratnasamy, Deputy Director, National Chemical Laboratory, Pune, for his generous advice, valuable guidance and encouragement throughout the course of this investigation.

Sincere thanks are due to Dr. V.P. Shiralkar for his encouragement and stimulating discussions and personal help rendered from time to time for the completion of this work.

I am grateful to Dr.P.N.Joshi, Dr.A.N.Kotasthane, Dr.B.S.Rao, Dr.S.G.Hegde, Dr. C. Gopinathan, Dr.S.Sivasankar, Dr.A.V. Ramaswamy and all other colleagues and friends in Catalysis division as well as from other divisions for their whole-hearted co-operation and help rendered at all the stages of this work.

Finally I wish to thank, The Registrar, Shivaji University, Kolhapur and The Director, National Chemical Laboratory, Pune, India, for allowing me to submit this work in the form of a thesis.

Ms.S.V.Awate

DECLARATION

I hereby declare that the thesis entitled, **'SYNTHESIS AND CHARACTERIZATION OF ZEOLITE CATALYSTS.'** completed and written by me has not previously formed the basis for the award of any Degree or Diploma or other similar title of this or any other University or examining body.

(Ms.S.V. Awate)

Research student

CONTENTS

LIST OF TABLES

LIST OF FIGURES

****

Chapter 1

GENERAL INTRODUCTION

****

CONTENTS

1.1 INTRODUCTION

Zeolites are microporous, crystalline, hydrated alumino-silicate molecular sieves, containing rigid three dimensional infinite framework structure comprising of SiO_4 and AlO_4 tetrahedra linked through oxygen bridges and enclosing cavities and channels of molecular dimensions. The net negative charge of the framework generated by alumina tetrahedra, is compensated by the nonframework cations generally belonging to the group I or II or organic cations. Structurally, the formula of zeolites can be represented[1] by its unit cell composition as,

$$M_{x/n} [(AlO_2)_x (SiO_2)_y] . z H_2O$$

where 'M' is an exchangeable cation of valence 'n'. The sum (x+y) is the total no. of tetrahedra in the unit cell. According to Loewenstein rule[2], the lower limit for y/x ratio tends to a value of 1.0. The parenthesis represents the framework composition and 'z' is the number of water molecules occluded in the zeolite cavities. The isomorphous substitution of Si^{4+} or Al^{3+} by other metal ions like B^{3+}, Ga^{3+}, Fe^{3+}, Cr^{3+}, V^{4+}, Ti^{4+} and Zr^{4+} in the zeolite framework is an emerging area in the zeolite catalysis. These are called as metallosilicate molecular sieves.

1.2 HISTORICAL BACKGROUND

Zeolites, a group of minerals, consisting of hydrated alumino—silicates were first recognized by Swedish mineralogist Cronstedt[3] in 1756 with the discovery of stilbite. The term zeolite was coined for these minerals because they exhibited a phenomenon of 'intumescence', when heated in a blow pipe flame.

The word is adopted from two Greek words viz. 'Zeos' meaning, to boil and 'lithos' meaning stone. In 1840, Damour[4] demonstrated that zeolites would be reversibly dehydrated without alteration of the structure and morphology. The property of dehydrated zeolites to occlude liquids such as alcohol, benzene and mercury was first observed by Friedel[5]. In 1909, Grandjean[6] reported that dehydrated Chabazite adsorbed gases like ammonia, air, hydrogen, carbon disulfide, hydrogen sulfide, iodine, bromine and even mercury at higher temperature. In 1925, Weigel and Steinhoff[7] observed that dehydrated chabazite rapidly sorbs the vapors of water, methyl and ethyl alcohol and formic acid. They also observed that acetone, ether and benzene are largely excluded. McBain[8] was the first to recognize the importance of these results and attributed them to the difference in molecular sizes. He coined the term "molecular sieves" for materials capable of exhibiting this type of selective adsorption.

1.3 NOMENCLATURE

The International Zeolite Association Structure Commission and IUPAC have assigned structural codes to the known synthetic and natural zeolites[9,10]. Designations consisting of three capital letters have been used to identify structural types. The codes for the zeolite identification have generally been derived from the names of the type species and exclude numbers and characters other than Roman letters. The codes for the type of the structure do not depend on the chemical composition, distribution of the various possible T atoms (Si^{4+}, Al^{3+}, P^{5+}, Ga^{3+}, Ge^{4+}, B^{3+}, Be^{2+}, Ti^{4+} etc.), unit cell dimensions or

crystal symmetry.

1.4 CLASSIFICATION

Since 1950, about 40 natural and more than 150 synthetic zeolite species have been investigated[11]. Zeolites are classified according to morphological characteristic[12], crystal structure[13-15], chemical composition[16], effective port diameter[17,18] and natural occurrences[19]. On the basis of morphological characteristics, zeolites are classified as fibrous, lamellar and those having three dimensional framework structures. The "fibrous" zeolites have their linkages of tetrahedra more numerous in one crystallographic direction. The "lamellar" zeolites are noted by having their structural linkages more numerous in one plane and are characterized by a platy cleavage. The "framework structures" have the binding of the aluminosilicate tetrahedra of similar strength in all directions. The tectosilicates in general and zeolites in particular are so diverse that secondary structure units, based on small groups of linked tetrahedra are needed in describing and systematizing their topologies. Meier[14] in 1967 proposed the secondary building units (SBU) as the smallest number of such units from which known zeolite topologies could be built. Depending on the differences in the SBU[14,15] the crystal structure of zeolites can be classified into ten groups viz. Analcime, Natrolite, Chabazite, Phillipsite, Heulandite, Mordenite, Faujasite, Laumontite, Pentasil and Clathrate.

Classification of zeolites according to their chemical composition (silica to alumina ratio) include, four distinct

groups, low silica, intermediate silica, high silica and pure silica molecular sieves as illustrated in Table 1.1.

Classification of zeolites according to their natural occurrences are of interest to earth scientists or geologists. Zeolite occurrences in bedded pyroclestics and siliceous volcanic flows comprise the commercially significant zeolite beds. Other natural occurrences of zeolites have been found in amyydaloidal basalt, deep sea sediments, fracture-filling of hydrothermal veins, plays lake beds, hot springs, and regional metamorphism[19].

Zeolites can be conveniently classified according to the pore opening defined by the number of TO_4 units that form the channel. Barrer[17] has made such a classification of zeolites into five groups. Sand[18] later modified this classification into three major groups, according to the largest ring present in the structure of each zeolite (Table 1.2). This classification does not give an indication of exact dimension of the pore opening or whether the zeolite has uni-, di-, or tri- dimensional pore system. Although not shown in Table 1.2 recently very large pore aluminophosphate molecular sieve (VPI-5)[20] containing 18 membered rings have been synthesized (pore size 1 nm).

Zeolite ZSM-5 is a medium pore zeolite having 10 membered pore system and belongs to the family of high silica aluminosilicates (type MFI) with silica to alumina ratio from 10 to infinity and 5-membered TO_4 rings occur predominantly (MFI). Due to structural peculiarities and broad range of acidity, ZSM-5 is a potential catalyst for certain industrially important

Table 1.1

Classification of zeolites according to chemical composition*

Class	Si/Al ratio	Examples
"Low" Silica	1.0-1.5	A, X, Sodalite
"Intermediate" Silica	2.0-5.0	(a) Natural zeolites : Erionite, Chabazite, Clinoptilolite, Mordenite
		(b) Synthetic zeolites : X, Y, L, Large-port Mordenite, Omega
"High" Silica	10-several thousand	(a) By thermochemical framework modification: highly siliceous variants of Y, mordenite, erionite.
		(b) By direct synthesis : ZSM-5, ZSM-11, EU-11 EU-2, Beta etc.
Silica molecular sieves	Several thousand to ∞	silicalite

* Ref. 16

Table 1.2

Classification of zeolites according to the largest pore opening*

Small port (8 membered)	Intermediate port (10 membered)	Large port (12 membered)
Zeolite A	ZSM-5	Cancrinite
ZK-5	ZSM-11	Faujasite
Bikitaite	ZSM-23	Linde X,Y,L
Brewsterite	ZSM-22 (Theta-1)	Gmelinite
Chabazite	ZSM-48 (EU-2)	Mazzite
TMA-E	ZSM-50 (EU-1)	Mordenite
Edingtonite	Dachiardite	Offretite
Erionite	Epistilbite	Omega
Gismondine	Ferrierite	ZSM-12
Merlinolite	Stilbite	Beta
Levyne	Heulandite	NCL-1
Laumontite		
Natrolite		
Paulingite		
Phillipsite		
Rho		
Thomsonite		
Yugawarolite		

* Ref.17

reactions. e.g. Xylene isomerization, aromatization of alkanes, cracking of higher alkanes and hydrodewaxing.

The present work mainly deals with the synthesis, characterization and hydrocarbon conversion reactions over pentasil (MFI) zeolites.

1.5 ISOMORPHOUS SUBSTITUTION

T-atoms of the zeolite molecular sieves can be isomorphously substituted by other di-, tri-, tetra- and pentavalent metal ions. The isomorphous substitutions, not only alter the physico-chemical properties but also change their catalytic behavior. The first isomorphous substitution in the lattice was reported by Goldsmith[21] in which Si^{4+} was replaced by Ge^{4+}. Barrer[22] classified the isomorphous replacements in zeolites in four different categories as, (1) Cation exchange, (2) Introduction of isomorphous element in the zeolite framework, (3) Isomorphous replacement of isotopes and (4) Replacement of intracrystalline salts and molecular water. The location of the substituted cations can be any one or more of the following sites in the zeolites :

1. Framework sites
2. Exchange positions
3. Inside the pores or on the external sites as a metal oxide.
4. Defect sites

The modification of zeolites by isomorphous substitution imparts additional properties to zeolites which may lead to interesting catalytic applications.

Pauling's theory[23] predicts the possibility of isomorphous substitution and the stability of that particular metal ion in the zeolite tetrahedral framework. According to the Pauling criterion, the substituent metal ion is stable in the tetrahedral framework when it is in the range $0.414 > \rho > 0.225$ ($\rho = r_c/r_o$ where r_o is the radius of oxygen and r_c is the radius of substituent cation). The above range can be modified as, $0.439 > \rho > 0.238$ by using Goldschmidt's[23] oxygen radius value as 1.32 Å. However, metal ions like Ga^{3+}, Fe^{3+}, Ti^{4+} and V^{4+} for which values of ρ are out of range, can be successfully substituted into zeolite tetrahedral framework due to their stability in tetrahedral environments.

The tetrahedral occupancy of the substituted metal ion can be characterized by the different techniques such as XRD, IR, MASNMR, ESR, UV-VIS, XPS, Photoacoustic spectroscopy, ion exchange capacities and by catalytic test hydrocarbon conversion reactions.

Isomorphous substitution can be achieved either by direct hydrothermal synthesis or by post synthesis methods. Wilson et al.[24] synthesized an important family of molecular sieves called aluminophosphates (ALPO) containing equal moles of Al^{3+} and P^{5+} ions in the lattice. Metalloalumino-phosphate (MeALPO) have been reported[24,25] by isomorphous substitution of Co^{2+}, Fe^{3+}, Mg^{2+}, Zn^{2+}, Be^{2+}, B^{3+}, Ga^{3+}, Cr^{3+}, Ti^{4+}, V^{4+} and Mo^{3+} in the framework of ALPO. In other class of molecular sieves, silico-aluminophosphates (SAPO's) in which silicon is substituted for aluminum or phosphorous in ALPO framework. ALPO does not have

Bronsted acidity because of neutral framework. SAPO has weak acidic properties and can exhibit ion exchange. Both ALPO and SAPO have good thermal and hydrothermal stability.

1.6 HYDROTHERMAL SYNTHESIS OF ZEOLITES

Much of the success in laboratory syntheses has come from the duplication of the conditions[26] that produce natural zeolites.

In the late 1940's the first systematic laboratory zeolite synthesis was carried out by Barrer[27]. He was able to synthesize successfully from silica-alumina gels and alkali metal hydroxides, the synthetic counterpart to the natural zeolite, mordenite. Since this time research on the synthesis of zeolites has accelerated and numerous synthetic zeolites, for which no known natural counterparts exist, have been synthesized. Zeolites A, L and ZSM-5 are examples of the success in this area. Since 1950, about 40 natural zeolites are known while more than 150 synthetic zeolites have been reported[11].

The essential process involved in the hydrothermal synthesis of most of the zeolites, is the conversion of amorphous reactive aluminosilicate gels into crystalline ones, in the presence of aqueous solution of alkali and/or alkaline earth metal hydroxide at higher temperature (298 - 573 K)[28]. Although zeolites are not often formed above 623 K in a hydrothermal system[29], high temperature synthesis of analcime, clinoptilolite, Ferrierite and mordenite have been reported[15].

The actual mechanism of zeolite crystallization is not well understood because of the complexity of the interactions

occurring in the hydrothermal magma. Sand[30] has summarized the simultaneous reactions that can occur during synthesis as:

1. Precipitation of a gel
2. Dissolution of the gel
3. Nucleation of zeolite
4. Continued crystallization and crystal growth of the zeolite.
5. Dissolution of the initial metastable phase
6. Nucleation of a more "stable" metastable phase or phases
7. Continued crystallization and crystal growth of the new crystalline phase while the initial crystals are dissolved.
8. Dissolution of the metastable phase
9. Nucleation of the equilibrium phase
10. Crystallization and crystal growth of the final stable phases.

The crystal growth occurs from the solution phase. The gel composition of structure, which determines the resulting zeolite composition and structure, is largely dependent on the solution chemistry prior to gel formation. Temperature, pH, aluminate, hydroxide and silicate ion concentrations, aging of other species present in solution (i.e. alkali cations) will each play role in determining this solution chemistry. There are other physical variables such as the order of mixing, rates of addition of aluminate to silicate solution, or vice versa and rate of agitation which affect the solution chemistry. The chief role of the solid gel is to supply silicate and aluminosilicate species to the solution and control its composition by solubility equilibria[31].

In the zeolite synthesis, the level of supersaturation is not

readily controlled. The high supersaturation, normally encountered, give many nuclei and lead to rapid crystal growth, consequently forming smaller and faulted crystals. These effects can be reduced if the solid phase of the reaction mixture is zeolite itself. In such recrystallization, the supersaturation is usually less than that formed by amorphous gel solids and hence the crystals formed are larger and more perfect[32].

For the low silica variety (i.e. zeolite A, X, Y), organic cations are not used. Here alkali cations play a major role in the nucleation mechanism by permitting depolymerization of the gel, through stabilization of aluminosilicate complexes such as secondary building units which come together to form nuclei or precursors to zeolite crystals. After 1960, siliceous zeolites (higher SiO_2/Al_2O_3 ratio) could be synthesized through the use of certain organic cations particularly alkylammonium cations[30]. The zeolite product is stabilized by the guest species that fills the channels and cavities of aluminosilicate framework. A thermodynamic treatment shows[31] that these guest molecules lower the chemical potential of the framework. In aluminous zeolites, inorganic cations and water molecules fulfill this function whereas in hydrophobic clathrasils neutral organic guest species lower the chemical potential of the framework[30].

The inorganic cations used during synthesis greatly influence crystal morphology, % crystallization and the yield of product[15]. The template used can be a charged, a neutral or an ionic pair. The role of templates like tetraalkylammonium bromide may be as,

1. to act as donors of hydroxyl ions, thus helping to increase

the solubility of aluminate and silicate ions,

2. structure-directing agent for the formation of zeolite crystals,

3. for balancing the framework charge.

The advances in the area of new molecular sieve materials have come into practice in the preparation of zeolite structures containing framework components other than aluminum and silicon. The isomorphous substitution of Al^{3+} or Si^{4+} by B^{3+}, Ga^{3+}, Ge^{4+}, Be^{2+}, Ti^{4+}, V^{4+} greatly modifies the properties like acidity, ion exchange, thermal stability and their catalytic behavior.

1.7 STRUCTURAL FEATURES OF ZEOLITE ZSM-5

The term pentasil was proposed by Kokotailo and Meier[33] to designate the group of structures having 5-1 secondary building units. The silica and alumina tetrahedra[34] which make up the framework of ZSM-5 consists of eight 5-membered rings. This structural unit is linked repetitively through its edges to form a chain configuration as shown in Fig. 1.1a. A skeletal diagram[34] of the unit cell of ZSM-5 along (010) and (100) face is shown in Fig. 1.1b and Fig. 1.1c respectively. The elliptical 10-membered ring apertures (5.2 X 5.8 Å) shown in Fig. 1.1b are entrances to structural channels parallel to the (010) crystallographic direction. The nearly circular 10-membered ring apertures (5.4 X 5.6 Å) as shown in Fig.1.1c, are the entrances to the sinusoidal channels which extend parallel to the (100) crystallographic direction. The channel system of ZSM-5, consisting of both sinusoidal and straight channels, is illustrated in Fig. 1.1d.

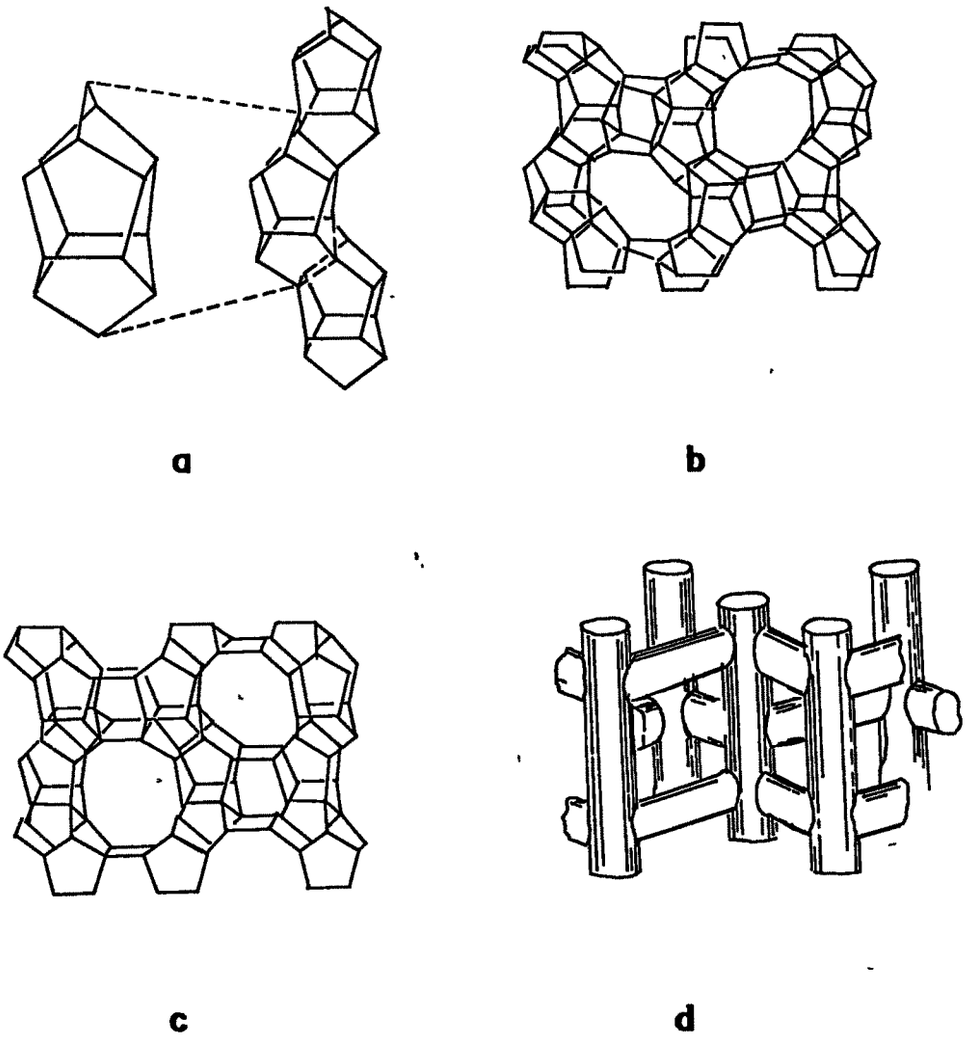

Fig. 1.1 : Structure of MFI type zeolite : **a**) Pentasil chains showing the building block of MFI , **b**) Skeletal diagram of the [010] face of the MFI unit cell, **c**) Skeletal diagram of the [100] face of the MFI unit cell , and **d**) Channels of the zeolite MFI.

Zeolite ZSM-5 has orthorhombic symmetry and belongs to the space group P_{nma} with lattice constants a = 20.1, b = 19.9 and c = 13.4 Å. However, a reversible transformation to monoclinic symmetry has been observed due to certain treatments such as calcination, SiO_2/Al_2O_3 ratio and ion exchange[35]. The framework density is 17.9 (Si+Al) per 1000 $Å^3$ while unit cell volume is 5363 $Å^3$. The ZSM-5 is a medium pore zeolite with unique channel structure. The composition of the unit cell of Na/ZSM-5 is :

$$Na_n[Al_n\ Si_{96-n}\ O_{192}] \cdot 16\ H_2O$$

where n < 27 and typically equal to 3[36]. This formula indicates the bulk SiO_2/Al_2O_3 ratio. It does not imply however, that the silicon and aluminum are homogeneously distributed within individual zeolite crystallites. The number of Al atoms per unit cell is obtained from the relation,

$$N_{Al} = 96 / [1 + (N_{Si}+N_{Al})]$$

where N_{Si}, N_{Al} are gm. atoms of Si and Al respectively.

1.8 PHYSICO-CHEMICAL CHARACTERIZATION OF ZEOLITES.

1.8.1 X-ray diffraction (XRD) : X-ray diffraction is one of the most important techniques used to identify (i) zeolite structure[37], (ii) purity of the zeolite, (iii) % crystallinity, (iv) unit cell parameters[38], (v) crystallite size and also (vi) to understand the kinetics and mechanism of crystallization[37-43]. Since the powder pattern is the fingerprint of the individual zeolite structure, % crystallinity and phase purity of the synthesized catalyst can be compared with the reference catalyst.

The unit cell volume calculated from different data is sensitive[44-46] to the framework aluminum content. The unit cell

volume expands with decreasing SiO_2/Al_2O_3 ratio and thus provides the valuable framework compositional information about the structure. The incorporation of elements other than Al in the framework of the zeolite, can be correlated with the change in the unit cell volume[44,47].

1.8.2 Infra red (IR) spectroscopy : The mid-infrared region (1200-400 cm^{-1}) is used to characterize and to differentiate various zeolite structures[48,49], particularly when XRD fails owing to the presence of very small crystallites and may even give an approximate crystallinity of the zeolite. Systematic investigations[50-52] on infrared spectroscopy on the framework and fundamental structure for many minerals and synthetic zeolites have been published[50-52]. It is found that asymmetric stretching vibration of Si-O or Al-O band occurs at about 1000-1100 cm^{-1} and is related to the amount of Al atoms present in the zeolite framework[53-55]. It was argued that the frequency of the double five membered rings is sensitive to the topology and building units of the zeolite framework[48,49]. A band at 550 cm^{-1} was assigned to the stretching vibration of these units in Pentasil (MFI,MEL) zeolites.

Isomorphic substitution and its effect on Bronsted acidity can be studied by IR spectroscopy. The IR absorption bands around 3600-3700 cm^{-1} confirm the presence of silanol and/or bridged hydroxyl groups in the zeolites[56-57] and their Bronsted acidity strength can be compared .

The FTIR studies on zeolites in the region 1400-1700 cm^{-1} after absorption of base molecules like pyridine and ammonia[58]

have been reported for the detection and the estimation of acid strength. Isomorphous substitution in place of aluminum causes shifts in the bands due to Bronsted acidity which correlate well with the resultant acidity[59-60].

1.8.3 Nuclear magnetic resonance (NMR) spectroscopy : Lippmaa et al.[61] have demonstrated that ^{29}Si-MAS (magic angle spinning) NMR spectra were sensitive to the nature and chemical environment of the atoms. The application of this technique to the study of synthetic zeolites has been reported for ZSM-5[62] and faujasites[63]. From the zeolites point of view NMR technique serves as a guide to find that there is strong paramagnetic influence of 4 co-ordinated Al^{3+} substituting for Si^{4+} in the second co-ordination sphere of Si^{4+}. Thus in the solid state ^{29}Si MASNMR of zeolite, the chemical shifts relative to $Si(CH_3)_4$ enables one to determine whether there are present groupings with Si^{4+} linked through oxygen to 4, 3, 2, 1 or 0 other silicon atoms (and hence to 0, 1, 2, 3, 4 aluminum atoms respectively).

Solid state MASNMR spectroscopy for ^{29}Si, ^{27}Al can show evidence[61-62] for the tetrahedrally coordinated atoms from the zeolite lattice and the concomitant deposition of octahedrally co-ordinated aluminum, if present in the pores of the zeolite. Thus considerable knowledge has been obtained during the last few years about the structures of zeolites from the study of their ^{29}Si, ^{27}Al, ^{71}Ga MASNMR spectra[64-65].

1.8.4 Thermal analysis : Thermo-analytical technique has been found[66-67] to yield the information on the mechanism as well as the thermal behavior of the synthesized zeolites. Thermal

properties can be related to other physico-chemical properties of zeolites. Thermal stability of zeolites is an important parameter for their application as selective sorbent and catalytic activity. The thermal stability of the zeolites[67-68] is determined by the DTA/TG curves. The splitting of low temperature endotherm[69] is used to identify the location of the water molecules and to study kinetics of desorption of water molecules[70]. It is known that thermal stability of zeolite framework structure increases with the increase in the silica to alumina ratio[71] and the method of thermal/acid treatment[72] or ion exchange. The silica-alumina ratio plays a major role in the symmetry change of ZSM-5 zeolite which has exceptionally high degree of thermal and hydrothermal stability[68]. Silicalite, the end member of ZSM-5 series is stable in air upto 1373 K and is then converted slowly to amorphous silica at 1573 K[73-74].

1.8.5 Sorption and diffusion properties : Zeolite molecular sieves have uniform pores and internal channels are of molecular dimensions. The channels and cavities constitute a high intracrystalline surface area accessible to molecule of comparable size. As early as 1846 Damour[3] demonstrated that water could be reversibly removed from a zeolite without altering its crystalline framework. Sorption of various gases and vapors on the natural as well as synthetic zeolites has been extensively studied by Barrer and coworkers[75,76]. The sorption properties of zeolites have been reviewed by Kiselev[77]. The selective adsorption of molecules into zeolites depends on,

1. molecular size of adsorbate,

2. polarizability and polarity of the adsorbate,
3. organophilicity and hydrophobicity of the zeolite host structure,
4. degree of unsaturation of organic adsorbates and
5. polarizing power of the host cations.

Studies on the sorption characteristic of zeolite can provide information about their,

1. void volume,
2. size of the pore openings which depends on the ring size,
3. level of crystallinity and crystal size,
4. acidity,
5. diffusion properties and crystal blockages if any.

The void volume of porous zeolite is often determined by low temperature (78 K) nitrogen sorption. Analysis of such sorption isotherm have been found to be useful in determining the micropore volume and pore size distribution of composite materials containing molecular sieves[78,79].

Meisel et al.[80] found that n-paraffins and monomethyl-paraffins diffuse more rapidly than dimethyl substituted paraffins in the ZSM-5 channel system. Olson et al.[81] have found that the sorption characteristic of ZSM-5 is composition dependent. They also observed that the ion-exchange capacity, the catalytic activity and the hydrophilicity of the zeolite is linearly dependent on the Al content in the framework. Moreover, silicalite exhibits surface adsorption selectivity and can distinguish between organic molecules and water. Flanigen et al.[82], while studying the sorption properties of silicalite, have

found that benzene with a diameter of 0.585 nm is adsorbed while neopentane with a diameter of 0.62 nm is rejected. The activation energies for diffusion of some alkyl benzenes in Na/ZSM-5 at 523 K and 623 K have been also reported by Weisz[83].

Sorption of basic molecules like nBA[84], NH_3[85] and of acidic molecules like CO_2[86], in zeolites gives useful information on the strength and density of acidic and basic sites respectively. Sorption isotherms of these molecules in zeolites enables us to arrive at sorption energetics including applications of different sorption models, evaluation of thermodynamic parameters like chemical affinity, isosteric heat of sorption and entropy of sorptions. In heterogeneous catalysis, adsorption and diffusion properties control the overall rate of the chemical reaction at the catalytic site. The diffusion in the zeolite catalysts may be divided into three types,

1. **Configurational diffusion** : It occurs in situations where the structural dimensions of the pores approach those of molecules. Even a subtle change in the dimensions of a molecule can result in a large change in its diffusivity.
2. **Kundsen diffusion** : It occurs when the mean free path of molecule is comparable to the pore diameter. Such conditions being usual in gas phase reactions on catalyst with pore diameters in the range of 30-1000 Å.
3. **Bulk diffusion** : occurs when the mean free path of the molecule is much smaller than the pore diameter. Molecular collisions are more frequent than collisions with the wall, the rate of diffusion under such conditions being independent of the

pore radius.

1.9 CATALYTIC REACTIONS OVER ZEOLITES.

1.9.1 As a characterization technique : Model test reactions can be used as tools for characterization of catalysts. Information concerning the pore structure of zeolite materials possessing potential catalytic applications can be obtained. These model reactions are classified into two categories,

1. Acid catalyzed reactions; 2. Bifunctional catalytic reactions.

In acid catalyzed reactions, the constraint index[87] compares the relative rate constants of n-hexane and 3-methylpentane cracking under a given set of conditions. From the ratio of rate constants, the pore size of zeolites can be differentiated. Acid catalyzed reactions[88] are sensitive to reaction temperature as well as the strength of Bronsted acid sites. These reactions affect the cracking rate ratio. For distinguishing large and medium pore zeolites, acid catalyzed reactions such as the isomerization of xylenes and disproportionation of ethylbenzene were used[89]. In the catalytic cracking of C_6 paraffins, changes in the product distribution with the change in the structure have been observed[90]. Conversion of napthenes[89] and conversion of n-decane[91] are the two bifunctional test reactions that have been considered for generating structural information.

1.9.2 As an industrial process : Zeolites are used as catalysts in various refinery operations, petrochemical and organic reactions because of their high thermal and hydrothermal stability, high acidity, molecular sieve action and regeneration capacity. These structural factors are of special interest in

various hydrocarbon conversion reactions. Weisz and coworkers[92] were the first to report molecular shape selective cracking of paraffin, olefin and alkyl aromatics and have established that the locus of the catalytic activity is within the intracrystalline pores. Acid sites are introduced into Na, K-zeolites by,

1. acid treatment,
2. ammonium exchange, followed by the thermal deammoniation to get hydrogen form of zeolite.

The strength and concentration of acidic sites can also be altered by isomorphous substitution of Al and Si in the framework by other elements.

The first zeolite used commercially in 1962 as a catalyst was the large pore X zeolite belonging to the naturally occurring faujasite family. Since then large number of purely synthetic zeolites have found application as catalysts. A large number of novel commercial processes have been developed in a relatively short time using ZSM-5 zeolite catalyst[93-101].

A list of commercial processes based on selective catalysis is given in Table 1.3. The catalysts used in these commercial process include Erionite, ZSM-5, wide pore zeolite LTL and USY.

A number of processes like selectoforming[102], M-forming[103], M-2 forming[104], cyclar[105] and Aromax[106] have been developed using zeolite catalysts and commercialized by Mobil Oil Co. and by British Petroleum Co. Gallium substituted ZSM-5 is reported[107-108] as a good catalyst for dehydrocyclization of normal alkanes.

Table 1.3

Industrial processes based on shape selective zeolite catalysts

Name of the process	Objective
SELECTO-FORMING	Octane boosting
M-FORMING	-do-
CATALYTIC CRACKING	-do-
MDDW	Distillate dewaxing
MLDW	Lube dewaxing
M-2 FORMING, CYCLAR	Gas to aromatics
MOGD	Light olefins to gasoline and distillate
MTG	Methanol to gasoline
MTO	Methanol to light olefins
MVPI,MLPI, MHTI XYLOFINING	Xylene isomerization
MTDP	Toluene disproportionation
MEB, ALBENE	Ethyl benzene synthesis
PARA SELECTIVE REACTION	P-Diethylbenzene synthesis p-Ethyltoluene synthesis

1.10 SCOPE OF THE PRESENT WORK

Isomorphous substitution of Al^{3+} by Ga^{3+} modifies the physico-chemical and catalytic properties of the zeolites. The objective of the present investigation was the synthesis and characterization of gallosilicate molecular sieves having MFI type structure. The scope of the present study includes the following aspects.

1. Hydrothermal synthesis of Al-, Fe-, Ga-, (Al+Ga) analogs of pentasil (MFI) type molecular sieves using tetra ethyl-butylammonium bromide.
2. Kinetic and mechanistic features of hydrothermal synthesis of MFI type zeolite.
3. Physico-chemical characterization of MFI phases by different techniques.
4. Evaluation of n-butylamine sorption isotherms in terms of different thermodynamic parameters and physical state of the sorbed phase.
5. Catalytic evaluation in hydrocarbon isomerization, alkylation, disproportionation and aromatization reactions.

1.11 REFERENCES

1. Breck, D.W., "Zeolite Molecular Sieves", J. Wiley and Sons., New York, 1974.
2. Loewenstein, W., Amer. Mineral. **39**, 92 (1954).
3. Cronstedt, A. Akad. Handl. Stockholm **18**, 120 (1756).
4. Damour, A., Ann Mines, **17**, 191 (1840).
5. Friedel, G., Bull, Soc. Fr. Mineral Cristallgr., **19**, 14 (1896).
6. Grandjean, F., Compt. Rendn, **149**, 866 (1909).
7. Weigel, O. and Steinhoff, E., Zeit. Krist. **61** 125 (1924).
8. McBain, J.N., "The Sorption of Gases and Vapors by Solids". George Routledge and Sons, London (1932). 9. Meier, W.M. and Olson, D.H."Atlas of Zeolite Structure Types", Structure Commission of the International Zeolite Association (2nd revised edition), Butterworths London (1987).
10. Barrer, R.M., "Chemical Nomenclcature and Formulation of Composition of Synthetic and Natural Zeolites," Pure and Appl. Chem., **51** 1091 (1979).
11. Whyte, Jr.T.E. and Dalla Betta, R.A., Catal. Rev. Sci. Eng. **24 (4)**, 567-598 (1982).
12. Bragg, W.L., "The Atomic Structure of Minerals", Cornell University Press, Ithaca, NY (1937).
13. Lok, B.M., Cannan, T.R. and Messina, C.A., Zeolites, **3**, 282 (1983).
14. Meier, W.M., "Molecular Sieves", Society of Chem. Ind., London, p.10 (1968).

15. Barrer, R.M., "Hydrothermal Chemistry of Zeolites", Academic press, London (1982).

16. Flanigen, E.M., Proc. of the Fifth International Conference on Zeolites, Rees, L.V.C., (ed) Heyden and Sons, London (1980).

17. Barrer, R.M., "Molecular Sieves", Society of Chem. Ind., London, p.10 (1968).

18. Sand, L.B., Econ. Geol., p.191 (1967).

19. Culfaz, A., Ph.D. Thesis, Worcester Polytechnic Institute (1973).

20. Davis, M.E., Saldarriaga, C., Montes, C., Garces, J., Crowder, C., Nature 331, 698-699 (1988).

21. Goldsmith, J.R., Min. Mag., 29 952 (1952).

22. Ref.17. Chap.6

23. Pauling, L.,"The Nature of Chemical Bond", Goskhimizdat, Moscow, p.521, (1947).

24. Wilson, S.T., Lok, B.M., Messina, C.A., Cannon, T.R. and Flanigen, E.M., J. Am. Chem. Soc., 104 1146 (1982).

25. Wilson, S.T. and Flanigen, E.M., ACS Symp. Ser., 298 (1988) 329.

26. Robson, H., CHEMTECH, March 1978.

27. Barrer, R.M., J. Chem. Soc., p.2158 (1948).

28. Milton, R.M.,"Molecular Sieves", Soc. Chem. Ind., London, p.199 (1968).

29. Stringhom, B., Econ. Geol., 47, 661 (1952).

30. Sand, L.B., Particle synthesis and properties of zeolite catalysts for synthesis Gas-Gasoline conversion research

proposal to the office of Fossil Energy Development of Energy (Re. No. FE-NPI-8001), p.1 (1982).

31. Lowe, B.M., Stud. Surf. Sci. Catal., 37 1 (1988).

32. Barrer, R.M., in "Zeolites", Stud. Surf. Sci. Catal., 24 1 (1985).

33. Kokotailo, G.T. and Meier, W.M., " The Properties and Application of Zeolites", R.P.Townsend (ed)., The Chem.Soc., London, 133 (1979).

34. Kokotailo, G.T., Chu, P., Lawton, S.L. and Meier, W.M., Nature 275, 119 (1978).

35. Wu, E.L., Lawton, S.L., Olson, D.H., Rohrman, Jr., A.C. and Kokotailo, G.T., J. Phys. Chem., 83, 21, 2777 (1979).

36. Argauer, R.J. and Landolt, G.R., U.S. Patent 3, 702, 886 (1972).

37. Kulkarni, S.B., Shiralkar, V.P., Kotasthane, A.N., Borade, R.B. and Ratnasamy, P., Zeolites, 2, 313 (1982).

38. Breck, D.W., U.S.Patent 3, 130,007 (1964).

39. Culfaz, A. and Sand, L.B., Adv. Chem. Ser., 121, 140 (1973).

40. Erdem, A., M.S.Thesis, Worcester Polytechnique Institute, Worcester, MA (1979).

41. von Balmoos, R., Collection of Simulated XRD powder pattern for zeolites, Butterworth, London (1984).

42. Szostak. R., Molecular Sieves, Principles of synthesis and identification, Van Nostrand Rheinhold, New York, p.285 (1989).

43. Chao, K.J., Tasi, T.C., Chen, M.S. and Wang, I., J. Chem. Soc. Faraday Trans. I, 77, 547 (1981).

44. Casci, J.L., Lowe, B.M. and Whittam, T.V., U.K. Patent 2077709 B.

45. Dempsey, E., Kuhl, G.H., Olson, D.H., J.Phys. Chem., 73 387 (1969).

46. Bibby, D.M., Aldridge, L.A., Milestone, N.B., J. Catal., 72, 373 (1981).

47. Pluth, J.J., Smith. J.V. and Benett, J.M., Acta Crystallog., C42, 283 (1986).

48. Flanigen, E.M., "Zeolite Chemistry and Catalysis", J.A. Rabo, ed. Adv. Chem. Ser. N 171, Chap 2, (1976).

49. Jansen,J.C., Van der Gaag, F.J. and Van Bekkum M., Zeolites, 4 369 (1984).

50. Flanigen,E.M. and Khatami, H. and Szymanski, H.A., Molecular sieve zeolite-1, 101 201 (1971).

51. Wright, A.C., Rupert, J.P., Granquist, W.T., Am. Miner., 53, 1293 (1968).

52. Zhdanov, S.P., Keselev, A.V., Lygin, V.I., Titova, T.I., Russ. J. Phys. Chem., 38, 1299 (1964).

53. Flanigen, E.M. and Grose, R.W., Adv. Chem. Ser., 101,76 (1971).

54. Milkey, R.G., Amer. Miner., 45, 990 (1960).

55. Lohodmy-Sarac, D. and White, J.L., J. Phys. Chem., 75, 2408 (1971).

56. Topsoe, N., Pedersen, R. and Derouane, E.G., J. Catal., 70, 41 (1981).

57. Jacobs, P.A. and Mortier, W.Y., Zeolites, 2, 226 (1982).

58. Vedrine, J.C., Auroux, A., Bolis, V., Dejaifive, P., Naccache, C., Wierzchowski, P., Derouane, E.G., Nagy, J.B., Gilson, T.P., Van Hooff J.H.C., Van Den Berg, J.P. and Wolthuizen, J.P., J.Catal., 59, 248 (1979).

59. Chu, C.J.W. and Chang, C.D., J. Phys. Chem. 89 1569 (1985).

60. Kutz, N., Heterogeneous Catalysis-II, Shapiro, B.L. (ed.) Texas A and M University press, College ststion, 121 (1984).

61. Lippmaa, E., Maggi, M., Samosen, P., Engelhardt, G., J. Am. Chem. Soc., 103, 4992 (1981).

62. Fyfe, C.A., Gobbi, G.C., Klinowski, J., Thomas, J.M. and Ramdas, S., Nature, 296, 530 (1982).

63. Klinowski,J., Thomas, J.M., Fyfe, C.A., Gobbi, G.C., Nature, 296, 533 (1982).

64. Fyfe, C.A., Thomas, J.M., Klinowski, J., Gobbi, G.C., Angew. Chem., 95, 257 (1983).

65. Nagy, J.B., Gabelica, Z. and Derouane, E.G., Chemistry Letters, 7, 1105 (1982).

66. Derouane, E.G., Detremmerie, S., Gabelica, Z. and Blom, N., Appl. Catal., 1, 201 (1981).

67. Barrer, R.M. and Langley, D.V., J. Chem. Soc., p. 3804, 3811 and 1817 (1958).

68. Nakamato, H. and Takahashi, H., Chemistry Letters, p.1013 (1981).

69. Gal, I.G., Tankocic, O., Malcis, S., Raoovanov, P. and Tadorovic, M., Trans, Faraday. Soc., 67 999 (1971).

70. Bremer, H., Morke, W., Schodel, R., Vogt, F., Adv. Chem. Ser. 121, 249 (1973).

71. Breck, D.W., "Zeolite Molecular Sieves" John Wiley and Sons, New York, p.449 (1974).

72. Kuhl, G.H., J. Catal., **29**, 270 (1973).

73. Flanigen, E.M., Bennett, J.M., Grose, R.W., Cohen, J.P., Patton, R.L., Kirchnee, R.M. and Smith, J.V., Nature, **271**, 512 (1978).

74. Grosé, R. W. and Flanigen, E.M., U.S.Patent 4,061,724, assigned to Union Carbide (1977).

75. a. Barrer, R.M., Proc. Roy. Soc., A, **167**, 392 (1938).
b. Barrer, R.M., Quart. Review London, p.3239 (1949).
c. Barrer, R.M. and Breck, D.W., Trans Faraday Soc.**59**, 2569 (1963).

76. Barrer, R.M., "Zeolites and clay minerals as sorbents and molecular sieves", Academic press, Inc., London.

77. Kiselev, A.V., "Molecular Sieve Zeolites-II" Adv. Chem. Soc., **102**, Amer. Chem. Soc., Washington, D.C., p. 37 (1971).

78. Hong-Xin. Li, Martins, J.A., Jacobs, P.A. et al., "Innovation in zeolite mater. sci.", Gribet, P.J.(ed.), p.75 (1987).

79. Tapp, N.J., Milestone, N.B., Bibby, D.M., ibid, p.393.

80. Meisel, S.L., McCullough, V.J.P., Lechthalev, C.H. and Weisz, P.B., ACS meeting, Chicago,I, p.11 (1977).

81. Olson, D.H., Haag, W.O. and Lago, R.M., J. Catal. **61**, 390 (1980).

82. Flanigen, E.M., Bennett, J.M., Grose, R.W., Cohen, J.P., Patton, R.C., Kirchner, R. and Smith, J.V., Nature (London), **271**, 512 (1978).

83. Weisz, P.B., Pure and Appl. Chem., **52**, 2091 (1980).

84. Rao, G.N., Joshi, P.N., Kotasthane, A.N. and Shiralkar, V.P. J. Phys. Chem., 94, 8589 (1990).

85. Reddy, K.S.N., Eapen, M.J., Soni, H.S. and Shiralkar, V.P., J.Phys. Chem., 96, 7923 (1992).

86. Joshi, P.N. and Shiralkar, V.P., J. Phys. Chem., 97, 619 (1993).

87. Frillette, V.J., Haag, W.O. and Lago, R.M., J. Catal. 67, 218 (1981).

88. Guisnet, M., Giannetto, G., Hilaireau, P. and Perot, G.J., J., Chem.Soc. Chem. Commun., p.1411 (1983).

89. Jacobs, P.A. and Martens, J.A., Proc. Seventh Int. Conf. on Zeolites, Tokyo, Japan, Elsevier, Amsterdam, p.23 (1981).

90. Barthomeuf, D. and Mirodatos, C., J. Catal., 93, 246 (1985).

91. Martens, J.A., Tielen, M., Jacobs, P.A. and Weitkamp, J., Zeolites, 4, 98 (1984).

92. Weisz, P.B., Frilette,V.I. and Golden, R.L., J. Catal., 1, 301 (1962).

93. Wise, J.J. and Silvestri, A.J., Oil and Gas J., 74, 140 (1976).

94. Chang, C.D. and Silvestri, A.J., J. Catal., 47, 249, (1978).

95. Silvestri, A.J., I and Ec Proc. Desi. and Dev., 17, 255 (1978).

96. Chen, N.Y., Kaeding, W.W. and Dwyer, F.G., J. Amer. Chem. Soc., 101, 6783 (1979).

97. Dwyer, F.G., Lewis, P.J. and Schneider, F. M., Chem. Eng., 83, 90 (1976).

98. Chang, C.D., Lang, W.H. and Silvestri, A.J., J. Catal., 56, 268 (1979).

99. Ceasar, P.D., Brennan, J.A., Garwood, W.E. and Ciric, J., J. Catal., 56, 274 (1979).

100. Chen, N.Y. and Garwood, W.E., J. Catal., 52, 453 (1978).

101. Cohen, A.D., U.S. Patent, 4,448,891, (1984).

102. Chen, N.Y., Mazink, J., Schwartz, A. B. and Weisz, P.B., Oil Gas J., 66, 154 (1968).

103. Heinemann, H., Catal. Rev. Sci, Eng., 15(1), 53 (1977).

104. Chen, N.Y. and Yan, T.Y., Ind. Eng. Chem. Proc. Res. Dev., 25, 151 (1986).

105. Johnson, J.A., Weiszmann, J.A., Hilder, G.K. and Hall, A.P.H., Paper presented at NPRA Annual Meeting, San.Antonio, Texas, March (1984).

106. Tamm, P.W., Mohr, D.H. and Wilson, C.R., Catalysis (1987), (Ed. ward, J.W.), Elsevier, Sci. Publi. Amsterdam, The Neterlands, p.335 (1988).

107. Sirokman, G., Sendoda, Y. and Ono, Y., Zeolite, 6, 299-303 (1986).

108. Kanai,J. and Kawata,N., Applied catalysis, 55, 115-122 (1989).

****

Chapter 2

SYNTHESIS OF MFI TYPE ZEOLITES

****

CONTENTS

Zeolites

2.1 INTRODUCTION

Zeolites are often crystallized by nucleation from the inhomogeneous supersaturated mother liquids. Therefore, the origin, the purity and the exact chemical composition of the reactants used for their synthesis may sometimes be critical. Hydrothermal synthesis of MFI type zeolites generally involve the preparation of reactant mixture comprising of sources of tri and/or tetravalent metal ions, an aqueous base and in some cases organic compounds such as quaternary ammonium compounds or an amine and heating it under autogeneous pressure. Under hydrothermal synthesis conditions, zeolitic structural units with linked AlO_4 or SiO_4 tetrahedra with associated cations and water molecules. In many instances achieving the right gel often becomes the primary requirement for obtaining crystalline material. The primary variables of this method are synthesis temperature, pH, reactivity of the silica source, silica to alumina ratio in the synthesis mixture and the nature and concentration of the alkali metals. In all cases the hydrogel of silica-alumina is prepared by keeping pH value in between 10 and 12. Such a system is always supersaturated with respect to the concentration of its chemical constituents. Under hydrothermal conditions (373-473 K) this supersaturation is then removed through nucleation of metastable zeolite phases. After nucleation of such a phase, the nuclei grow further to give larger crystals. These crystals can subsequently be dissolved in the mother liquor and eventually other zeolite phases may nucleate from it. As a consequence, the synthesis time is also a primary variable.

The use of quaternary organic ammonium salts in initial gel mixture bears the two effects as to influence Si/Al ratio and also structure of the zeolite.

The synthesis conditions of important zeolites using Na_2O-Al_2O_3-SiO_2-H_2O systems have been reviewed[1-3]. Because of the lack of thermodynamic equilibrium there is an infinite scope for modifying the reactants and physical conditions to produce new zeolites or to modify the chemical composition and physical properties such as size and shape of the zeolite crystals.

Lok et al.[4] examined the 'gel-chemistry' in detail. They traced the importance of gel-aging in zeolite synthesis. Usually the aging is carried out at room temperature (298 K) during which the bulk physical nature and consequently intimate atomic linkages change. Fyfe[5] reported the higher probability of the crystallization of metastable phases from highly reactive gel-mixtures. In such systems, the initial maximum free energy excess must be high with respect to final stable state. With increasing temperature of the synthesis, more compact zeolites are formed because of the greater reaction rates towards true equilibrium.

Lowe[6] has proposed a simple equilibrium model based on the assumption that in the initial reaction gel-mixture, the amorphous solid is in true or quasi-equilibrium with the solution phase and on completion of the crystallization a similar equilibrium is established between the zeolite and its mother liquor. The scope and objective of the present investigation on zeolite crystallization covers two areas :

(1) optimize synthesis procedure for partial (1:1 mole ratio of Al and Ga) and total incorporation of Ga in the MFI type framework with different Ga content,

(2) kinetic and mechanistic studies of such Ga incorporation.

2.2. SYSTEM FOR CRYSTALLIZATION OF PENTASIL (MFI) ZEOLITE

During the last 25 years, hydrothermal synthesis of high silica zeolites in presence of organic cations was studied extensively[7]. The addition of quaternary ammonium cations to the gel during the synthesis of high silica zeolites e.g. pentasil family has two effects viz :

(i) They act as strong bases and add more OH^- ions to the system, and hence increase the pH and solubility of silica and the degree of supersaturation of the system. Consequently zeolites with higher silica content are formed ($SiO_2/Al_2O_3 > 20$)

(ii) They are able to form water clathrates and possibly can "clathrate" silica in such a way as to generate new zeolite structures.

The isomorphous substitution of other tri- and tetravalent elements like B^{3+}, Ga^{3+}, Fe^{3+}, Zr^{4+} in place of Al^{3+} is of great interest to the scientists.

Materials which supply the approximate oxides for preparing zeolites of particular composition are sodium silicates/potassium silicates/silica gel/silicic acid for SiO_2 , Ga salts for Ga_2O_3, Al salts for Al_2O_3 , Fe salts for Fe_2O_3,sodium hydroxides for Na_2O and quaternary ammonium compounds. The crystallization of different isomorphs of ZSM-5 is usually carried out from a

hydrogel system with oxide mole composition :

$$M_{2/n}O : Y\ (R_4N)_2O : T_2O_3 : X\ SiO_2 : Z\ H_2O$$

where T is Fe^{3+}, Al^{3+}, Ga^{3+} or mixtures thereof; Y are moles of R_4N^+, the quaternary ammonium cation; M is the alkali metal cation of valence n and X are moles of SiO_2 and Z are water molecules. In general R_4N^+ can be triethyl-n-butylammonium (TEBA), triethyl-n-propylammonium (TEPA), tetra-ethylammonium (TEA), tetra-propylammonium (TPA) ions, equimolar mixture of alkylamines + alkyl-bromides and from the alkali metal or ammonium cation[8-10].

2.3 EXPERIMENTAL

2.3.1 Preparation of triethyl-n-butyl ammonium bromide (TEBA-Br): TEBA-Br was prepared by refluxing equimolar solution of n-butyl bromide (Sisco 98%) and triethylamine (Loba 99%) using isopropanol as solvent till the condesation reaction is complete. The excess alcohol was distilled off and TEBA-Br crystals were separated by filtration, washed with isopropanol and dried at 363 K overnight. The microanalysis of the dry product for C, N and Br agreed with the theoretical values within ± 0.5%. The product yield was 80%. The product being highly hygroscopic was preserved in an air-tight container. The reagents used for the hydrothermal synthesis of the pentasil isomorphs zeolites are listed in Table 2.1 with their commercial specifications.

2.3.2 Synthesis of pentasil zeolites : Synthesis runs were carried out using various composition in stainless steel (316) autoclaves (Fig. 2.1) of 250 ml capacity under static condition and at autogeneous pressure at different temperatures. A source

Table 2.1

Reactants used for the synthesis of pentasil zeolites and their specifications.

No.	Reagents	Manufacturer	Analysis
1	Sodium silicate Na_2SiO_3	-	27.89% SiO_2, 8.04% Na_2O, 64.07% H_2O
2	Gallium sulfate $Ga_2(SO_4)_3$	Aldrich	99.9%
3	Gallium nitrate $Ga_2(NO_3)_3$	Aldrich	99.9%
4	Aluminum sulfate $Al_2(SO_4)_3$ .16 H2O	Merck	99.8%
5	Sulfuric acid	BDH	98% AR
6	n-Butyl bromide	Sisco	98%
7	Triethylamine	Loba	99%
8	Isopropanol	Loba	99%
9	Triethyl-n-butyl ammonium bromide (TEBA-Br)	synthesized	50% C, 10.2% H, 5.7% N, 34% Br

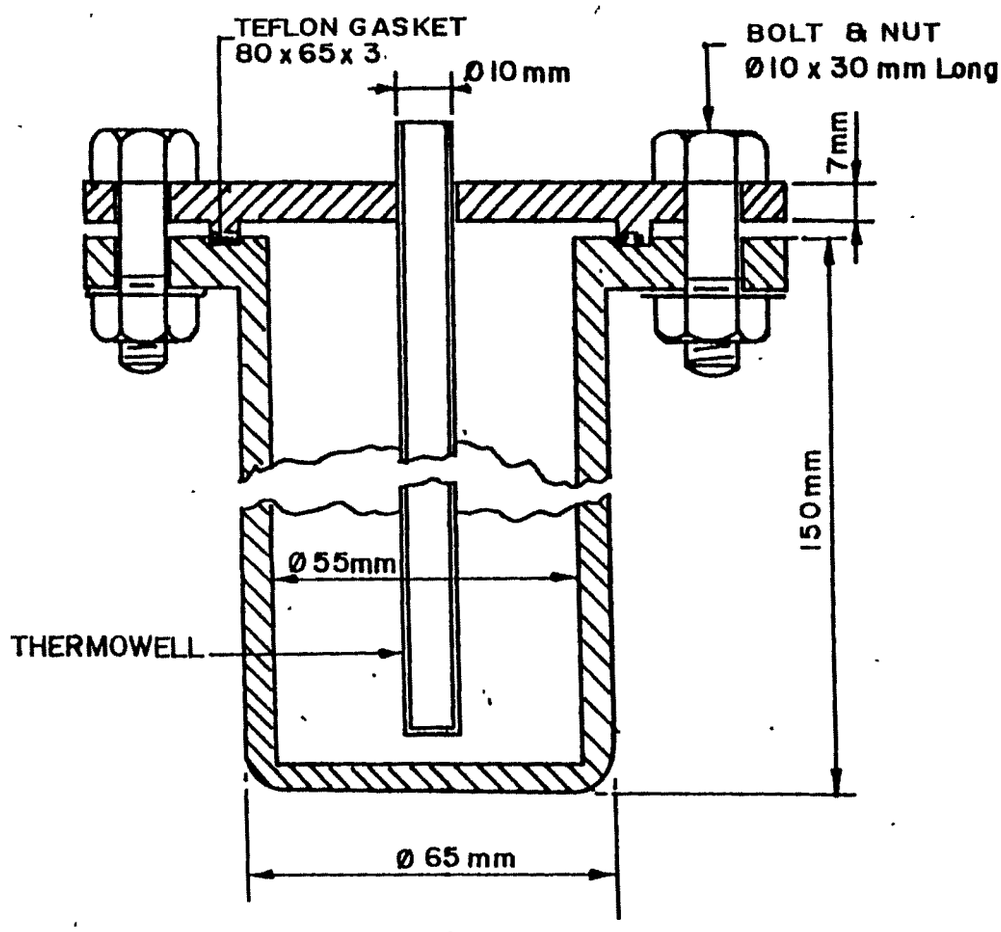

Fig.2.1. Stainless steel (316) autoclave with teflon gasket for hydrothermal synthesis.

of trivalent cation/(s) was dissolved in known amount of boiling water and sulfuric acid. This solution is then added dropwise to the mixture of TEBA-Br and sodium silicate diluted with water under constant stirring . The final gel (pH = 10.2) was stirred for half an hour and was autoclaved. The autoclave was then heated to desired temperature and the gel was crystallized over a certain length of period. The crystalline solid thus obtained was filtered, washed with distilled water and dried at 393 K. In a typical experiment, 0.92 g. of $Ga_2(SO_4)_3$ was dissolved in 3.52 g of H_2SO_4 and 50 g of water (solution A). In 40 g of sodium silicate 4.52 g TEBA-Br dissolved in 30 g of water was added with stirring (solution B). Then solution A was added to solution B with constant stirring for 15 minutes. Then gel formed was autoclaved and was kept in the oven at 453 K.

2.4 CHARACTERIZATION

2.4.1 X-ray diffraction (XRD) : The synthesized samples were analyzed by X-ray powder diffraction for qualitative and quantitative phase identification. **Philips X-ray diffractometer, model PW 1730** and Ni filtered cuK radiation (λ = 1.5406 Å) was used for the sample analysis. The most crystalline sample in each system was arbitrarily assumed to be 100% crystalline and was used as a reference standard for quantitative phase identification. The degree of crystallization of the solid product was estimated from the formula[11].

$$\% \text{ Crystallization} = \frac{\text{peak area between } 2\theta = 22\text{-}25^\circ \text{ of the product}}{\text{peak area between } 2\theta = 22\text{-}25^\circ \text{ of the reference sample}} \times 100$$

2.4.2 Infrared (IR) spectroscopy : The infrared spectra were recorded in the frequency range between 400-1300 cm^{-1} on a **PYE UNICAM SP-300** spectrometer using KBr pellets or nujol mulls of samples and by FTIR between 400-4000 cm^{-1} on **BRUKER IFS 48** IR spectrometer by adsorption of pyridine on zeolite.

For quantitative phase identification, a reference sample was used and % crystallization was calculated from the area under the band at 550 cm^{-1}. This band is due to double five membered rings in the zeolite. The extent of crystallization was estimated by using the formula[12].

$$\% \text{ Crystallization} = \frac{\text{peak area of the band at 550 } cm^{-1} \text{ of the product}}{\text{peak area of the band at 550 } cm^{-1} \text{ of the reference sample}} \times 100$$

The degree of crystallization can also be evaluated[13,14] from the IR optical density ratio of 550 and 450 cm^{-1} bands.

2.4.3 Thermal analysis (TG-DTA-DTG) : Simultaneous TG-DTA-DTG analysis of the crystalline phases were performed[15] on an automatic derivatograph **MOM BUDAPEST, Type 102B.** The thermograms of the samples were recorded under the following conditions.

Weight of the sample : 100 mg

Heating rate : 10 K min^{-1}

Pressure : flowing air at atmospheric pressure

Sensitivity :

TG - 100 mg

DTA - 0.2 mV

DTG - 0.2 mV

Preheated and finely powdered α-alumina was used as a reference material.

2.4.4 Scanning electron microscopy (SEM) : The morphology of synthesized samples was investigated using the scanning electron microscope, **STEREOSCAN MODEL 150 Cambridge, U.K.** The shape of the crystals obtained was investigated by dusting the samples on aluminum pegs by coating it with an Au-Pd evaporated film.

2.4.5 Sorption measurements : The sorption measurements have carried out with a calibrated McBain silica spring balance. The experimental set up is shown in Fig. 2.2. About 70-100 mg zeolite sample was pressed into a pellet and weighed into an aluminum bucket which was then suspended from the silica spring. The assembly was evacuated by means of a two stage rotary pump and mercury diffusion pump to a vacuum of 10^{-6} Torr. The sample was heated slowly to 673 K by continuous pumping till a constant weight was obtained. The temperature of the sample was then lowered to 298 K and the sorbate vapor admitted to the sample at constant temperature and pressure. The amount sorbed was measured from the extension of the spring which was recorded using a cathetometer.

In the preliminary runs, pentasil (MFI) zeolite exhibited the maximum uptake of water and hydrocarbons in the 1.5 hrs. Therefore, it was considered, the equilibrium saturation capacity when sorbate was exposed for the period of 2 hrs. The same sample was used for studying the sorption of another sorbate after desorbing the previous sorbate at 673 K and 10^{-6} Torr. All sorption measurements were carried out at 298 K and relative

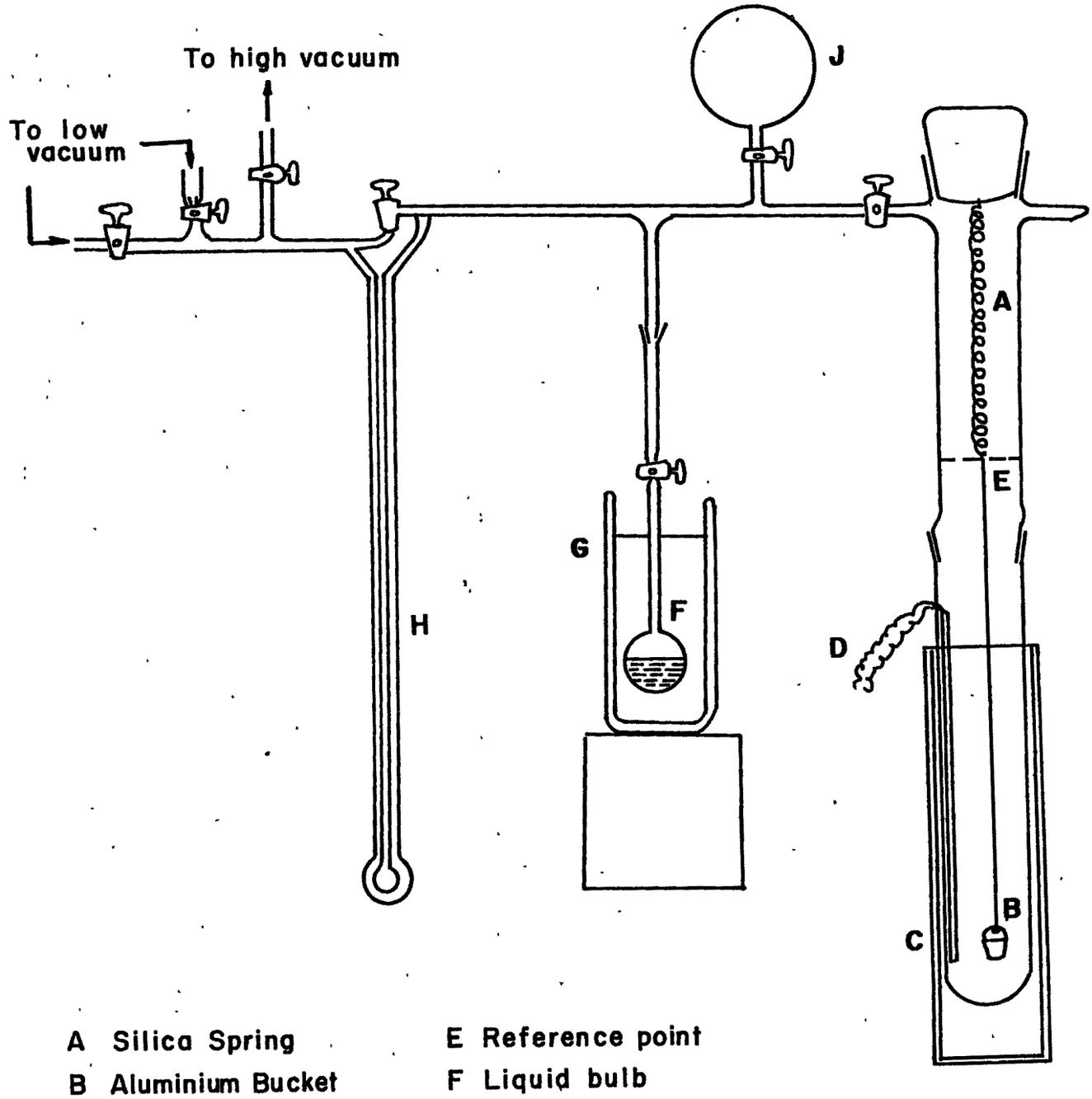

A Silica Spring
B Aluminium Bucket
C Furnace or Thermostat
D Thermocouple
E Reference point
F Liquid bulb
G Thermostat
H Manometer
J Gas Reservoir

FIG. 2.2 : GRAVIMETRIC ADSORPTION UNIT.

pressure P/P_o = 0.8.

2.4.6 Chemical analysis : A known quantity (0.2-0.3 g) of the sample was heated at a high temperature (1073 K) in a preweighed platinum crucible (in duplicates) for several hours till constant weight is obtained. The crucible was weighed to get % loss on ignition of the sample. The ignited sample was treated with 1:1 aqueous hydrofluoric acid (48% electronic grade) and a drop of sulfuric acid and was evaporated slowly. The HF treatment was repeated thrice. After the last treatment with HF, the sample was ignited to higher temperature (1073 K) for several hours to get a constant weight. From the loss in weight % SiO_2 in the sample was estimated. The residue was fused with potassium pyrosulfate (Merck, electronic grade) and was extracted with acidified deionized water and the solution was made up to a constant volume and the same was used for the estimation of the desired elements by the atomic absorption spectrophotometer, HITACHI Z 8000. The Si/Ga ratio was also confirmed by X-ray fluorescence spectrometry, (RIGAKU 3070).

2.4.7 ^{29}Si, ^{27}Al and ^{71}Ga MASNMR spectroscopy : Solid state MASNMR were recorded using a BRUKER MSL 300 spectrometer at 293 K. ^{29}Si spectra were collected using 45° pulse and with 3 sec. delay time) and chemical shifts were referred to TMS (tetra-methyl silane) as an internal standard. ^{27}Al spectra were recorded with 45° pulse (1 sec. delay time) using 0.1 M aqueous solution of $AlCl_3$ as a reference. ^{71}Ga spectra were recorded with 45° pulse (1 sec. delay time) using 0.1 M aqueous solution of

$Ga(NO_3)_3$ as a reference. All the samples were spun at a frequency of 3.5 KHz and 500-3000 FID's (free induction decay's) were recorded.

2.5 RESULTS AND DISCUSSION

2.5.1 Synthesis : Various synthesis experiments were carried out under static condition in the temperature range of 433 - 473 K, to investigate the kinetic features of the crystallization process. Table 2.2 lists the hydrogel compositions of the reaction mixtures (in terms of oxide moles) studied in the studies.

Fig. 2.3 depicts the XRD patterns of the fully crystalline as-syntheized Al, Fe and Ga isomorphs of ZSM-5 zeolites. All the XRD patterns from Fig. 2.3 resemble closely with the reported data for ZSM-5 zeolites[8,15,16]. The XRD profiles, however, for the as-synthesized Ga-ZSM-5 and Fe-ZSM-5 zeolites show a shift in interplaner spacings (d, Å) towards higher value as compared to that for Al-ZSM-5 of the same SiO_2/M_2O_3 (M = Al^{3+} or Ga^{3+}) ratio. The order of 'd' spacings of these zeolites is HGa-ZSM-5 > HFe-ZSM-5 > HAl-ZSM-5. The observed shift in (d Å) correlates with the lattice expansion[17] when comparatively shorter Al-O (1.74 Å) bonds are replaced by longer Ga-O (1.82 Å) in the zeolite framework. The results and more detailed discussion based on the X-ray diffraction data obtained in the present study is presented in the next chapter.

2.5.2 Kinetics of crystallization : A selected batch composition (System II, Table 2.2) was adopted to study the kinetic features of processes for the nucleation and crystallization. XRD

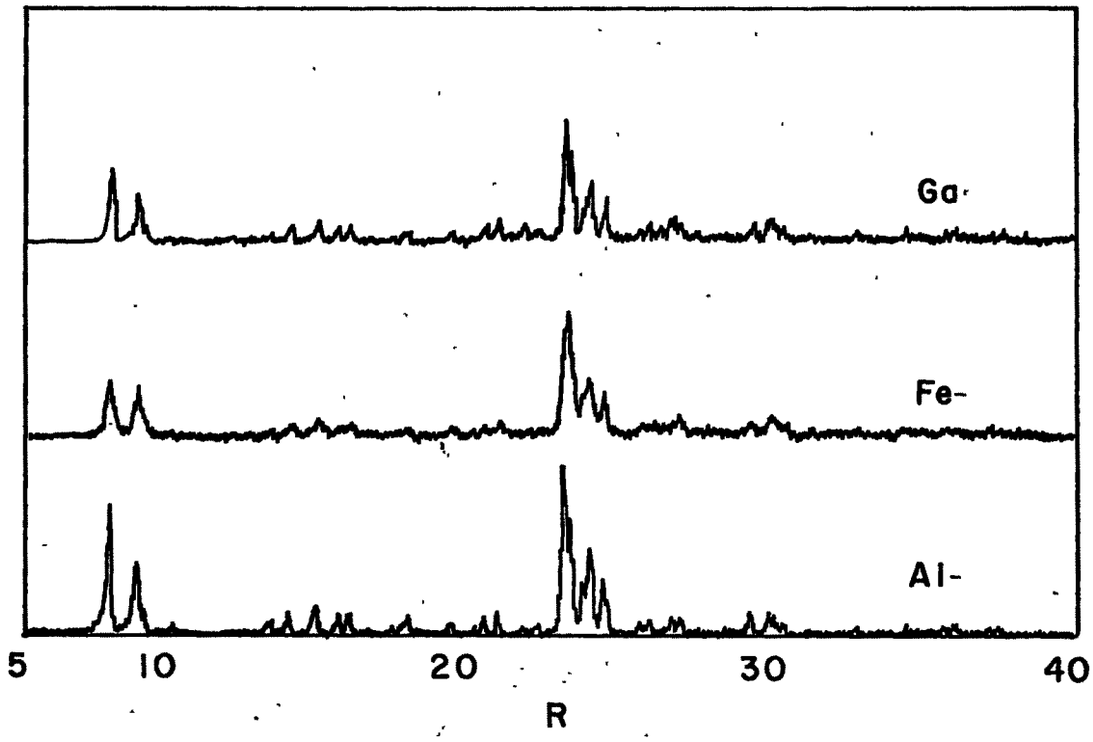

FIG.2.3 : X-RAY POWDER DIFFRACTION PROFILES OF Al-, Fe- AND Ga- ANALOGS OF PENTASIL (MFI) FRAMEWORK STRUCTURE IN AS-SYNTHESIZED (C/N) FORMS.

Table 2.2

Composition of hydrogel expressed in oxide moles.

System	$(TKBA)_2O$	Na_2O	Al_2O_3	Ga_2O_3	Fe_2O_3	SiO_2	H_2O	Product designation
I	2.03	11.08	-	1	-	39.64	1492	Ga-ZSM-5(40)
II	4.41	24.10	-	1	-	86.18	3243	Ga-ZSM-5(97)
III	15.04	82.12	-	1	-	293.6	11050	Ga-ZSM-5(289)
IV	4.42	24.28	1	-	-	87.0	3304	Al-ZSM-5(85)
V	1.89	10.38	1	-	-	37.2	1413	Al-ZSM-5(36)
VI	4.41	25.32	-	-	1	85.0	3243	Fe-ZSM-5(80)
VII	2.03	11.08	0.5	0.5	-	39.64	1492	AlGa-ZSM-5 (40)*
VIII	4.42	24.10	-	-	-	87.0	3243	Silicalite (> 3000)
IX	3.83 % Ga_2O_3 impregnated on silicalite							3.83 % Ga_2O_3 impreg. silicalite
X	2 % Ga_2O_3 impregnated on the crystalline product obtained from system IV							2 % Ga_2O_3 impreg. HAl-ZSM-5

*$SiO_2/(Al_2O_3+Ga_2O_3)$ = 40

profiles (Fig. 2.4) show the typical progressive crystallization of the gallosilicate phases obtained from system II at 453 K at different crystallization periods. The characteristic peaks of the pentasil phase started appearing after 10 hrs and the fully crystallized phase is obtained at 32 hrs. Fig. 2.5 illustrates the typical crystallization curves of gallosilicates at 433, 453 and 473 K for the system II. The curves show that the kinetics of crystallization depends on the temperature, as expected. With longer crystallization times (usually after attaining 100 % crystallinity), a decrease in crystallinity (not shown in Fig. 2.5) was observed due to the formation of a secondary dense phase (like α quartz) at the expense of the crystallized pentasil phase. Hence, the metastability region for gallosilicate pentasil zeolite is found to be smaller in the present studies compared to that for the aluminosilicate pentasil zeolite. The crystallization curves exhibit a sigmoid nature characteristic of two distinct stages viz.,

(1) an induction period when nuclei are formed, and

(2) a crystal growth period when nuclei grow into crystals.

The induction period (θ) may be defined as the time required for providing the condition for the formation of nuclei and the crystal growth period (K) as the time necessary for the growth of nuclei to a critical size[18].

As the main period of crystallization curve (20 - 80 %) is almost linear, the crystallization of gallosilicate was treated[19] as a first order reaction. The formation of nuclei during the induction period is assumed to be an energetically activated

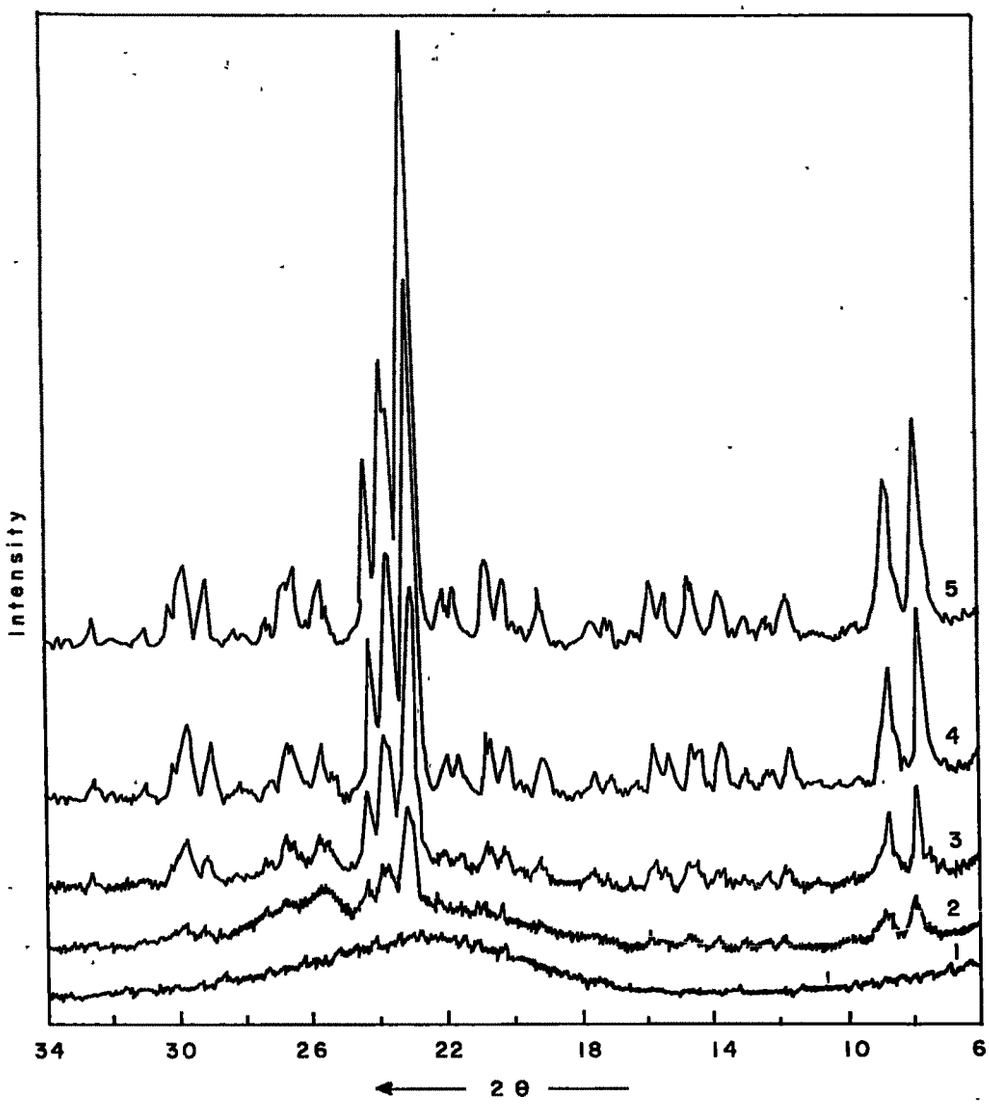

FIG. 2.4 : X-RAY DIFFRACTION PROFILES OF AS-SYNTHESIZED (C/N) Ga-ZSM-5 ZEOLITE SYNTHESIZED AT 453 K WITH DIFFERENT DEGREE OF CRYSTALLIZATION 1) 0%, 2) 18%, 3) 46%, 4) 81% AND 5) 100%.

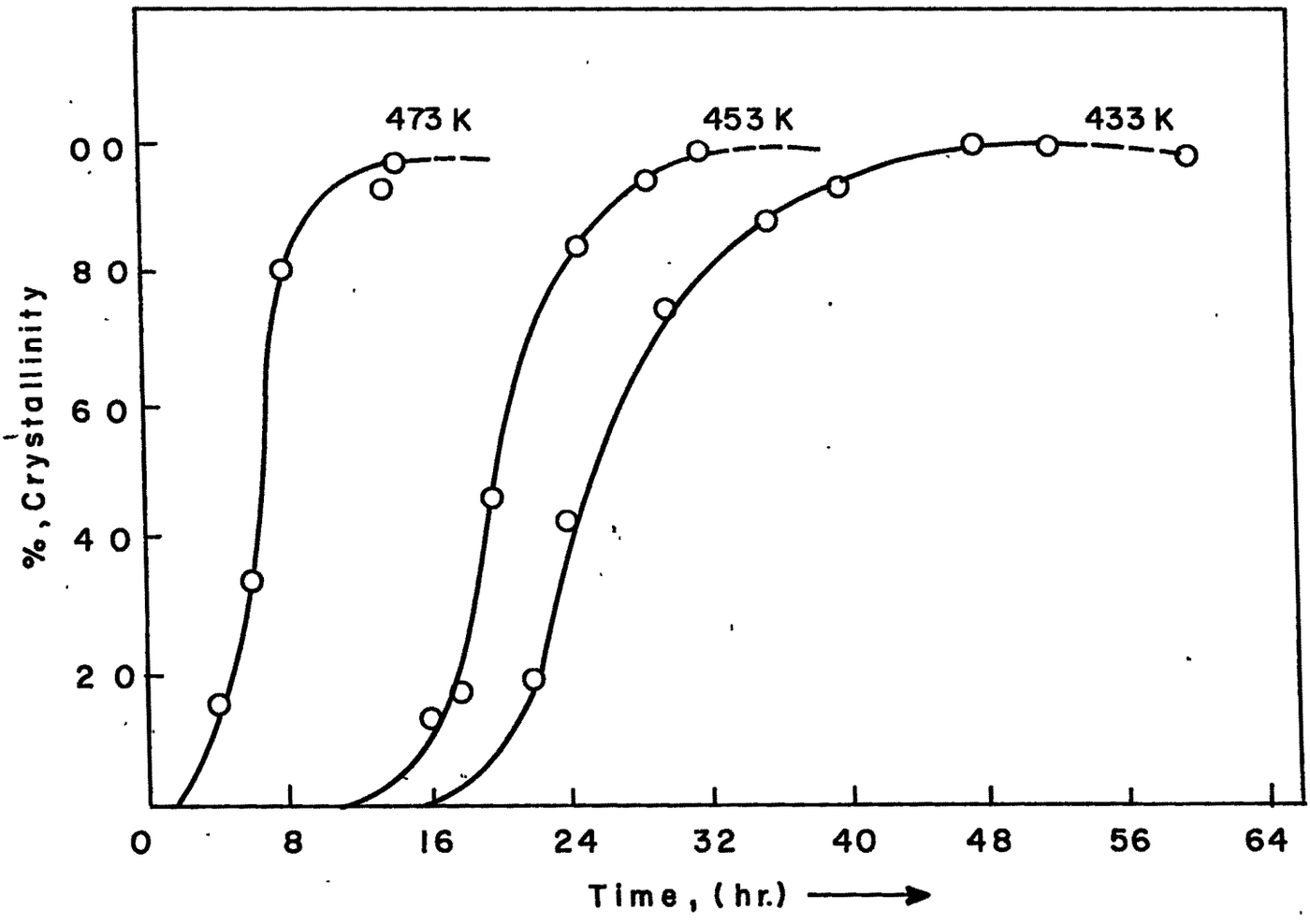

FIG. 2.5 : CRYSTALLIZATION KINETICS OF GALLIUM ANALOG OF PENTASIL (MFI) FRAMEWORK ZEOLITE FOR SYSTEM II.

process and since nucleation is the rate determining step during the induction period, the apparent activation energy for nucleation E_n was calculated from temperature-dependence of the rate of nucleation. The rate of nucleation has been assumed to be inversely proportional to the nucleation period. Apparent activation energy for nucleation was calculated from the Arrhenius equation which expresses the temperature dependence of the rate of nucleation,

$$\frac{d \ln(1/\theta)}{d (1/T)} = \frac{-E_n}{R} \qquad (1)$$

where θ is the induction period, that is the time on the crystallization curve where the conversion to the crystallization phase is just starting, T is the absolute temperature and R is the molar gas constant.

Similarly the apparent activation energy for the crystal growth 'E_c' was calculated from the temperature dependence of the rate of crystallization and was obtained from the point on the crystallization curves where 50% crystallization is complete. The temperature dependence of the rate of crystallization may be represented as,

$$\frac{d \ln(1/K)}{d (1/T)} = \frac{-E_c}{R} \qquad (2)$$

where K is the point on the crystallization curve (in hrs) where 50% crystallization is complete, T is the absolute temperature and R is the molar gas constant. Fig. 2.6 illustrates Arrehenius plots of the temperature dependence of the rate of nucleation and

crystallization. The values of the apparent activation energy of nucleation (E_n = 155.7 kJ $mole^{-1}$ as well as that of crystallization (E_c = 94.3 kJ $mole^{-1}$) for gallosilicate analog of pentasil formation were evaluated from the slopes of these linear plots. The above values of E_n and E_c obtained during the present studies appear to be higher than those reported previously[20] for the Al analog (E_n = 118, E_c = 78.6 kJ $mole^{-1}$) and Fe analog[21] (E_n = 145, E_c = 92.5 kJ $mole^{-1}$) of pentasil zeolites. The increase in E_n and E_c values in the order ($Al^{3+} < Fe^{3+} < Ga^{3+}$) may be due to their increasing ionic radii.

A number of reports[22-24] have described zeolite crystallization as a process that follows first order kinetics equation by the so called Avarami-Erofeev equation and the apparent activation energies for the processes of nucleations (E_n) and crystal growth (E_c) have been evaluated by applying Arrhenius equations. However, recently Thompson[25] and co-workers[26] have suggested that these analytical treatments to crystallization curve and the applications of Arrhenius equations to the crystallization kinetics cannot be used to reveal details regarding the crystallization kinetics or to compute activation energies from such as analysis principally due to the insensitivity of measurements of the mass of zeolite by conventional methods. Linear plots were, however, obtained when zeolite crystallization kinetics data were analyzed in terms of Avrami-Erofeev (linear) equation. Avarami-Erofeev parameters (m and k) obtained from the slopes and intercepts respectively are tabulated in Table 2.3 only for comparative purpose.

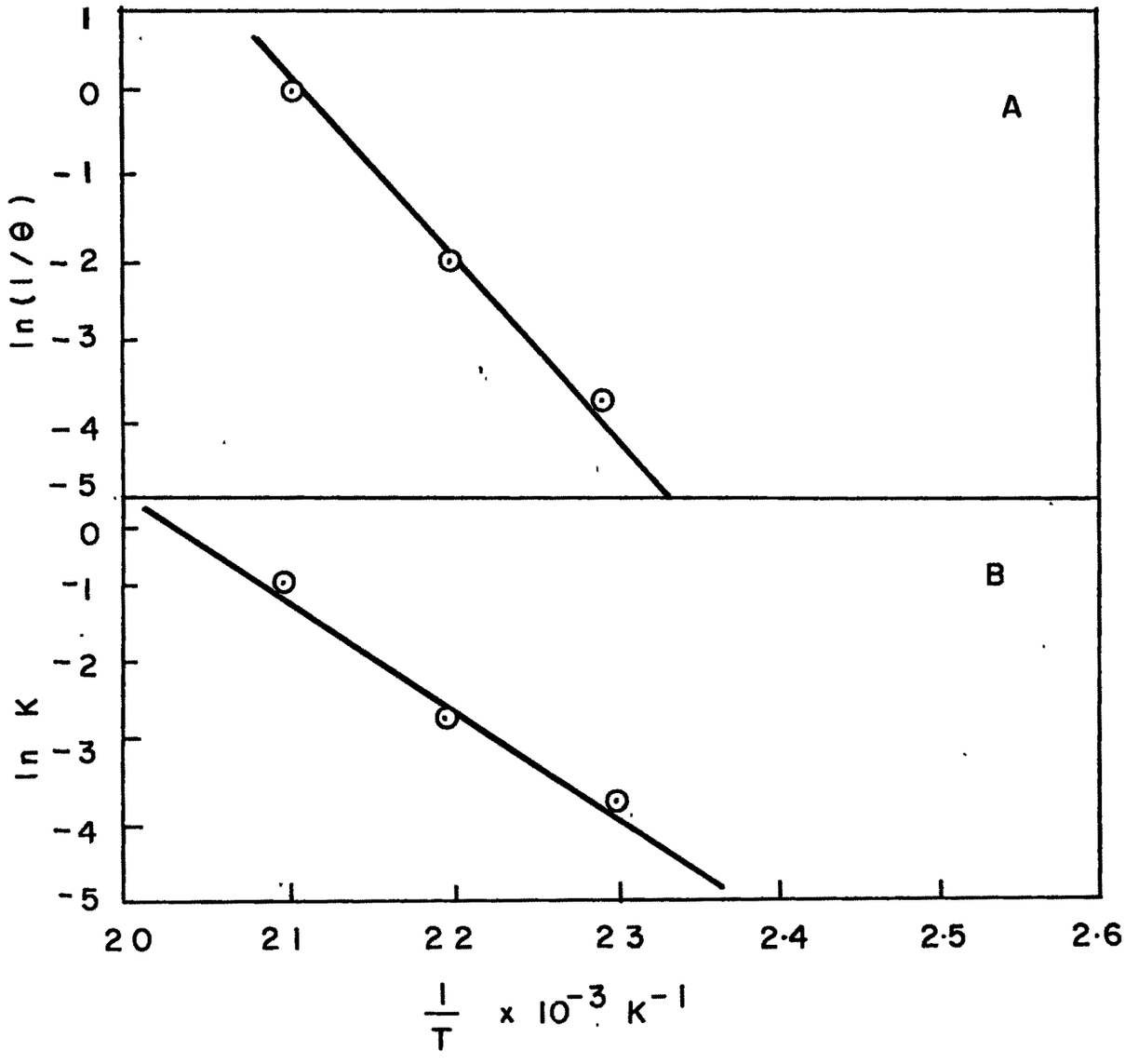

FIG. 2.6: ARRHENIUS PLOTS FOR A) NUCLEATION AND B) CRYSTALLIZATION OF GALLIUM ANALOG OF MFI TYPE ZEOLITE OBTAINED FROM SYSTEM II.

Table 2.3

Avrami-Erofeev Parameters for gallosilicate synthesis using TEBA-Br.

Synthesis temp. K	10^2 x k	m
433	3.27	4.72
453	4.58	3.60
473	11.73	2.44

2.5.3 Effect of SiO_2/Ga_2O_3 ratio on the kinetics and crystallization : Fig 2.7 shows the typical crystallization curves at 453 K for pentasil gallosilicate gel composition of varying SiO_2/Ga_2O_3 (system I, II and III) at a constant $(TEBA)_2O/SiO_2$, Na_2O/SiO_2 and Ga_2O_3/SiO_2 mole ratio. These curves are of typical sigmoid nature, characteristic of processes involving nucleation and crystal growth. The decrease in Ga concentration in the hydrogel enhances the rate of nucleation and crystal growth processes of gallosilicate. Similar results were reported[11,27,28] for Al-ZSM-5 when Al concentrations were varied. Perhaps the higher concentration of Ga^{3+} in a gel may require higher amount of silica monomers for the formation of nuclei.

Increase in the crystallization period beyond the metastability period decreases the crystallinity of the pentasil phase and increases the formation of quartz (not shown in Fig. 2.7) in the solids obtained.

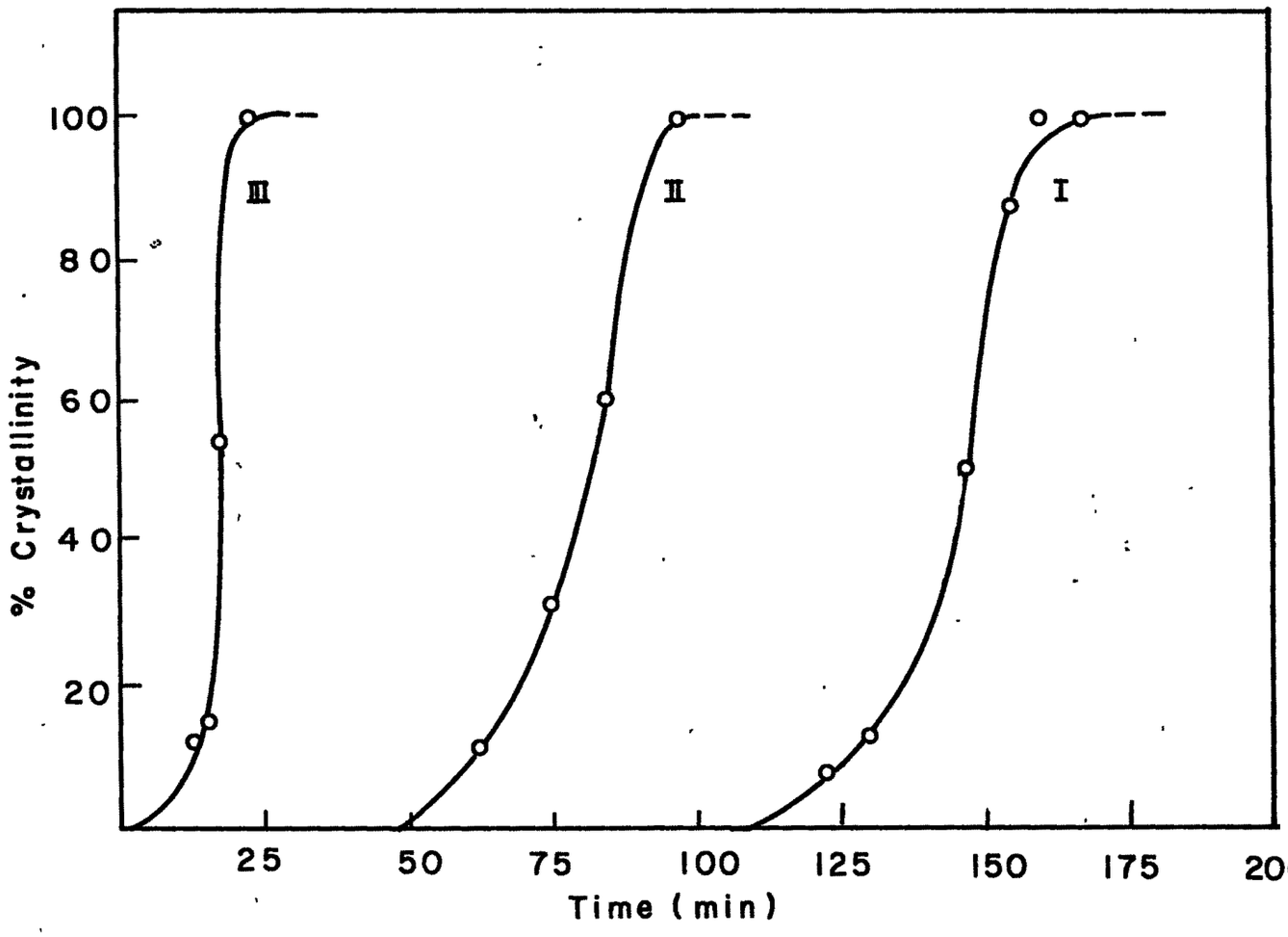

FIG. 2.7 : CRYSTALLIZATION CURVES AT 453 K FOR PENTASIL (MFI) GALLOSILICATE OBTAINED FROM SYSTEM I, II AND III.

2.5.4 Effect of OH^-/H_2O ratio on the kinetics of the crystallization : As polymerization - depolymerization equilibrium of the soluble gallosilicate is influenced by alkalinity of the reactants, the functional dependence of zeolite crystallization kinetics on OH^-/H_2O ratio was studied.

Fig. 2.8 represents the crystallization curves for gallosilicate, system II at 453 K with varying alkalinity of the reaction mixture. Variation in alkalinity was accomplished by varying the amount of sulfuric acid added.

As seen in Fig. 2.8, an increase in OH^-/H_2O ratios in the reaction mixture increases the rate of nucleation. Concentration of OH^- ions in the gel accelerates the dissolution of the gel materials and enhances the formation of $Ga(OH)_n$ species. The dissolved species (Si and Ga) can also undergo polymerization forming gallosilicate or polysilicate ions and those in turn, in presence of quaternary ammonium ions, $(TEBA)^+$, condense to form the nuclei of the ordered zeolite framework. Thus induction and nucleation period is inversely proportional to the OH^- ion concentration. As seen from Fig. 2.8, the nucleation period for the Ga-ZSM-5 system II was shortened from 30 to 10 h when the OH^-/H_2O concentration was increased from 1.0×10^{-3} to 5×10^{-3}. It was observed (not shown in Fig. 2.8) that still higher alkalinity of the hydrogel mainly gives rise to a dense phase, α-quartz due to the rapid decomposition of the template (TEBA-Br)[28].

2.5.5 Infra red spectroscopy : The structural details of the zeolitic phase formed from gallosilicate mixture was studied by infra red technique in the framework vibrations region (400 -

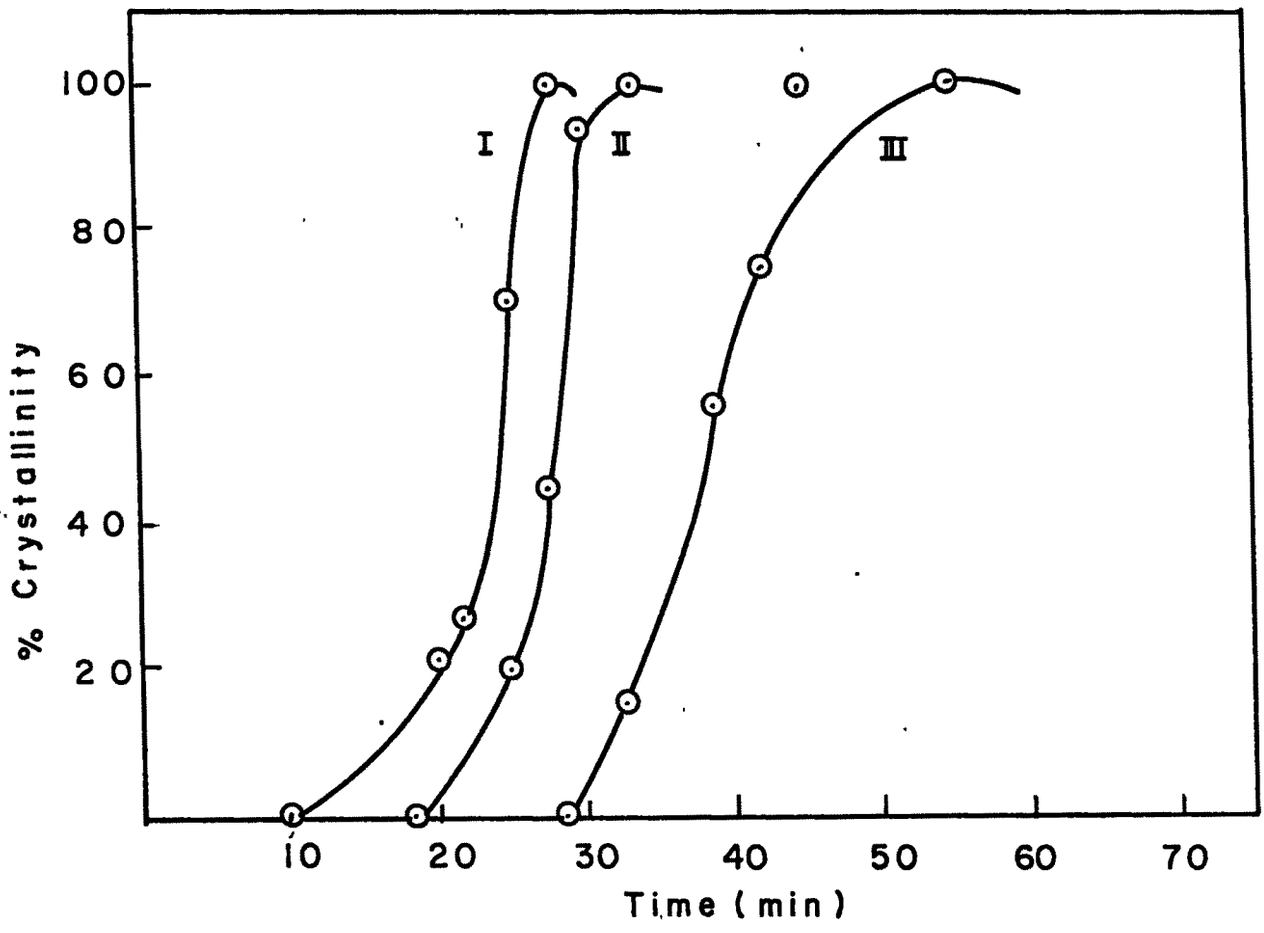

FIG. 2.8 : INFLUENCE OF OH^-/ H_2O CONCENTRATING A) 5×10^{-3} b) $2{\cdot}7 \times 10^{-3}$ c) $1{\cdot}0 \times 10^{-3}$ ON CRYSTALLIZATION KINETIC OF PENTASIL (MFI) GALLOSILICATE AT 453 K OBTAINED FROM SYSTEM II.

1200 cm^{-1}). The spectra were recorded using nujol mull technique. Fig. 2.9 shows framework region IR spectra of gallosilicate products of different crystallinity obtained from system II at 453 K. Absorption in the mid region (200-1300 cm^{-1}) in the IR spectra can be classified[29a] into (1) internal vibrations of the TO_4, which are sensitive to the structural vibrations, and (ii) vibrations related to the external linkages of TO_4 units in the zeolite structures. The IR band assignments[29a] for internal and external vibrations are shown in Table 2.4. The gradual increase in the intensity of 550 cm^{-1} band[27-28] in addition to the one at 450 cm^{-1} shows the increase in the concentration of MFI phase in the product. According to

Table 2.4

The IR band assignments for internal and external vibrations

Zeolite Infra-red assignments		cm^{-1}
(i)	Internal tetrhedra	
	Asym. stretch	1250 - 950
	Sym. stretch	720 - 650
	T-O bond	420 - 500
(ii)	External linkages	
	Double ring	650 - 500
	Pore opening	300 - 420
	Sym. stretch	750 - 820
	Asym. stretch	1050 - 1150

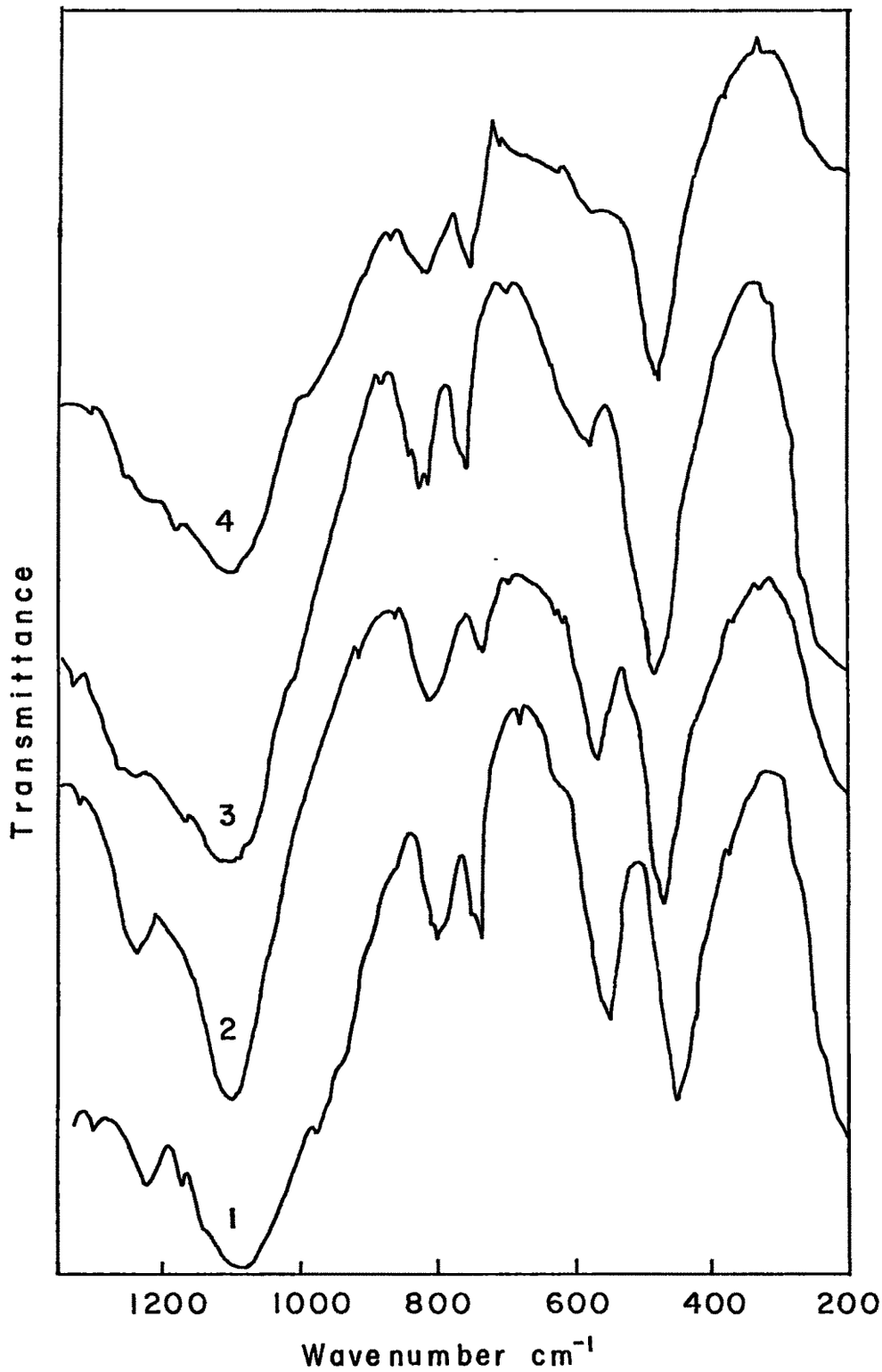

FIG. 2.9 : IR SPECTRA OF GALLOSILICATES (MFI) ZEOLITE WITH DIFFERENT DEGREE OF CRYSTALLINITY. 1) 100%, 2) 46%, 3) 18% AND 4) 0% OBTAINED USING SYSTEM II. COMPOSITION AT 453 K.

the Flanigen-Khatami Szymanski correlation[29], the absorption near 1100, 700 and 450 cm^{-1} are assigned to infrared vibration of $Si(Al)O_4$ tetrahedra and are also seen in silica and quartz[30]. The absorption bands near 1200 and 550 cm^{-1} were assigned by Jacobs et al.[31] and Vedrine et al[32]. to the presence of double five membered ring systems. The strongest absorption band at around 1100 cm^{-1} is related to the internal asymmetric stretching vibration of T-O bond. This band is shifted to lower wave number with respect to silicalite[14] (1100 cm^{-1}). The shift in the frequency can be explained on the basis of T-O bond distance. In case of T-O stretch frequency, substitution of Ga for Si in the framework causes a shift to lower frequency owing to longer Ga-O bond distance (1.82 Å) as compared to Si-O bond distance (1.60 Å).

2.5.6 Thermal Analysis : The gallosilicates synthesized from system II were studied by thermogravimetry. Both the weight loss and the magnitude of the corresponding thermal effects are utilized to characterize the intermediate phases. Fig 2.10A represents the TG patterns for the samples of different crystallinity of gallosilicate pentasil phases obtained at 453 K. It is seen from the figure that the % weight loss on heating increases with the crystallinity of the samples. This is because of the incorporation of more and more template with increasing crystallinity of the zeolite. For the amorphous sample, the weight loss is in the temperature range 345 to 750 K. Fully crystalline, as-synthesized gallosilicate sample shows three distinct zones of weight loss (Fig. 2.10B) in the temperature

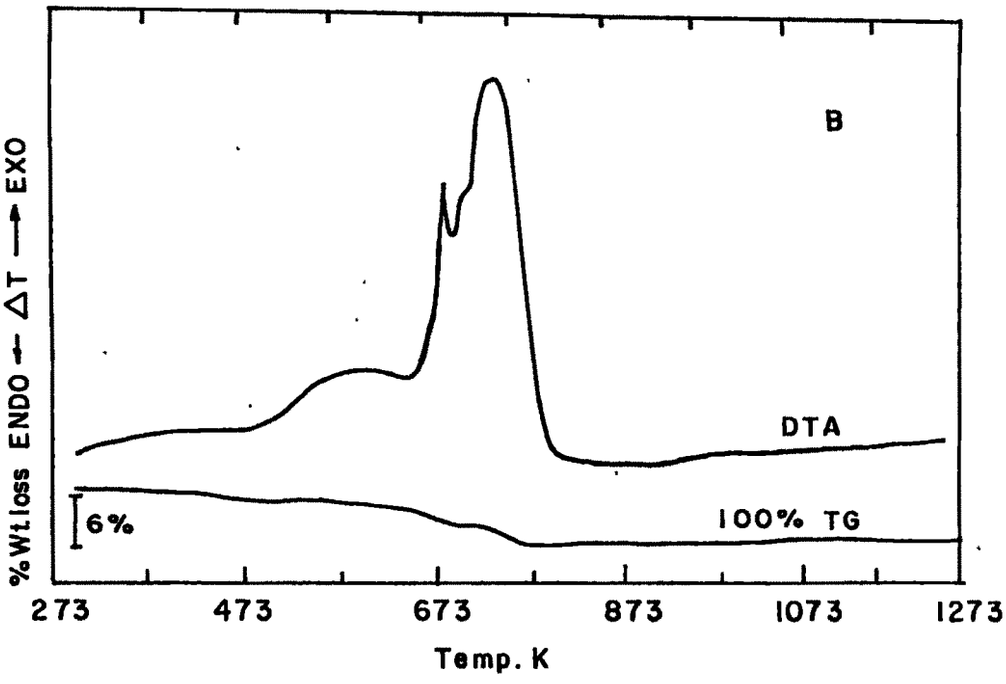

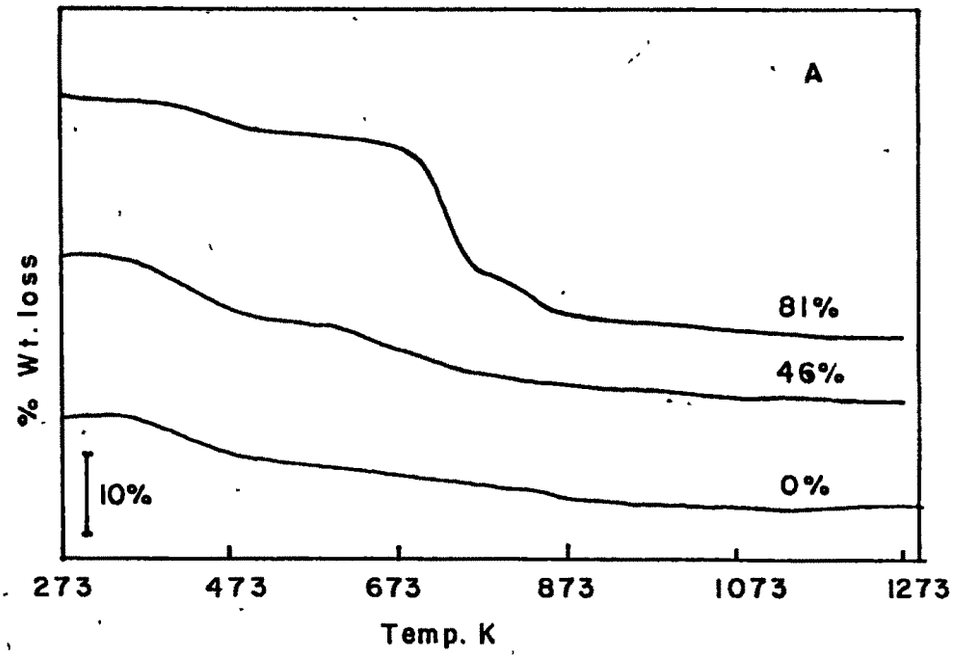

FIG. 2.10: A) THE TG PATTERENS FOR THE SAMPLES OF DIFFERENT CRYSTALLINITY OF PENTASIL (MFI) PHASES OBTAINED AT 453K USING THE COMPOSITION OF SYSTEM II. B) TG/DTA CURVES FOR 100% CRYSTALLINE AS SYNTHESIZED PENTASIL MFI GALLOSILICATE OBTAINED FROM SYSTEM II.

ranges, (1) 434-647 K, (2) 647-699 K and (III) 699-834 K. The first step results from dehydration of physically sorbed water. Almost all the water is lost in a narrow temperature interval. It is observed that the peak area under the endotherm varies with the crystallinity. The other two steps are exothermic (DTA curve) and are related to the oxidative decomposition of organic material occluded during the crystallization. This is consistent with the characteristic two step exotherm in the Al analog of MFI framework zeolite[33]. The low temperature (705 K) peak is believed to be due to decomposition of loosely held $TEBA^+$ ions in gallosilicate, while the high temperature (757 K) peak corresponds to the oxidative decomposition of $TEBA^+$ cations which are strongly bonded and associated with gallium sites in the channels. The exotherm around 1253 K shows breaking down of the structure due to degalliation or the transformation of the pentasil phase into a dense phase. It shows that organic $TEBA^+$ is decomposed at 834 K and are removed from the zeolite framework. It is observed that the increase in crystallinity resulted in the increase in weight loss due to decomposition of organic cations accompanied by the decrease in loss in weight due to dehydration in the temperature range 647-834 K. It thus indicates that the products tends be more hydrophobic as organic templating species are progressively incorporated during the crystallization[33]. Fig. 2.11 represents the % weight loss corresponding to the decomposition of organic cations as a function of crystallinity measured by X-ray diffraction for the gallosilicates synthesized from system II at 453 K. The linear relationship is observed in

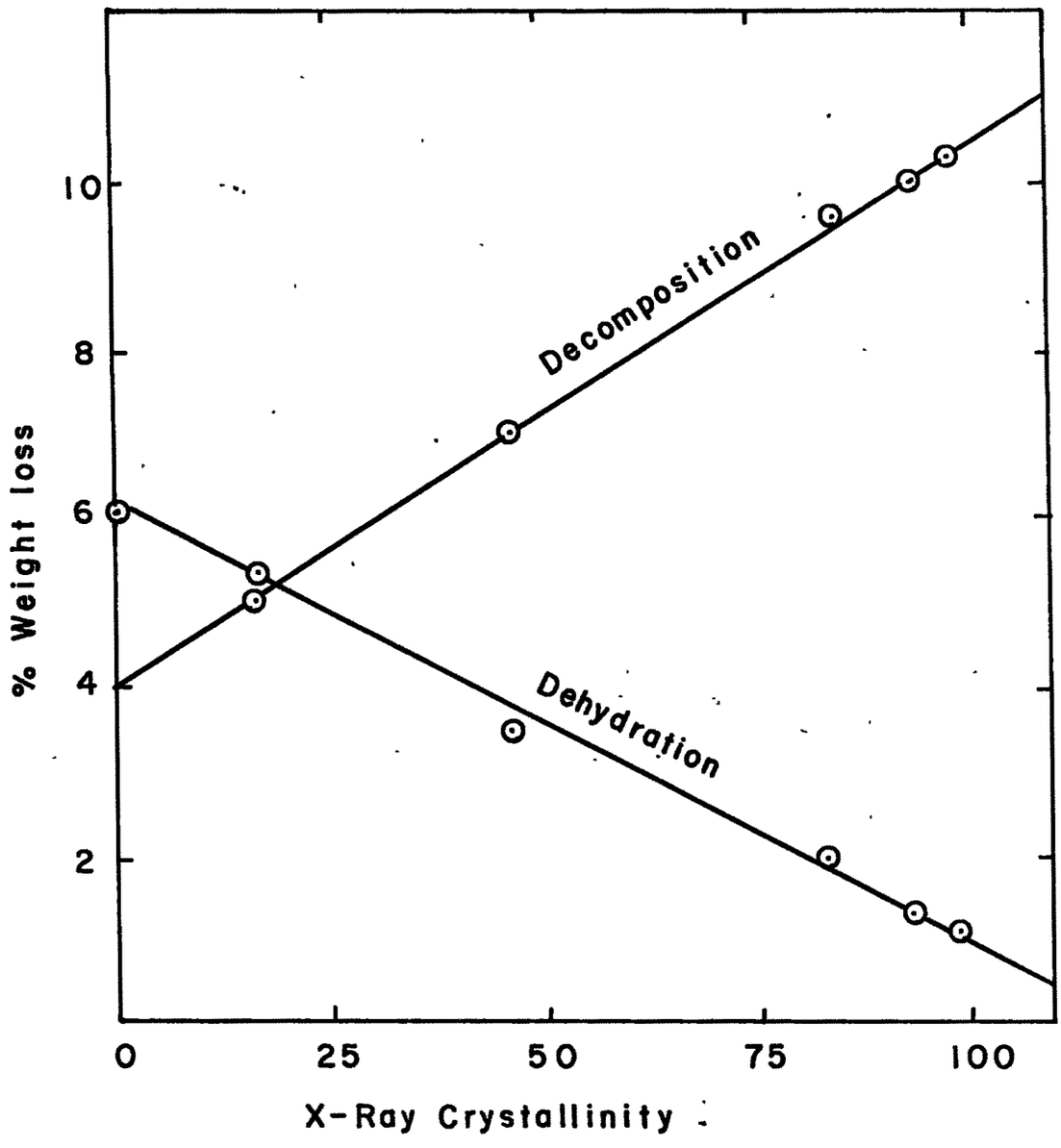

FIG. 2.11 : X-RAY CRYSTALLINITY Vs % LOSS IN WEIGHT DUE TO DECOMPOSITION OF ORGANIC AND WATER PENTASIL (MFI) GALLOSILICATES OBTAINED FROM SYSTEM II.

both i.e. in the loss due to dehydration as well as that due to template decomposition processes. An extrapolation of the line to the ordinate shows that the nuclei of Ga-ZSM-5 are also present in amorphous gel, which are probably not detected by the crystal below its lower limitation (< 5nm). The temperature of the maximum of the high temperature exotherm is often taken[34] as a criterion for the thermal stability of the zeolite lattice. The absence of an exotherm in DTA curve of fully crystalline sample upto 1273 K indicates that the gallosilicate zeolite lattice is stable at least upto 1273 K.

2.5.7 Sorption properties : Equilibrium sorption capacities of different probe molecules like water, benzene, n-hexane[35] often help to estimate or confirm the crystalline nature and the void volume of the zeolites. Table 2.5 lists the equilibrium sorption capacities (at P/P_o = 0.8, 298 K, 2h) for different probe molecules in the samples of different crystallinity obtained from system II and also in the samples of maximum crystallinity from systems I, III, V, VIII and IX. It is observed from the sorption data, that the sorption uptake increases with increase in the crystallinity. The amorphous material adsorbs 20% of the total capacity of the water in 100% crystalline sample, whereas it adsorbs 5-10 % of the total sorption capacities of larger hydrocarbons in fully crystalline sample.

The water molecule is comparatively smaller in size (kinetic diameter 2.65 Å) with polar character and hence gets occluded depending on the concentration of Ga content. Table 2.5 shows decrease in water uptake consistently with a decrease of Ga

Table 2.5

Equilibrium sorption capacities of the gallosilicate pentasil and other pentasil (MFI) isomorphs.

System	Sample name	% crystallinity	Sorption* gm 100 gm^{-1}		
			Water	n-Hexane	Cyclohexane
I	Gallosilicate(40)	100	9.14	10.00	4.52
II	Gallosilicate(97)	0	1.60	0.56	0.40
		18	2.16	2.28	1.86
		46	2.66	4.62	2.20
		81	6.40	10.70	3.50
		100	8.13	11.01	4.07
III	Gallosilicate(289)	100	3.09	11.50	3.98
IV	Silicalite (>3000)	100	2.00	11.90	2.60
V	Aluminosilicate(36)	100	10.06	11.10	5.29
VI	3.83% Ga_2O_3 impregnated silicalite	-	3.3	12.1	3.50

* At 298 K, P/P_o = 0.8, 2h.

content in the zeolite (system I,II,III). This shows an increase in the hydrophobic character of the gallosilicate with the increase in SiO_2/Ga_2O_3 ratio. The sorption uptake of the non-polar cylindrical n-hexane molecule (kinetic diameter 4.3 Å) seems to be least affected by the variation of the gallium content in gallosilicate pentasil samples. The nearly constant equilibrium sorption of n-hexane corresponds to general expectation for zeolite ZSM-5[16,36]. The equilibrium sorption capacity of spherical cyclohexane molecule of the size 6.2 Å (kinetic diameter) comparable to the pore diameter, decreases with the increase in the SiO_2/Ga_2O_3 ratio. However, relatively higher values for water and cyclohexane adsorption on gallosilicate, compared to those for silicalite and impregnated samples, further indicate some change in the void volume when Ga^{+3} is present and occupying tetrahedral positions in the lattice. These data support the observation that under direct hydro-thermal treatment Ga containing hydrogels yield a Ga^{3+} containing MFI framework and not the silicalite with occluded Ga_2O_3. Although aluminosilicate (system V) and gallosilicate (system II) MFI samples show almost comparable sorption uptakes, the former shows slightly higher sorption uptakes than those in the latter.

Crystallinity evaluated from the uptake of n-hexane by the samples obtained from system II at different crystallization period shows a close relationship with the XRD crystallinity as shown in Fig. 2.12. Both the XRD and sorption crystallinity plots are sigmoid in nature indicating that the nucleation and

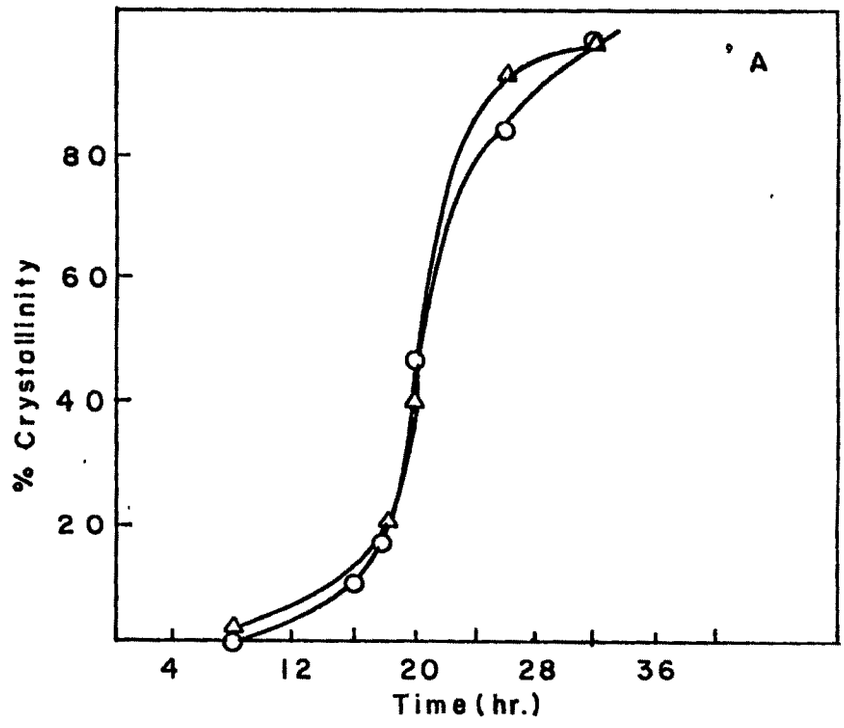

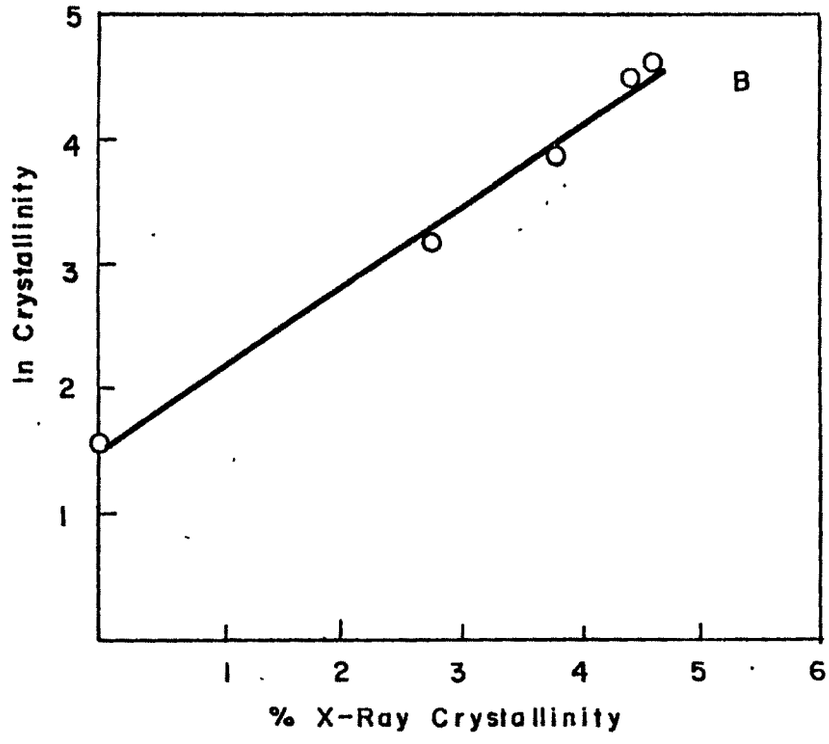

FIG.2.12: A) THE CHANGE IN CRYSTALLINITY OF GALLOSILICATE (MFI) PHASE WITH SYNTHESIS TIME ESTIMATED BY (△) n-HEXANE SORPTION AND (O) XRD. (B) RELATION BETWEEN THE CRYSTALLINITY EVALUATED FROM n-HEXANE SORPTION AND XRD.

crystal growth occurs successively. The lower value of crystallinity obtained by XRD is attributed to its inability to see crystals smaller than 5 nm[37]. The linear correlation between the two values of crystallinity is also seen in Fig. 2.12b.

2.5.8 Scanning electron microscopy : Fig. 2.13 (a to d) show the representative phases during the crystallization of gallosilicate from system II at 453 K. The well-defined crystallites start appearing with the increase in the crystallinity of the zeolite. Amorphous samples obtained at 8h, do not show the MFI peak in XRD (Fig.2.4, curve 1) and 550 cm^{-1} peak in IR (Fig. 2.9, curve 4). Small amount of crystals (Fig. 2.13a) along with large amount of amorphous phase appeared in the product obtained at 18 h which is reflected in the partly crystalline nature in XRD pattern (Fig. 2.4, curve 2) and IR pattern (Fig. 2.9, curve 3). It seems that crystalline phase increased more and more and gel was mostly converted into MFI phase (Fig. 2.13c) at 25 h. The contribution of a crystalline phase increased with conversion of a gel into MFI phase (2.13c) at 25 h. With further increase in the crystallization time, the fully crystalline phase was obtained (Fig. 2.13d) at 32 h. This increase in crystallinity is reflected in IR spectra also. Two bands at 550 cm^{-1} and 450 cm^{-1}, characteristic of a double ring and pore opening respectively in the MFI structure are exhibited in IR (Fig. 2.9, curve 1) spectrum.

The increase in the crystallite size was observed with the increase in the crystallization temperature. However, with increase in concentration of Ga, the crystallite size was found to decrease.

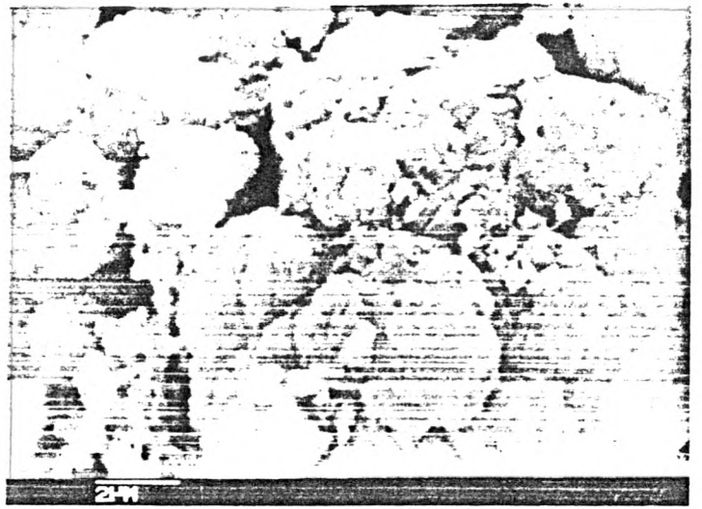

(a)

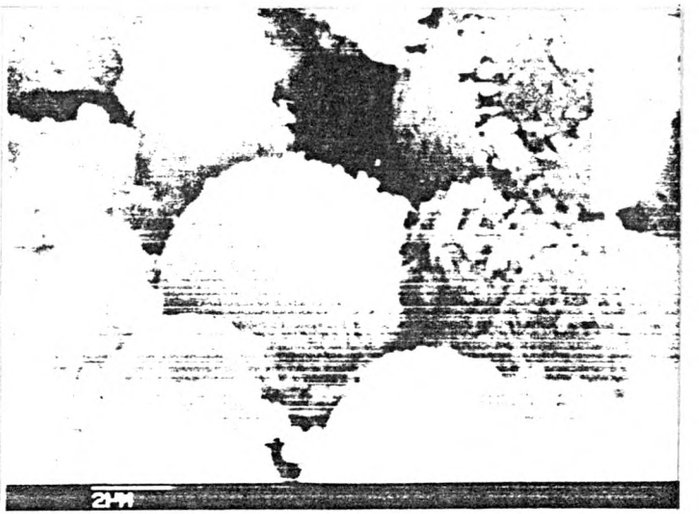

(b)

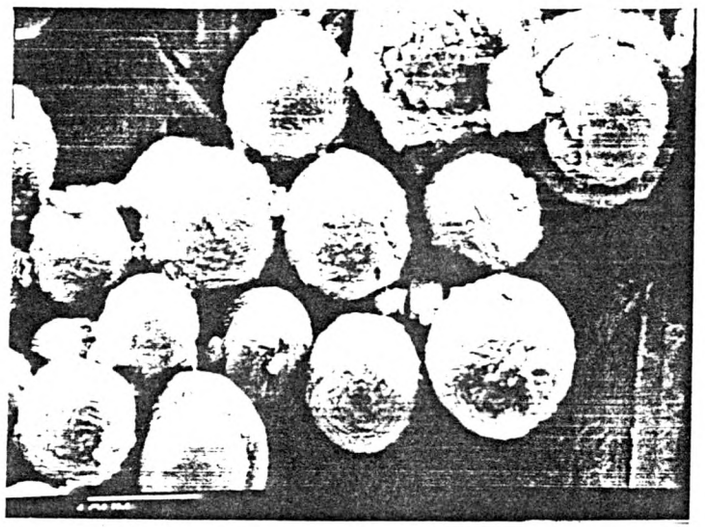

(c)

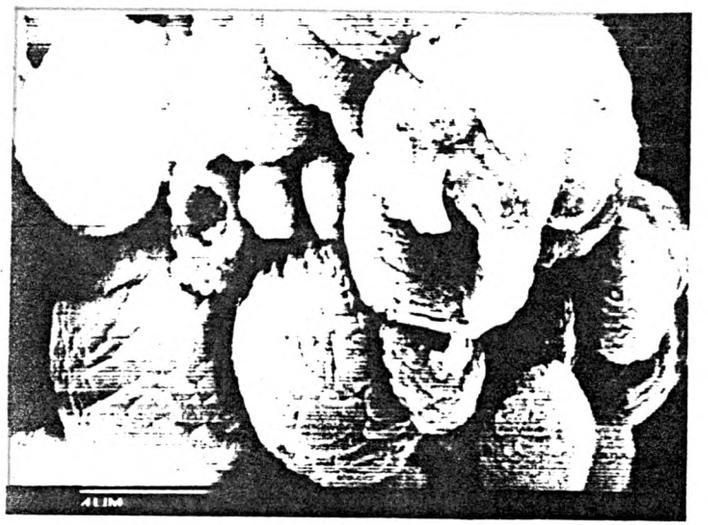

(d)

FIG.2.13 : SEM PHOTOGRAPHS OF PENTASIL (MFI) GALLOSILICATE PHASES WITH a) 18%, b) 46%, c) 81% AND d) 100% CRYSTALLINE SAMPLES OBTAINED FROM SYSTEM II AT 453 K.

The morphology of a fully crystalline pentasil zeolite of Ga and Al analog prepared from different systems (from Table 2.1 has been illustrated in Fig. 2.14. The crystallite size of Al-analog of pentasil zeolite was found to be smaller (1.5 μm) than Ga-analog of pentasil zeolite (3.5 μm) of same product SiO_2/M_2O_3 ratio. The crystallite size of Al+Ga analog of pentasil was found to be (2-3 μm). Silicalite sample (free from both Al^{3+} and Ga^{3+}) shows a well defined cuboid shaped crystallites of 8-10 μm (Fig. 2.14 d).

The shape of the crystallites obtained was found to be spherical irrespective of the gel composition and crystallization temperature.

2.5.9 Zeolite crystallization mechanisms : As the synthesis of zeolite is carried out from a complex mixtures of reactants and multiple phases (aqueous solution, amorphous solid and crystalline solid) and both the composition and quantities of these phases vary continuously during the course of crystallization, it is indeed expected that a single mechanism to explain zeolite formation may be unrealistic. Over past three decades[4,33,38-42] many investigators paid an extensive attention to the mechanism involved in the zeolite crystallization. To date two theories have been proposed,

1. Crystallization via liquid phase transformation
2. Crystallization via solid - phase transformation

In addition to the zeolite formation via either of the two transformations, an evidence has been presented indicating that both the types of transformations can occur simultaneously in the

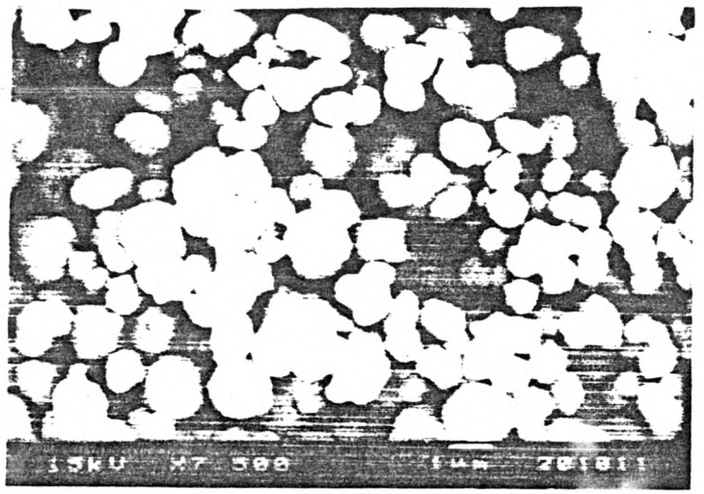

(a)

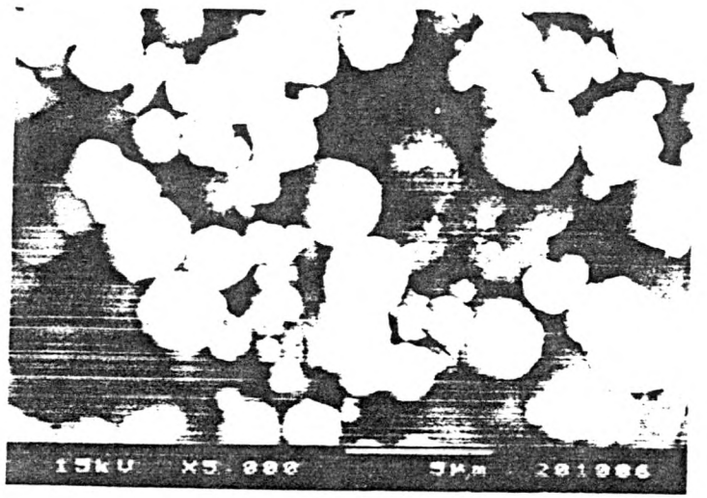

(b)

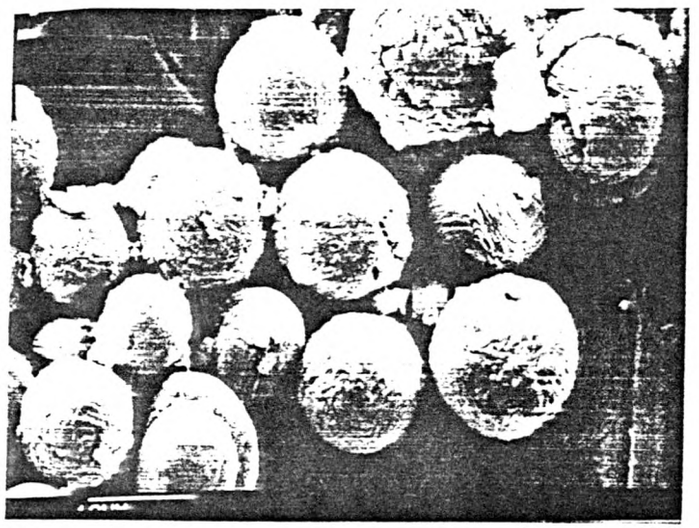

(c)

(d)

FIG.2.14: SEM PHOTOGRAPHS OF FULLY CRYSTALLINE a) Al-ZSM-5(85), b) AlGa-ZSM-5(40), c) Ga-ZSM-5(40) AND d) SILICALITE (>3000)

same reaction system. In general, based on the evidence presented to date, it appears that the mechanism for crystallization of these systems is strongly directed by the components making up the reaction system and the conditions of synthesis.

1. Crystallization by liquid phase transformation : In liquid phase transformation, the crystallization mechanism is controlled by the soluble aluminate and aluminosilicate species. The nuclei of the zeolite crystals are formed in the liquid phase of the gel or at the interface of the gel phases. The growth of the crystal nuclei proceeds at the expense of aluminosilicate hydrated anion species in the solution. An equilibrium exists between solid gel phase and solution phase. Whenever nucleation occurs in the solution, this equilibrium shifts so as to provide more nutrients to the solution. The gel dissolves continuously and the dissolved species from the gel are transported to the nuclei crystals in the solution phase. Therefore, the concentration of the soluble aluminosilicate species in the solution increases and more crystal nuclei are formed from these soluble species in the solution.

2. Crystallization by solid phase transformation : In the solid phase transformation, a hydrogel is rapidly formed from a solution composed of monomeric silica and alumina[39] species at higher pH (>10). The gel composition should be nearly same as that of expected reagent ratios. The nucleation of hydrogel occurs rapidly in presence of organic cations, which further interact intimately with the numerous reactive aluminosilicate anions and direct recrystallization process involving the solid-

hydrogel transformation or surface nucleation. A rapid and sharp increase in nucleation and growth leading to a large number of small polycrystalline zeolite crystallites occurs. Sand and coworkers[30,53] have confirmed the existence of these two types of different mechanisms.

To delineate the behaviour of gallium during crystallization, the bulk chemical composition of the intermediate phases, obtained by AAS and ICP techniques and expressed as a Si/Ga and Ga/Na atomic ratios, are presented in Fig. 2.15. Initially (up to 15 h) the Si/Ga ratio is high and the composition of solid phase when separated from the liquid phase was found to be closer to the final crystalline composition[44]. This suggests that the solid phase transformation may be operative during the formation of gallosilicate MFI zeolite. In addition, the Ga/Na atomic ratio is initially low but rapidly increases (Ga/Na = 4) indicating that Na^+ are compensating for about 25 % of the Ga present. However, it indicates that the amount of Na^+ ions occluded into the gallosilicate is lower than the number of negative charges present in the framework. It is more likely that the $TEBA^+$ ions incorporated during the synthesis may also be acting as charge compensating cations on GaO4 tetrahedra and thus contributing to the neutralization of the gallosilicate zeolitic lattice.

2.5.10 Solid state ^{29}Si, ^{71}Ga and ^{27}Al MASNMR spectroscopy : Fig. 2.16 illustrates the solid state ^{27}Al, ^{71}Ga and ^{29}Si MASNMR for the fully crystalline sample in as-synthesized form obtained from system VII. A single peak with a chemical shift of 51.37 ppm was observed indicating tetrahedral[53] coordination of aluminum

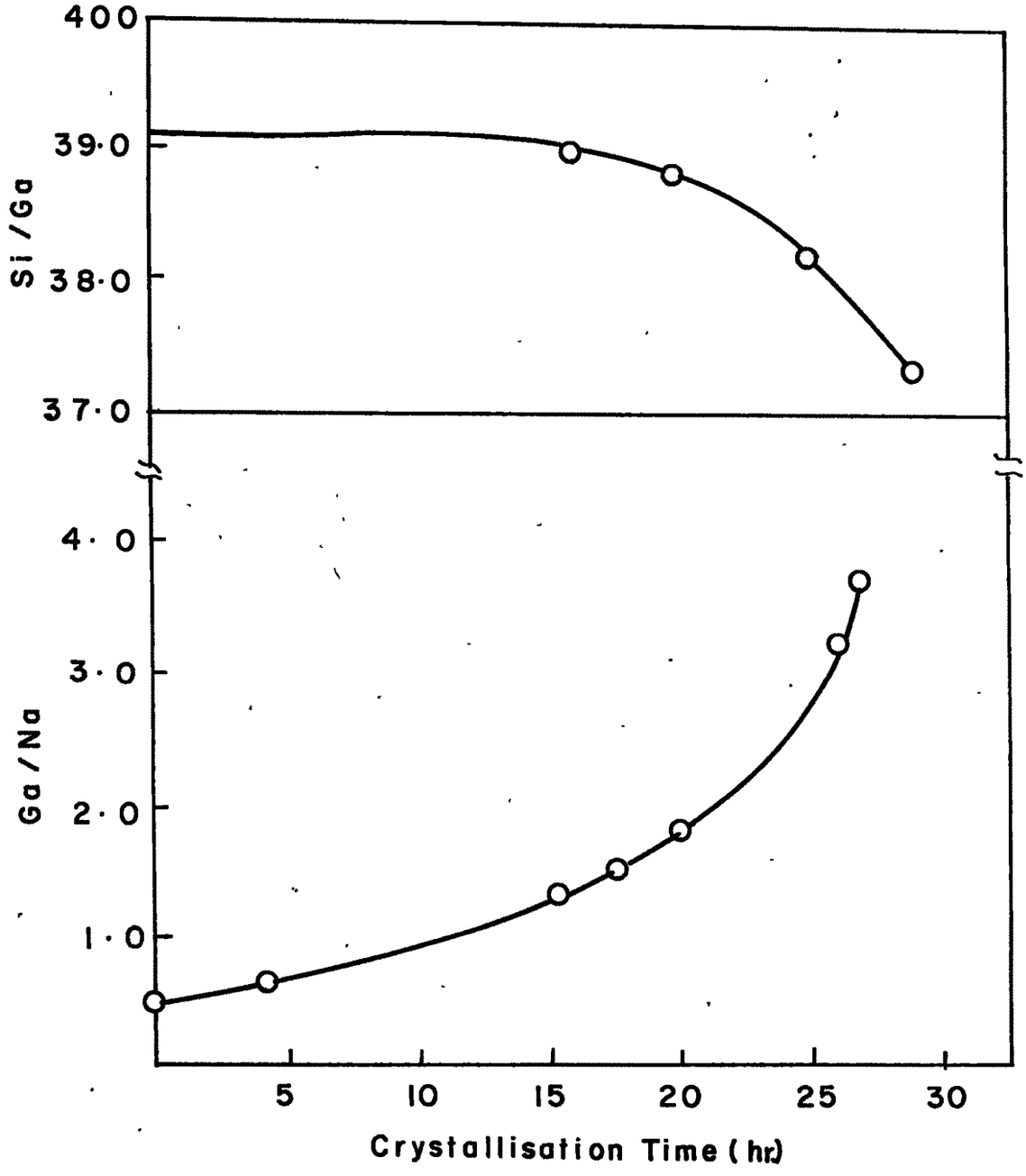

FIG. 2.15 : VARIATION OF Si/Ga AND Ga/Na ATOMIC RATIOS OF THE INTERMEDIATE SOLID PHASES FORMED DURING CRYSTALLIZATION OF GALLOSILICATE (MFI) ZEOLITE OBTAINED FROM SYSTEM II.

in the zeolite and absence of extraframework octahedral[54] aluminum.

For the comparing ^{71}Ga MASNMR spectrum, ^{71}Ga MASNMR spectrum of gallium sulfate in which gallium is known to have an octahedral coordination[55] is also shown. The chemical shift δ = - 87 ppm for gallium atoms in solid $Ga_2(SO_4)_3$ is characteristic of Ga in octahedral sites. The ^{71}Ga MASNMR spectrum for as-synthesized gallosilicate analog containing gallium showed a large chemical shift at δ = 163 ppm for Ga^{+3}. Thus the position of the δ = 163 ppm peak is attributed to Ga^{+3} ions in tetrahedral environments with respect to oxygen in the gallosilicate analog of pentasil zeolite framework[56,57].

^{29}Si MASNMR spectrum shows three signals at -112, -107 and -105 ppm with respect to TMS (tetra methyl silane). These signals can be assigned to Si(0T), Si(1T) and Si(2T) respectively on the basis of the ranges of chemical shifts, characteristics of the different environments proposed by Lippamaa et al[58].

Thus solid state NMR spectra of ^{27}Al, ^{71}Ga and ^{29}Si show the occupancy of Al^{3+} and Ga^{3+} in the tetrahedral positions of aluminogallosilicate of pentasil zeolite.

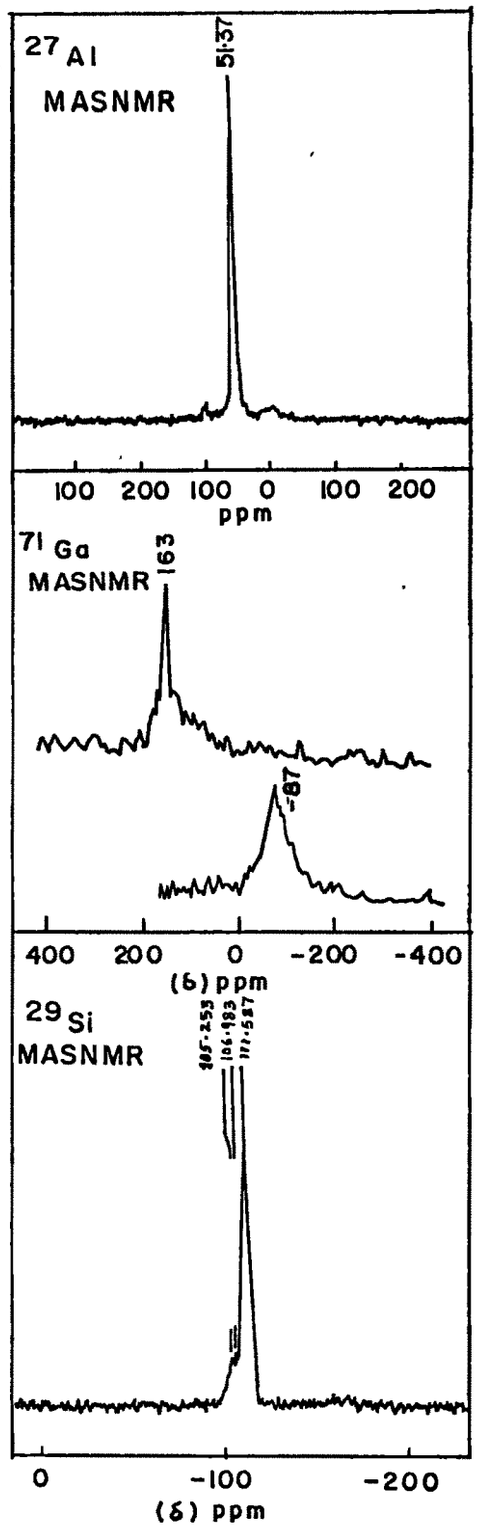

FIG. 2.16 : ^{27}Al, ^{71}Ga AND ^{29}Si MASNMR SPECTRAM OF AS-SYNTHESIZED PENTASIL (MFI) AlGa-ZSM-5(40), OBTAINED FROM SYSTEM VII.

2.6 REFERENCES

1. Barrer, R.M. and White, E.A.D., J. Chem. Soc., 156 (1961).
2. Regis, A.I., Sand, L.B., Calman, C. and Gilwood, M.E., J. Phys. Chem., 64, 1567 (1980).
3. Schwochow, F.E. and Heinze, G.W., Adv. Chem. Ser., 101, 102 (1971).
4. Lok, B.M., Cannan, T.R. and Messina, C.A., Zeolite, 3, 282 (1983).
5. Fyfe, W.S., J. Geol., 61, 553 (1960).
6. Lowe, B.M., Zeolite, 3, 300-305 (1983).
7. Lok, B.M., Cannan, T.R. and Messina, C.A., Zeolites 4, 289 (1984).
8. Erdem, A. and Sand, L.B., J. catal., 60, 241 (1979).
9. Gabelica, Z., Derouane, E.G. and Blom, N., Appl. Catal. 5,109 (1988).
10. Nastro, A. and Sand, L.B., Zeolites, 3, 57 (1983).
11. Chao, N.J., Tasi, T.C., Chen, N.S. and Wang, I.,J. Chem. Soc. Faraday Trans. I, 57, 547 (1981).
12. Jacobs, P.A., Derouane, E.G. and Weitkamp, J., J. Chem. Soc. Faraday Trans. I, 57, 547 (1981).
13. Flanigen, E.M., "Zeolite chemistry and catalysis", J.A.Rabo, Ed. Adv. chem. ser. 171, chap.2 (1976).
14. Jansen,J.C., Van der Gaag, F.J. and Van Bekkum, H., Zeolites, 4 369 (1984).
15. Argauer,R.J. and Landolt, G.R., U.S. Patent 3,702,886 (1972).
16. Deelee, H.J., Hearing, J., Riekert, L. and Marosi, L., J. Catal.,71, 27 (1981).

17. Awate, S.V., Joshi, P.N., Shiralkar, V.P. and Kotasthane, A.N., J. Incl. Phenon. & Mol. Recogn., **13**, 207-218, 1992.

18. Culfaz, A. and Sand, L.B., Adv. chem. ser., **121** 140 (1973).

19. Tsitsishvilli, G.V., Krupenikov, A. Yu., Mamulashvili, M.V. and Urushadze, M.V., Russ. J. phy. chem., **53**, 975 (1979).

20. Joshi, P.N., Rao, G.N., Kotasthane, A.N. and Shiralkar, V.P., J. Incl. Phenom. & Mol. Recogn. in Chem., **9**, 91 (1990).

21. Kotasthane, A.N., Ph.D. Thesis, University of pune (1985).

22. Shiralkar, V.P. and Clearfield,A., Zeolites, **9**, 363 (1989).

23. Kulkarni,S.B., Shiralkar, V.P., Kotasthane, A. N., Borade, R.B. and Ratnasamy, P., Zeolites **2**, 313 (1982).

24. Joshi, P.N., Kotasthane, A.N. and Shiralkar V.P., Zeolites, **10**, 598 (1990).

25. Thompson, R. W. Zeolites, **12**, 680-684 (1992).

26. Ouden C.J.J. den and Thompson R.W., Am. Chem. Soc, Ind. Eng. Chem., **31(1)**, 369-373 (1992).

27. Borade, R.B., "Synthesis and Characterization of ZSM-5 zeolites", Ph.D. Thesis, Pune Univ., July 1983.

28. Borade,R.B., Chandwadkar, A.J., Kulkarni, S.B. and Ratnasamy, P., Ind. J. Technology, **21**,9 358 (1983).

29. (a)Flanignen, E.M., Khatami, H. and Szymanski, H.A., Adv. Chem. Ser., **101**, 201 (1971).

(b)Flanigen, E.M.,"Zeolite chemistry and catalysis," Ed. J.A. Rabo, Adv. Chem.Ser., **173**, 80 (1976).

30. Gamami, M. and Sand, L.B., Zeolite, **3** 155 (1983).

31. Jacobs, P.A., Bayer, H.K. and Valyon, J., Zeolite, **1**, 161-168 (1981).

32. Coudurier, G., Naccache, C. and Vedrine, J.C., J. Chem. Soc., Chem. Comm. 1982, 1413 .

33. Derouane, E.G., Detremmerie, S., Gabelica, Z. and Blom, N., Appl. Catal., 1, 201 (1981).

34. Bremer, H., Morke, W., Schodel, R., Vogt, F., Adv. chem.ser. 121, 249 (1973).

35. Shiralkar, V.P. and Kulkarni, S.B., Z. Phys. Chemie., 265, 313 (1984).

36. Anderson, J.R., Foger, T. Mole, Rajadhyaksha, R.A. and Senders, J.V., J. Catal. 58, 114 (1979).

37. Jacobs, P.A., Derouane, E.G. and Weitkamp, J., J. Chem. Soc. Chem. Communication., 591 (1981).

38. Breck, D.W. and Flanigen, E.M., "Molecular Sieves", Society of chem. Ind. London, 47 (1968).

39. Barrer, R. M., Baynman, J.W., Bultitude, F.W., Meier, W. M., J. Chem. Soc., 195 (1959).

40. Barrer, R.M., " hydrothermal chemistry of zeolites" Academic press, London (1982).

41. Flanigen, E.M., Adv. chem. ser., 121, 119 (1973).

42. Flanigen, E.M. and Breck, E.W., ACS 137th meeting, Cleveland, Ohio, (1960).

43. Myrsky, Ya.V., Mirtofanov, M.G., Dorogochiniski, A.V., `New Adsorbents- Molecular Sieves', Grosnyi, (1964).

44. Zhdanov, S.P., `Molecular Sieves', Soc. Chemical Industry, London, p. 68 (1968).

45. Senderov, E.E., Khitarov, N.E., `Zeolites, Their Synthesis and Conditions of Formation in Nature, Nauka Publishing

House, Moscow, (1970).

46. Zhdanov, S.P., ACs Advances in Chem. Series., **101**, 20 (1971).

47. Rubin, M.K., Plank, C.J. and Rosinski, E.J., Eur. Pat. 3144 (1979) Mobil Oil Corp, USA.

48. Davis, M.E., Saldarriaga, C., Montes, C., Garoes, J. and Crowder, C., Zeolites, **8**, 362, (1988).

49. Breck, D.W., " Zeolite Molecular", John Wiley and Sons, New York, 1974.

50. Barrer, R.M., Zeolites, **1** 130 (1981).

51. Lechert, H., Stud. Surf. Sci. & Catal. **18**, 107 (1984).

52. Mostowich, R. and Sand, L.B., Zeolite, **2**, 143 (1982).

53. Khusid, B.L., Chukin,G.D., Gullyev, Ch. and Nefedov, B.K., Kinetika i Kataliz, **28 (No.4)**, p.938-942 (1986).

54. Szostak, R., "Molecular Sieves", Ed. Van Nostrand Reinhold, New York, p. 338, (1989).

55. Mastikhin, V.M. and Zamaraev, K.I. :Z. Phys. Chem. Neue Folge **152**, 59 (1987).

56. Akitt, J.W. Annu. Rep. NMR spectroscopy 5A, 465 (1972).

57. Thomas, J.M., Klinowsky, J., Ramadas, S., Anderson, M.W., Fyfe, C.A. and Gobbi, G.C.: Intrazeolite Chemistry, ACS Symp. Series, ACS Washington DC, **218**, 159 (1983).

58. Lippmaa, E., Magi, M., Samoson, A., Tarmak, M., Engelhardt, G., J. Am. Chem. Soc. **103**, 4992 (1981).

****

Chapter 3

PHYSICO-CHEMICAL CHARACTERIZATION OF MFI TYPE ZEOLITES

****

CONTENTS

3.1 INTRODUCTION

This chapter deals with the detailed characterization of gallosilicate with MFI type structure. Evidence for the incorporation of Ga^{3+} in the silicate framework has been obtained using XRD, IR, ^{29}Si, MAS NMR, sorption kinetics and equilibrium sorption capacities of different probe molecules like water, n-hexane, cyclohexane, n-butyl amine (nBA), tributylamine (TBA) and xylene isomers etc.

3.2 EXPERIMENTAL

3.2.1 Heat treatment : Na/ZSM-5 samples are heated in an air at different temperatures ranging from 873 to 1393 K over a period upto 24 h. After the heat treatment zeolites were cooled to room temperature and were moisture-equilibrated by keeping them over saturated solutions of ammonium chloride for 24 h in a desiccator.

3.2.2 Preparation of protonated (H^+) gallosilicate with MFI type structure : As-synthesized Ga-ZSM-5 zeolite contain occluded quaternary ammonium cationic species and is designated as C/N Ga-ZSM-5. These organic cations occupying the channels in the zeolite crystals are removed by slow heating of the sample in the muffle furnace at 823 K for overnight. The catalyst is cooled to room temperature and moisture equilibrated by keeping it over saturated ammonium chloride solution for a week. This sample is designated as Na/Ga-ZSM-5.

The Na/Ga-ZSM-5 catalyst is refluxed with 5M ammonium nitrate at solid to liquid ratio 10 for overnight, then it is filtered, washed with hot water and dried at 373 K overnight. To obtain

the samples with higher degree of exchanges, the procedure was repeated for number of times. This catalyst is designated as NH_4/Ga-ZSM-5.

The acidic or protonated forms (HGa-ZSM-5) were obtained by air deammoniation of NH_4/Ga-ZSM-5 samples at 673 K for 6 hrs. Then the samples were cooled to room temperature and is kept over saturated ammonium chloride for a week.

3.2.3 X-ray diffraction (XRD): The X-ray diffraction patterns were recorded to ascertain the purity of the samples on **Philips PW 1730** X-ray diffractometer using nickel filtered Cu-K_α radiation (λ = 1.5404 Å). To calculate the unit cell parameters of Na/Ga-ZSM-5 and silicalite sample, the spectra were recorded at scanning rate of 0.2° (2θ), min^{-1} using extra pure silicon powder as an internal standard .

3.2.4 Thermal Analysis : The thermograms of the samples were recorded on an automatic Hungarian derivatograph (**MOM 102-Budapest**) under the following conditions.

Sample weight	:	100 mg
Rate of heating	:	10 K min^{-1}
Atmosphere	:	Flowing air
Sensitivity	:	DTA 1/1
		DTG 1/5
		TG 100

Precalcined and finely powdered α - alumina was used as a reference sample.

3.2.5. Nitrogen adsorption : Surface area measurements were carried out by low temperature (78 K) nitrogen sorption using a

conventional all glass BET unit as shown in Fig. 3.1. It consists of three burettes B_1, B_2 and B_3 (B_3 is not shown in figure), a manometer M and a sample bulb S. High vacuum system consisting of a two stage rotary pump, mercury diffusion pump, Mcleod gauge and a series of cold traps were used for degassing the sample.

The volume of the burette bulbs were precalibrated with mercury before joining to the adsorption system. The burettes B_1 and B_2 were immersed in water jackets, provided with thermowell for temperature measurements. The dead space volume in the system was determined by using spectrally pure Helium supplied by British Oxygen Co. (UK). About 0.2 to 0.3 gm of hydrated sample weighed in the sample bulb was activated by increasing temperature slowly under continuous pumping. The sample was activated at 673 K by evacuation to about 10^{-6} Torr for a period of 6 hrs. The sample was cooled and dead space volume was determined by using Helium at liquid nitrogen temperature. After pumping the helium gas, a dose of nitrogen was admitted and calibrated. The sample was exposed to Nitrogen gas at 78 K. The adsorption measurements were continued by admitting consequent calibrated doses, till a sufficient number of points were obtained. The reversibility was checked by carrying desorption measurements. The volume of a gas adsorbed at STP was estimated as follows,

$$V_{ads} = V_1 - V_2 - V_3 \ (1 + \alpha(P/760)) \qquad (1)$$

Where V_1, V_2, V_3 are volume of gas taken, remaining in the system and in the bulb respectively. The α is the correction for non-

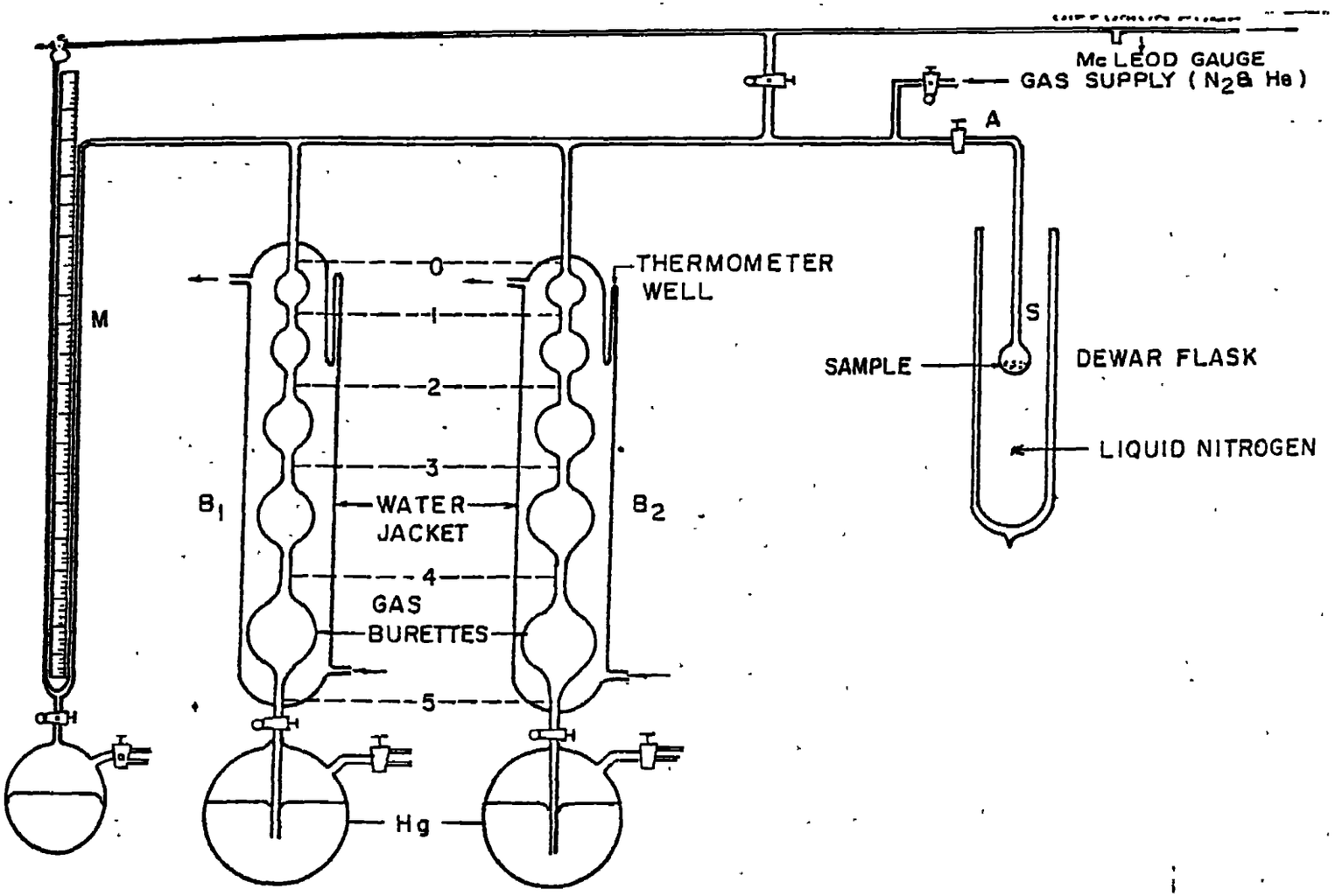

FIG.3.1. GAS ADSORPTION UNIT FOR THE MEASUREMENTS OF BET SURFACE AREA.

ideality of nitrogen at 78 K. The applicability of the Langmuir or BET isotherms equations for the estimation of surface area was checked by using the following relations,

$$\frac{P}{P_oV} = \frac{1}{b.V_m} + \frac{P}{V_m.P_o} \qquad (2)$$

$$\frac{P}{V_{ads}\,(P_o-P)} = \frac{1}{V_m\,C} + \frac{C-1}{V_m.C} \times \frac{P}{P_o} \qquad (3)$$

Where $C = e^{(E-E_o)/RT}$ is constant and depends on the sorbate sorbent system, V_m is the monolayer volume, P_o is the saturation vapor pressure of nitrogen at 78 K, P is the equilibrium pressure and b is the constant.

The void volume of the zeolite sample was determined from the Dubinin plots log (a) V_s $(\log P_s/P)^2$.

The equation used was,

$$\log a = C - D\,(\log P_s/P)^2 \qquad (4)$$

Where C and D are constants[1], P is equilibrium pressure and P_s is the saturation pressure.

3.2.6 Sorption and diffusion studies : The equilibrium sorption capacities of alumino- and gallosilicates (MFI) at $P/P_o = 0.8$ at 298 K were measured on an all glass gravimetric apparatus using McBain Baker type silica spring (sensitivity 50 cm/g) balance as described in chapter II, section 2.4.5. nBA sorption isotherms in the temperature range 323 - 523 K were measured up to 100 Torr of pressure on the all glass gravimetric apparatus as described

earlier. About 70 mg of sample in a pellet form was degassed under vacuum (10^{-6} Torr) at 673 K following the procedure reported[2] by Shiralkar et al. After degassing to a constant weight, the balance case containing the sample was maintained at the isotherm temperature for at least 2 h before the commencement of the measurement. The sorbate pressure was measured with a cathetometer, and the amount sorbed was measured accurately from the change in the weight of the sample after equilibrating for 2 h at each equilibrium pressure. The sorption isotherm was obtained by a progressive increase in the sorbate vapor pressure and by noting the amount sorbed. The sorption isotherms were obtained sequentially from lower temperature (323 K) to higher temperature (523 K) after following the same degassing procedure prior to the sorption measurement. In order to check the reversibility of the sorption, desorption measurements were carried out. The X-ray diffractograms were also recorded for each sample before and after the sorption measurements to check the structural stability.

3.2.7 Infra red (IR) spectroscopy : The framework IR spectra of the samples of interest were recorded in the frequency range of 200-1300 cm^{-1} using nujol mull technique on **PYE UNICAM SP-300** spectrophotometer. Also FTIR spectra of samples with/without pyridine sorption in the hydroxyl stretching vibration region 3000-4000 cm^{-1} and in the region of 1700 to 1400 cm^{-1} was recorded on **Nicolet 60 SXB U.S.A FTIR** spectrophotometer following the procedure as described below.

The powder sample was pressed (5 ton/$inch^2$) into self

supporting wafers (5-12 mg/cm^2) introduced into a conventional all silica in-situ transmittance FTIR cell which was connected to an evacuation gas manipulation manifold (Micromeritics-Accusorb 2000 B). The sample was activated at 673 K for 4h in vacuum (10^{-6} Torr) and cooled to 323 K. Pyridine vapor (5 Torr) was then introduced and equilibrated for 1 hr. and then evacuated at 373 K and cooled down to 323 K before recording the spectrum (2 cm^{-1} resolution, 100 scans). Again sample was evacuated at 423 K and the spectra were recorded after cooling it to 323 K.

FTIR spectra of gallosilicate (MFI) samples heated at different temperatures were also scanned on Perkin-Elmer 1600 FTIR in the frequency range 400-1400 cm^{-1}

3.2.8 X-ray photoelectron spectroscopy (XPS) : X-ray photoelectron spectroscopy studies were carried out in a V.G. Scientific ESCA-3-MK-2 electron spectrometer with an AlK_{α} X-ray source (non-monochromatic). For the present measurements the anode was operated at 140 W (14kV, 10mA) and the analyzer was operated at a constant pass energy of 50 eV. The residual gas pressure in the spectrometer chamber during data acquisition was less than 10^{-7} Torr. All the spectra were recorded with similar spectrometric parameters. The binding energy (B.E) scale was calibrated by determining the B.E. of $Au4f_{7/2}$ (84 eV), $Ag3d_{3/2}$ (368.4 eV) and $Cu2p_{3/2}$ (932.4 eV) levels using spectroscopically pure metals from Johnson-Matthey, London. A binding energy 285 eV for C1s level was used as an internal standard for all the samples. The B.E. values (measured to an accuracy of 0.2 eV) are in good agreement with literature values[3]. The resolution in

terms of the full width at half maximum (FWHM) of the $Au4f_{7/2}$ level is 1.6 eV.

3.2.9 ^{29}Si MASNMR : ^{29}Si MASNMR spectra were recorded on a Bruker-MSL-300 spectrometer for silicalite, gallosilicate (MFI) samples with different SiO_2/Ga_2O_3 ratio and gallosilicate (MFI) samples heated at different temperatures. Chemical shifts were calibrated using tetramethylsilane (TMS) as a reference material with 0.3S as a relaxation time. The data were recorded over 3000 cycles.

3.3 RESULTS AND DISCUSSION

The unit cell compositions of gallosilicate and aluminosilicate analogs of pentasil (MFI) structure are determined by chemical analysis (Chapter II, Section 2.4.6) and tabulated in Table 3.1.

3.3.1 X-ray diffraction : The X-ray diffraction patterns of gallosilicate catalyst obtained from system II in C/N, Na, NH_4 and H forms are shown in Fig. 3.2. The XRD patterns and 'd' values for these samples were found to be in good agreement with reported data[4].

The most intense peak was observed at 2θ = 23.08° in C/N Ga-ZSM-5 form. The intensity of the peaks at 7.8° and 8.0° were found to be affected by the nature and concentration of nonframework cationic species. When C/N form was modified to Na form, the intensity of the peaks at 7.8° and 8.0° were found to increase due to removal of the bulkier organic cations situated in intracrystalline voids[5]. Further modification to NH_4 and H form, the intensity of these peaks was found to decrease and

Table 3.1

Unit cell compositions of MFI zeolites.

System	SiO_2/M_2O_3*	Unit cell composition
I	40	$H_{4.50}Na_{0.03}[(GaO_2)_{4.53}(SiO2)_{91.47}]$
II	97	$H_{1.86}Na_{0.08}[(GaO_2)_{1.94}(SiO_2)_{93.86}]$
III	289	$H_{0.65}Na_{0.01}[(GaO_2)_{0.66}(SiO_2)_{95.35}]$
IV	85	$H_{2.12}Na_{0.08}[(AlO_2)_{2.20}(SiO_2)_{93.80}]$
V	36	$H_{4.95}Na_{0.07}[(AlO_2)_{5.02}(SiO_2)_{90.98}]$
VI	80	$H_{2.27}Na_{0.08}[(FeO_2)_{2.35}(SiO_2)_{93.60}]$
VII	40	$H_{4.50}Na_{0.02}[(GaO_{22.26}(AlO_2)_{2.26}(SiO_2)_{91.48}]$
VIII	> 3000	$Si_{96}O_{192}$
IX	-	3.83% $Ga_2O_3\{Si_{96}O_{192}\}$
X	-	2% $Ga_2O_3\{H_{2.12}Na_{0.08}[(AlO_2)_{2.20}(SiO_2)_{93.80}]\}$

* M = framework Al or Ga

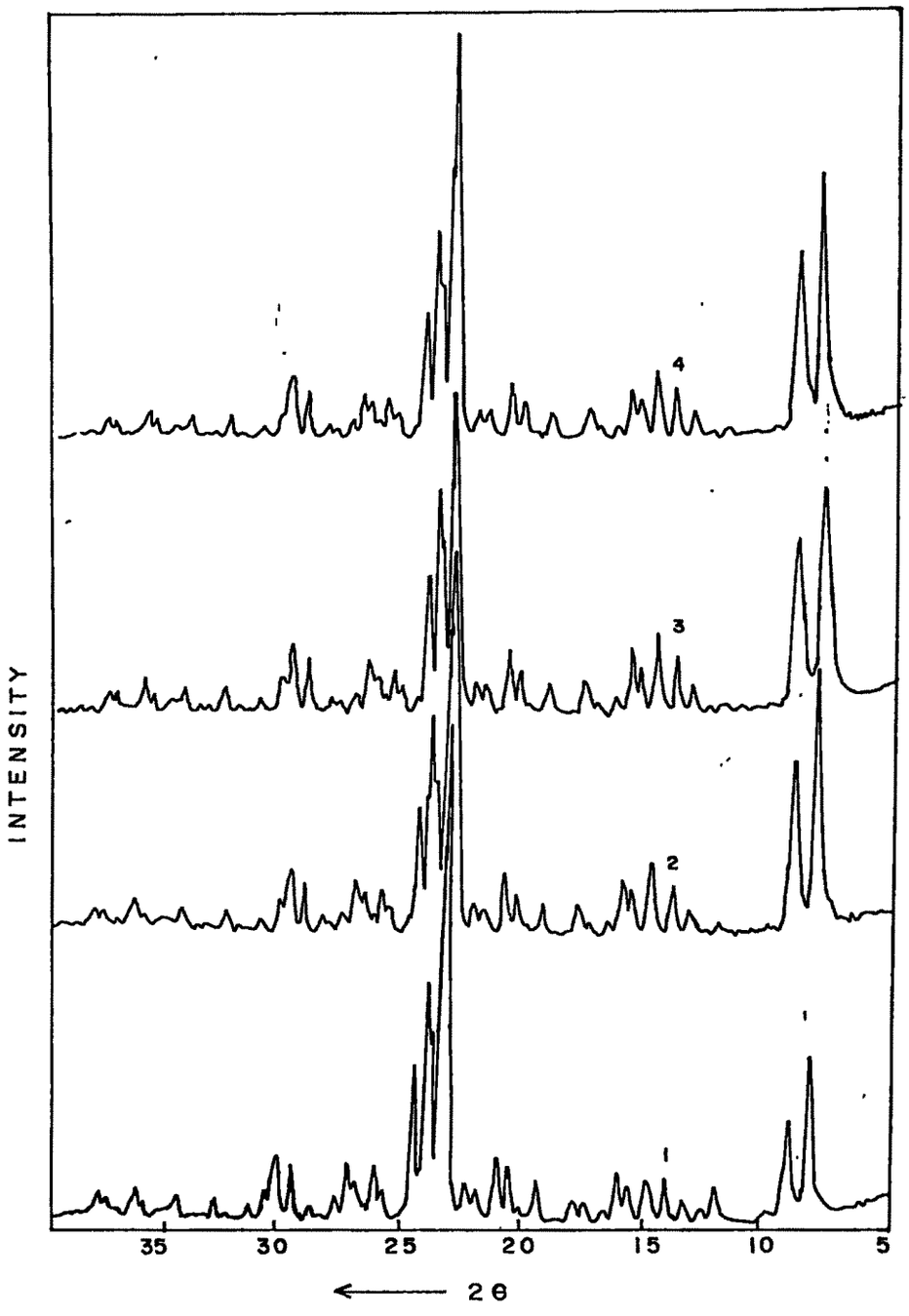

FIG.3.2 : X-RAY DIFFRACTION PROFILES OF PENTASIL (MFI) GALLOSILICATE 1) AS-SYNTHESIZED (C/N), 2) Na–, 3) NH_4– AND 4) H-FORM.

increase respectively on account of their cationic charge and size.

Fig. 3.3 illustrates the XRD profiles of Al-ZSM-5 and its partial and total substituted Ga- analogs and 2% Ga_2O_3 impregnated HAl-ZSM-5. It is clearly demonstrated, that the peak positions and their relative intensities remains unaltered by impregnation of 2% Ga_2O_3 on Al-ZSM-5. But framework substitution was found to affect the interplaner spacings (d Å). It was observed that the extent of shift in the interplaner spacings is dependent on the degree of isomorphous substitution. Total framework substituted Ga-ZSM-5 (curve c) sample showed the maximum shift in interplaner spacings (d Å). This can be explained on the basis of the extent of lattice expansion taken place due to different degree of substitution by larger gallium ion in the tetrahedral framework of the zeolite.

The replacement of Al^{3+} by the larger ions like Ga^{3+}, Fe^{3+} etc. in the tetrahedral zeolite framework causes a slight increase in unit cell parameters and hence increase in the volume[6,7]. Insertion of gallium ions in the faujasite framework causes an unit cell expansion was also reported[8]. As seen in Fig. 3.4, the unit cell volume expands linearly with decreasing SiO_2/Ga_2O_3 ratio indicating successful insertion of larger Ga^{3+} ions during the hydrothermal synthesis. Simmons et al[9]. also observed a similar trend while confirming Ga^{3+} framework incorporation in pentasil (MFI) gallosilicate.

Fig. 3.5 represents the correlation observed between the 'd' spacings difference between two peaks at 2θ, 45.1 and 45.5° and

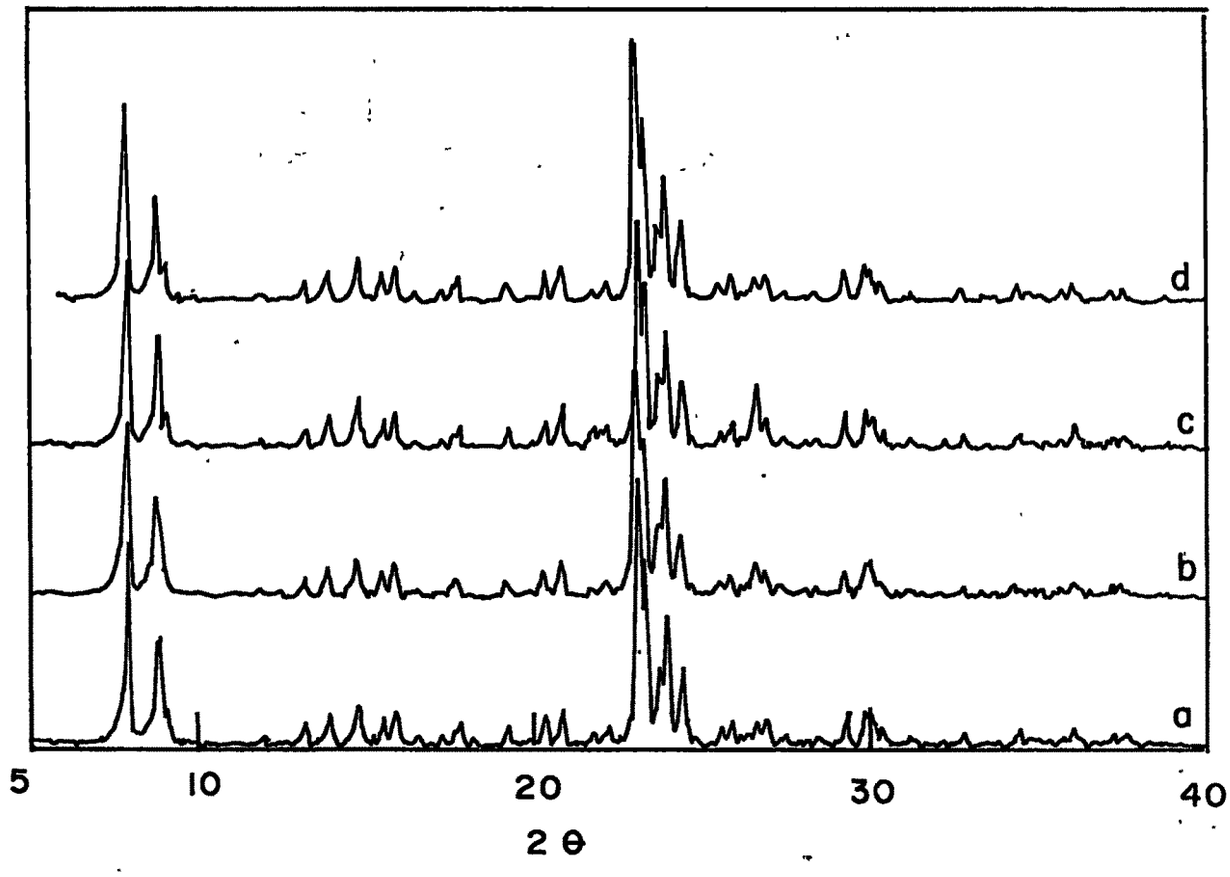

FIG.3.3: X-RAY DIFFRACTION PROFILES OF DIFFERENT PENTASIL (MFI) ZEOLITES a) HAL-ZSM-5(85); b) HAlGa-ZSM-5(40), c) HGa-ZSM-5(97) AND d) 2% Ga_2O_3 IMPREGNATED HAl,-ZSM-5.

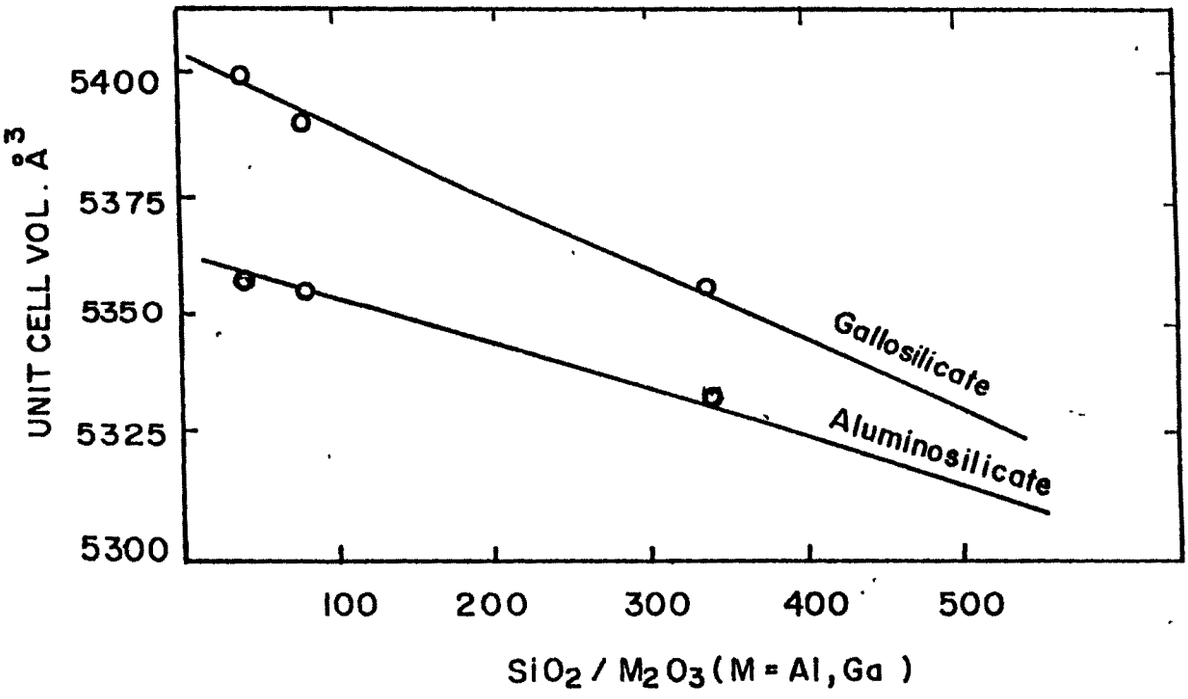

FIG. 3.4 : RELATIONSHIP BETWEEN UNIT CELL VOLUMES OF PENTASIL (MFI) ALUMINO AND GALLOSILICATES.

SiO_2/Ga_2O_3 ratio. The linear plot is yielded which suggests the linear dependence of the splitting of the peaks at 45.1° and 45.5° on the framework gallium content. Thus Fig. 3.5 can be served as a calibration curve to find out the framework gallium content in the test sample if splitting of the peaks at 45.1° and 45.5° is known.

Fig. 3.6 shows the influence of calcination temperature (range 873 - 1393 K) on the structural changes of Ga-ZSM-5(97) studied with the aid of powder X-ray diffraction technique. The parent sample calcined at 873 K for the period of 2 hrs does not show any change in XRD pattern as well as the peak intensities. The area under the XRD peaks between 2θ = 23°-25° of this sample was arbitrarily expressed as 100 and the relative drop in the crystallinity was evaluated as a function of calcination temperature. The parent sample was calcined for 2 hrs at different temperatures in the temperature range 873 - 1393 K and it was observed that the transformation to cristoballite occurs at the cost of gallosilicate from 1213 K onwards. The area under the XRD peaks 2θ = 21.8° and 23.0° of the sample without any ZSM-5 impurity was arbitrarily chosen as 100% and the contribution due to cristoballite was evaluated in the mixture. Fig. 3.7A illustrates the influence of calcination temperature on the extent of transformation. It can be seen from the figure that the increase in % cristoballite content shows `S' shaped relation to the calcination temperature. Fig. 3.7A also demonstrates the highest rate of transformation of ZSM-5 to cristoballite phase in the temperature range 1273 - 1298 K. At constant temperature, the

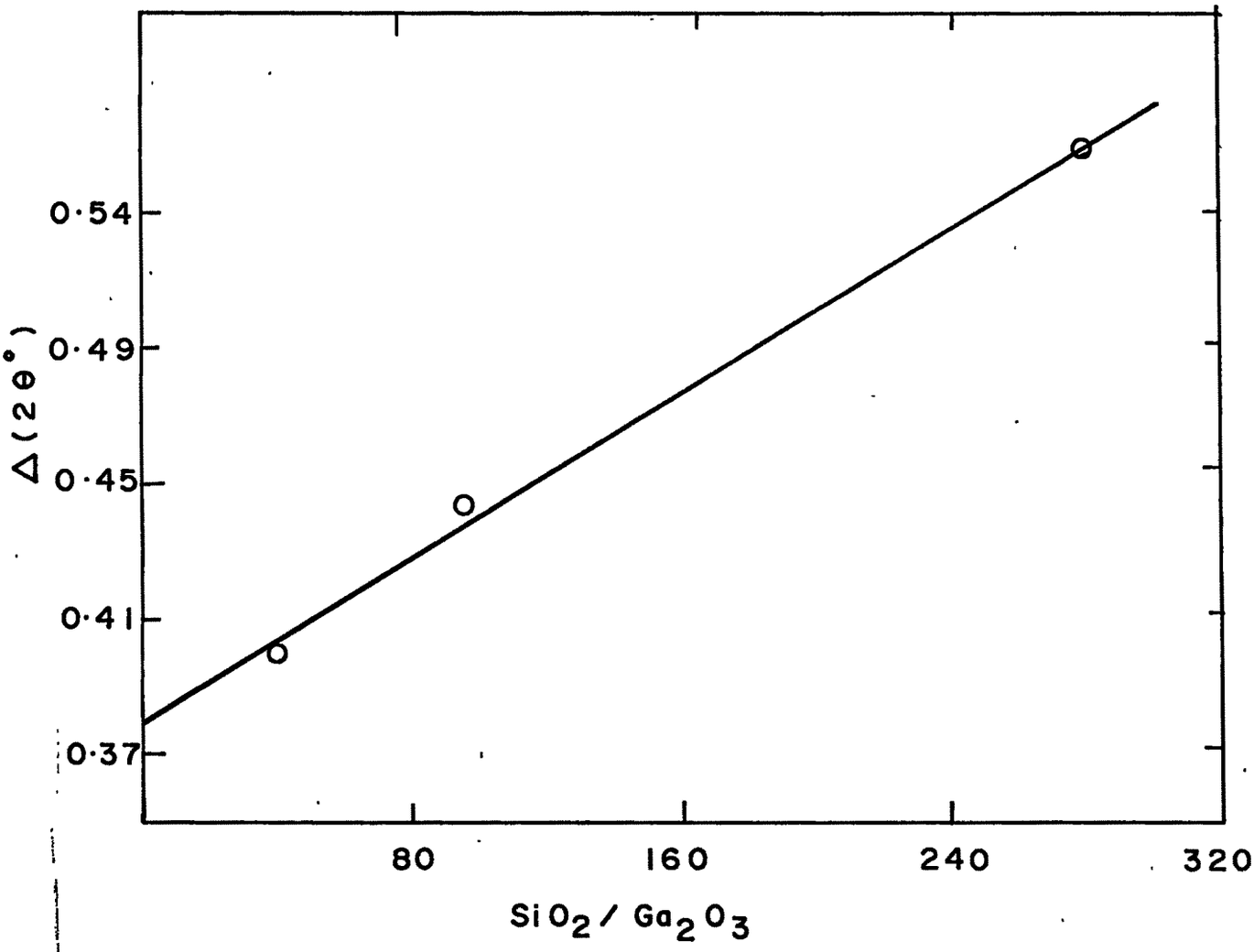

FIG. 3.5: INFLUENCE OF SiO_2/Ga_2O_3 RATIO ON SPACING 'Δ' BETWEEN THE PEAKS AT 45·0° AND 45.4°, 2θ IN XRD PATTERN.

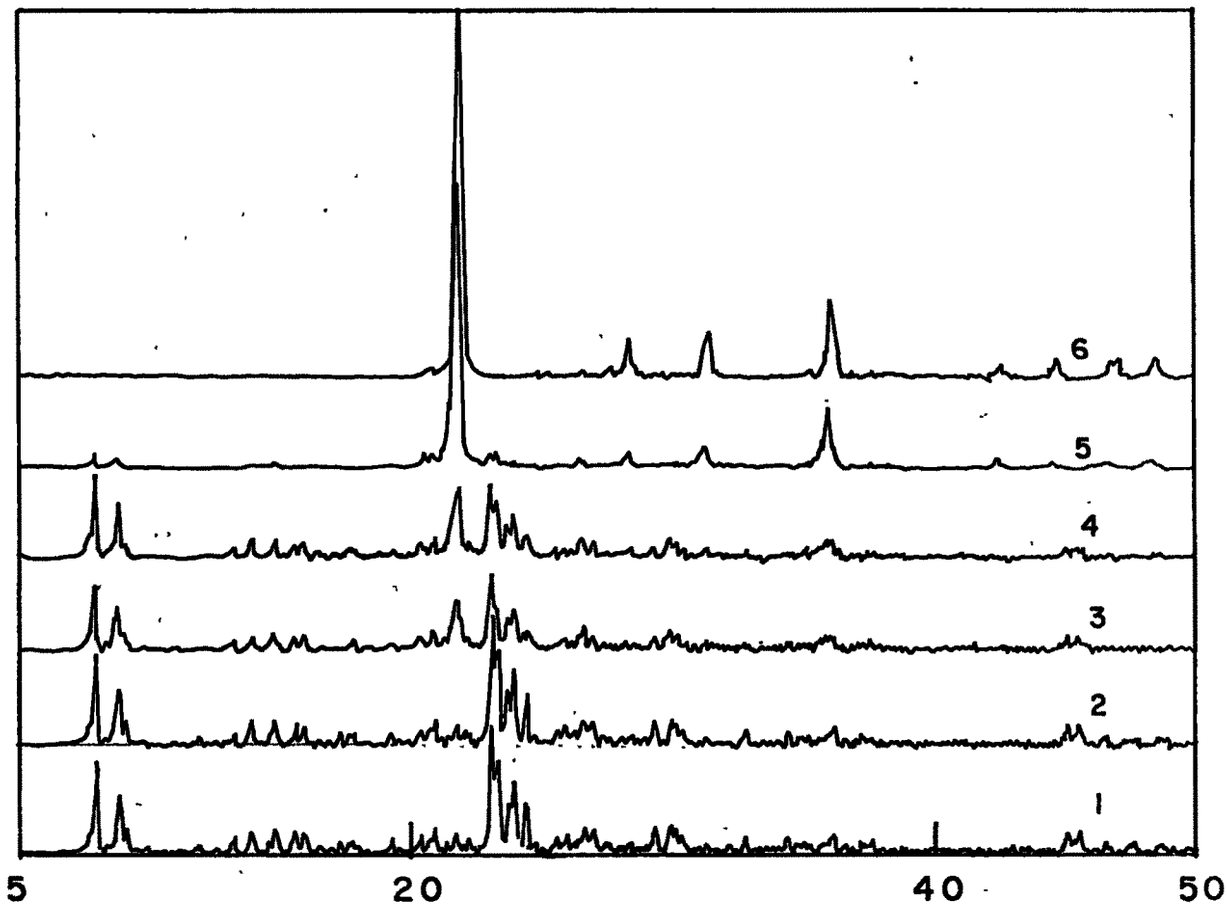

FIG.3.6: INFLUENCE OF CALCINATION TEMPERATURE ON THE XRD PROFILES AT 1) 873 K 2) 1213 K, 3) 1248 K, 4) 1273 K, 5) 1298 K AND 6) 1393 K FOR PENTASIL (MFI) GALLOSILICATE OBTAINED FROM SYSTEM II.

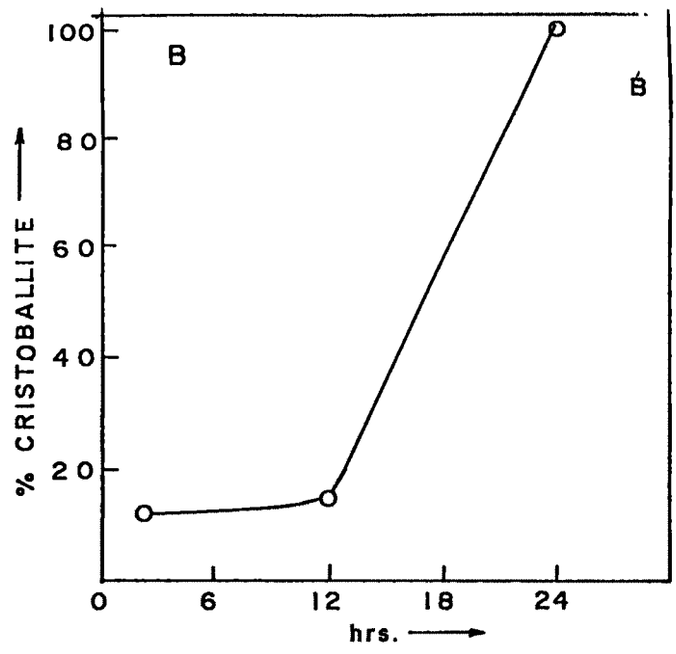

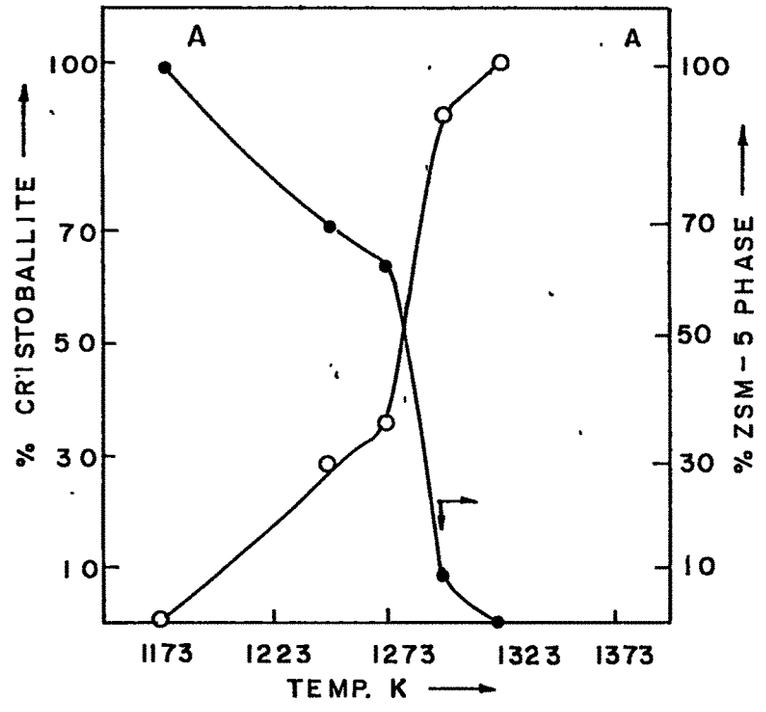

FIG. 3.7: (A) INFLUENCE OF CALCINATION TEMPERATURE ON THE CRYSTALLINITY OF PENTASIL (MFI) GALLOSILICATE OBTAINED FROM SYSTEM II (B) INFLUENCE OF CALCINATION PERIOD ON THE CRYSTALLINITY OF PENTASIL (MFI) GALLOSILICATE OBTAINED FROM SYSTEM II AT 1248 K.

calcination period plays an important role in the phase transformation. Fig. 3.7B shows the transformation of Ga-ZSM-5 into cristoballite as a function of the period of heat treatment at 1248 K. It is seen from the figure that the contribution of cristoballite increases with the calcination period and after 24 hrs at 1248 K, the product is only cristoballite.

Framework cations were also found to influence the thermal stability of the catalyst. Fig. 3.8 shows the XRD profiles of Ga- and Al- analogs of pentasil (MFI) structure (with almost identical silicon/framework cation ratio) calcined at 1073 and 1298 K for 2 hrs. Upto 1298 K, no marked structural changes are exhibited by the Al- analog while Ga- analogs showed the transformation of MFI phase to cristoballite in the temperature range 1073 - 1298 K.

3.3.2 Thermal Analysis : Fig. 3.9 shows DTA/TG curves of as-synthesized (C/N), sodium (Na), ammonium (NH_4) and hydrogen (H) forms of Ga-ZSM-5 obtained from the system II. The structural collapse of the zeolite crystal is accompanied by liberation of heat. So the position of this exotherm peak is considered as measure of the thermal stability. All forms of pentasil (MFI) gallosilicates as depicted in Fig. 3.9 show exothermic effect at 1253 K. An endothermic effect due to dehydration of physisorbed water was observed in the temperature range 300-453 K. In addition to this endotherm, an exothermic effect due to decomposition of organic template was observed in the temperature range 553 - 773 K in as-synthesized (C/N) form. The deammoniation in NH_4 form commenced at 553 K and was found to complete at

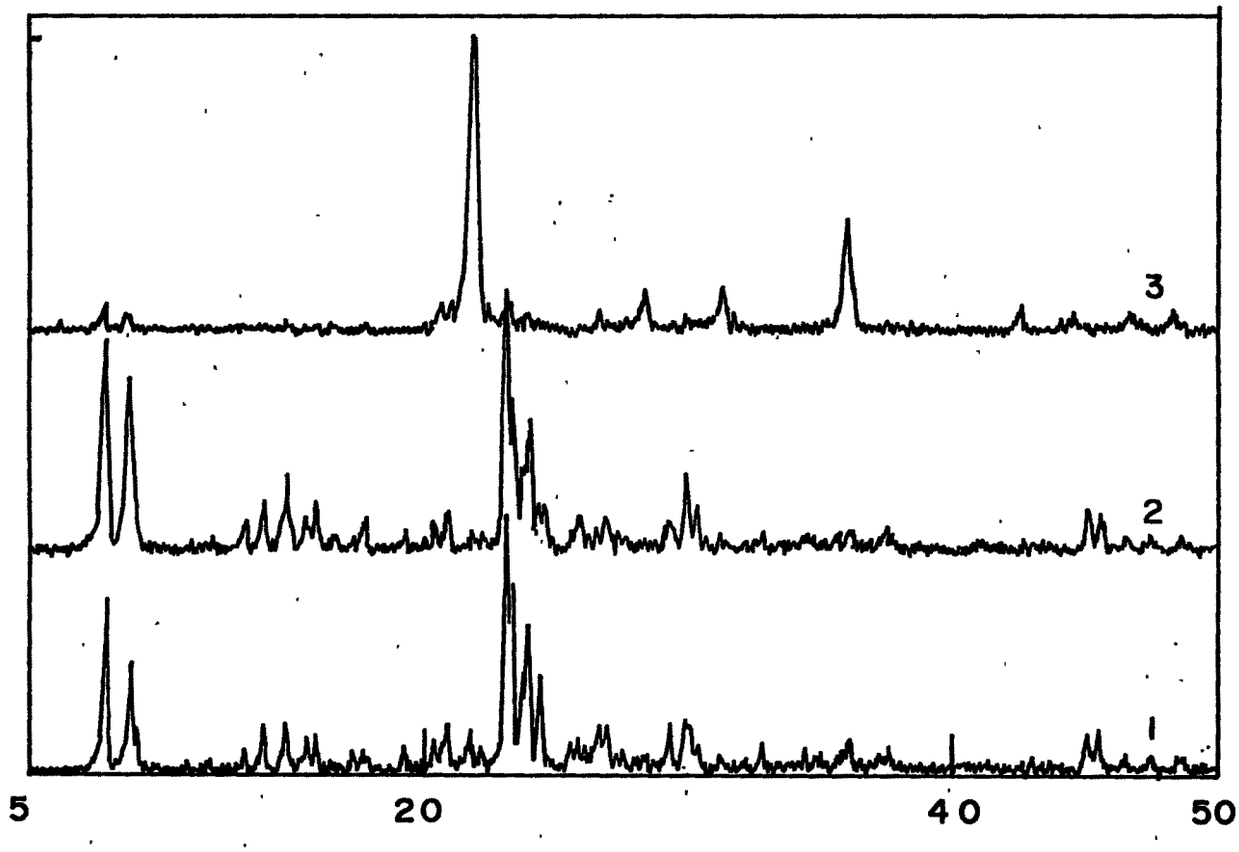

FIG. 3.8 : XRD PROFILES OF (1) HGa-ZSM-5(97) HEATED AT 1073 K, (2) HAl-ZSM-5(85) HEATED AT 1298 K AND (3) HGa-ZSM-5(97) HEATED AT 1298 K.

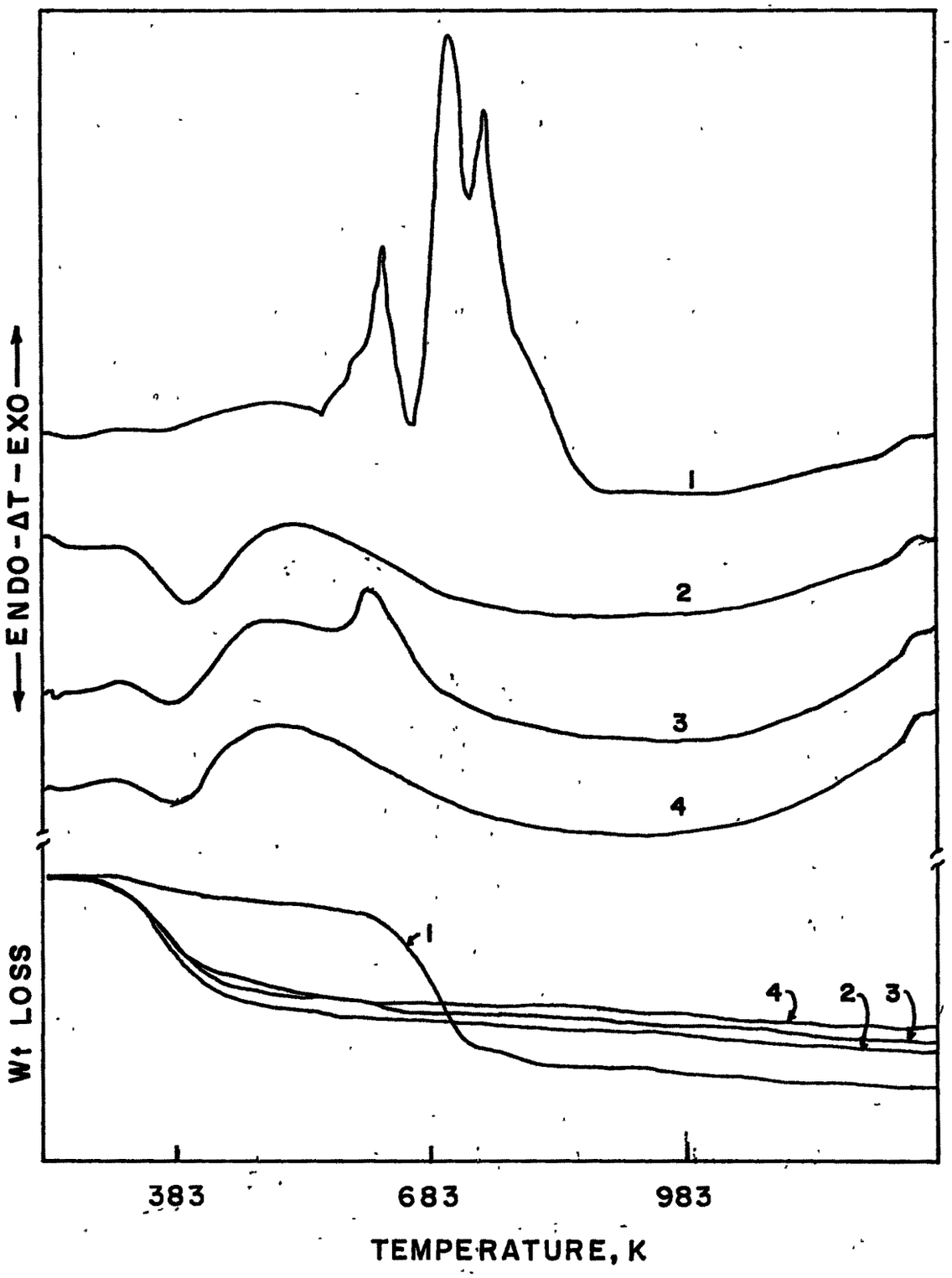

FIG. 3.9: DTA AND TG CURVES OF Ga-ZSM-5 ZEOLITES 1,2,3 AND 4 REFER TO C/N, Na, NH_4 AND H FORMS OF Ga-ZSM-5 RESPECTIVELY.

773 K. The template or NH_3 removal followed after decomposition and dehydration of physisorbed water was confirmed by two stepped weight loss in TG as well as DTA curves. The area under the endotherm of the different forms follows the increasing trend as NH_4 < H < Na. This can be inversely related to their rehydration capacity.

3.3.3 Nitrogen Adsorption : Fig. 3.10 shows the nitrogen adsorption isotherms for samples obtained from system II with varying crystallinity (as determined from XRD) and fully crystalline sample (100%) obtained from system I, III and V. For highly crystalline samples a very rapid uptake at low relative pressure followed by a nearly flat region at increased relative pressure was observed, while zeolites with lower degree of crystallinity show slow uptake with increase of relative pressure. Thus the isotherms exhibit different behaviour for the samples having different crystallinity. Fig. 3.11A shows a plot of amount of nitrogen sorbed at P/P_o = 0.5 with XRD crystallinity data. It is seen that with increase in the crystallinity there is also an increase in the number of N_2 molecules sorbed per unit cell. Fig 3.11B depicts the N_2 sorption at P/P_o = 0.5 as a function of Ga content. Although there is no linear increase in N_2 molecules/u.c., a systematic increase is found with the increase in Ga content/u.c. The crystallinity and the Ga content of the sample were found to influence the nitrogen sorption due to a change in surface area and void volume accessible for N_2. The values of surface areas obtained by BET and Langmuir plots and void volumes from Dubinin plots are tabulated in Table 3.2.

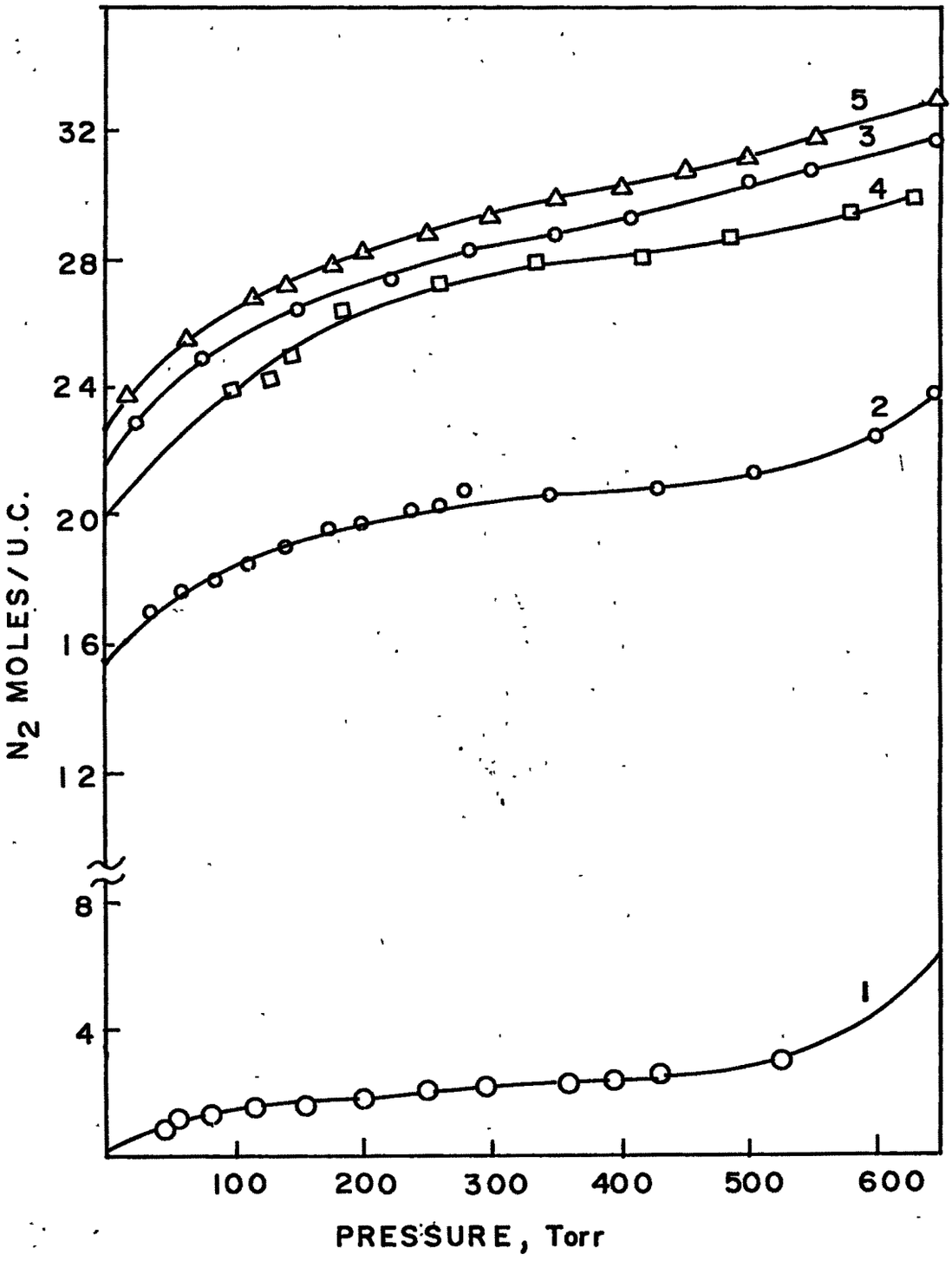

FIG.3.10: NITROGEN ADSORPTION ISOTHERMS FOR (1) 0%, (2) 46%, (3) 100% CRYSTALLINE SAMPLES OBTAINED FROM SYSTEM II AND (4) 100%, (5) 100% FROM SYSTEMS I AND III RESPECTIVELY.

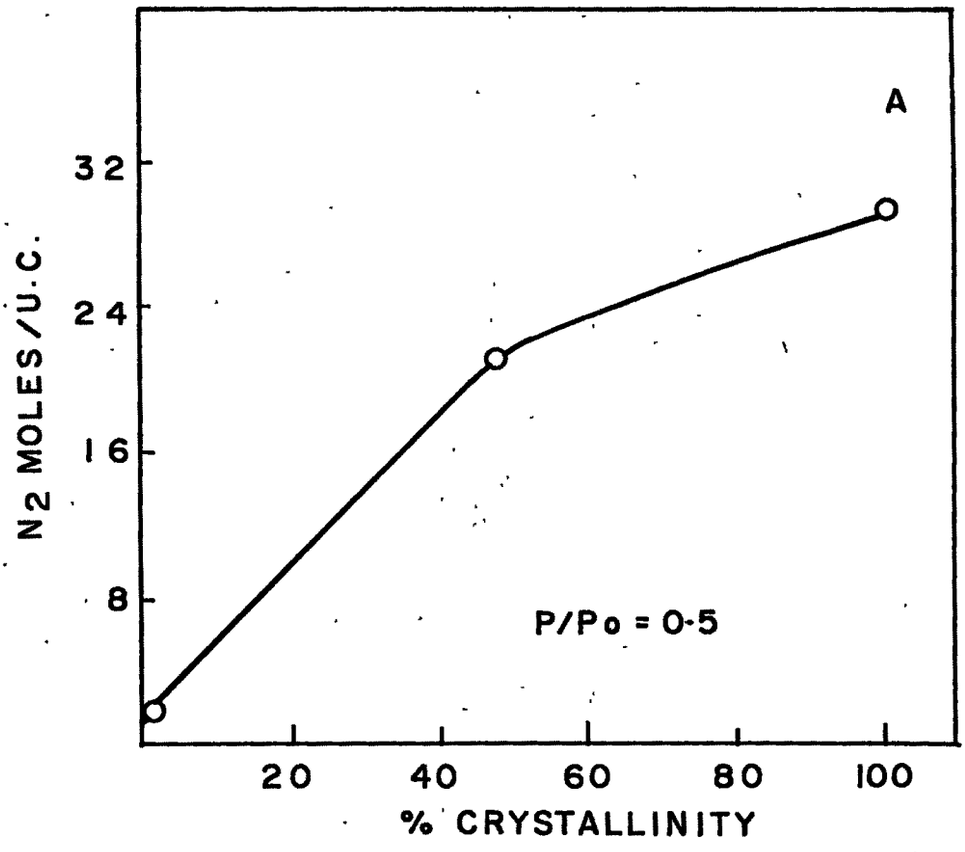

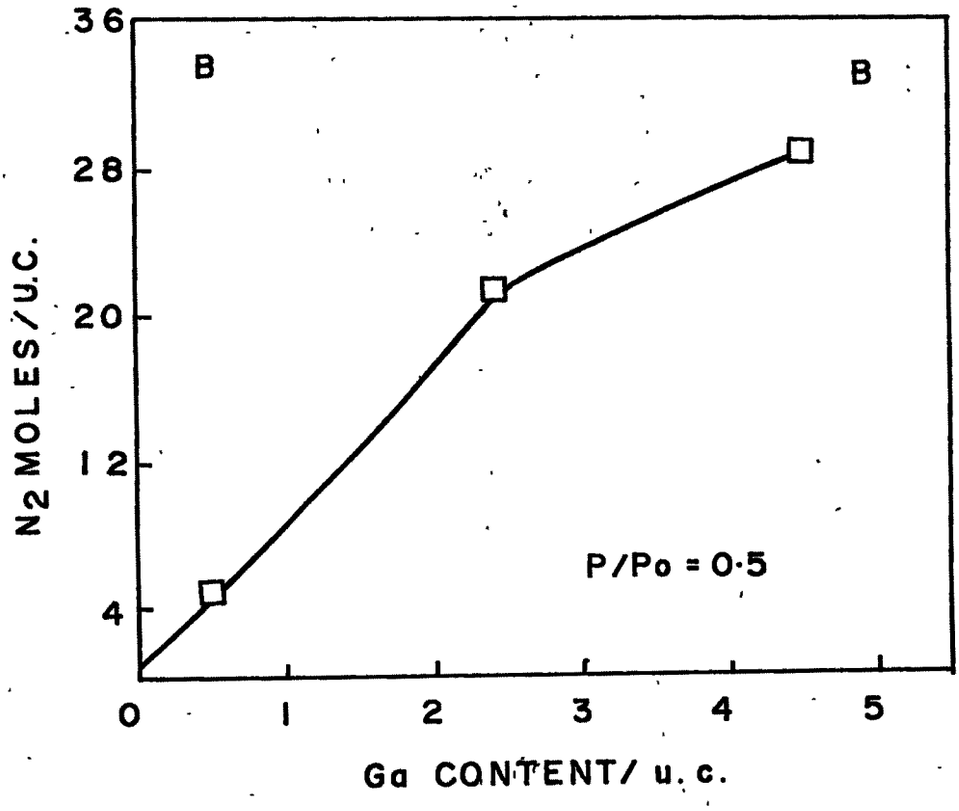

FIG.3.11: CORRELATION BETWEEN (A) XRD CRYSTALLINITY AND NITROGEN SORPTION AT P/Po=0·5 AND (B) NITROGEN SORPTION AT P/Po = 0·5 AND Ga CONTENT/u.c.

The specific surface areas obtained from nitrogen sorption data by applying Langmuir approach are found to be rather higher than those obtained by applying the conventional BET approach. Since Langmuir plots were linear over a wide range of relative pressures (P/P_o = 0.8) compared to the BET plots (linear up to only 0.15 relative pressure), the specific surface areas obtained by the Langmuir approach probably represent a more realistic estimate[10,11]. The specific surface area is rather lower for HGa-ZSM(40) (470 m^2 g^{-1}) than that of HAl-ZSM-5(36) (490 m^2 g^{-1}) and this is consistent with the slightly higher crystallite size (2 μm) and unit cell volume of the former. In fact isomorphous replacement of Al by Ga in the MFI structures has shown[12] a marginal increase in the unit cell volume. However, larger Ga^{3+} species themselves may be responsible for some reduction in the effective void volume. Table 3.2 also shows the void volume of these zeolites obtained from nitrogen sorption by Dubinin-Radushkevich equation[1]. As discussed above, the void

Table 3.2

Characterization of HAl-ZSM-5 and HGa-ZSM-5 zeolites.

Zeolite	Surface area m^2 g^{-1}		Dubinin void vol, ml g^{-1}
	Langmuir	BET	
HAl-ZSM-5(36)*	490	420	0.190
HGa-ZSM-5(40)	470	404	0.186
HGa-ZSM-5(97)	463	380	0.178
HGa-ZSM-5(289)	424	334	0.171

* Number in parenthesis indicate SiO_2/M_2O_3 ratio (M = Al or Ga).

volume of HAl-ZSM-5(36) (0.190 ml g^{-1}) is only slightly higher than that of HGa-ZSM-5 (40) (0.186 ml g^{-1}). The decrease in void volume in the case of Ga isomorphs from 0.186 mL g^{-1} for HGa-ZSM-5 (40) to 0.171 ml g^{-1} for HGa-ZSM-5(289) may be a consequence of an increase in crystallites from 2 μm for the former to 4 μm for the latter.

3.3.4 Equilibrium sorption capacities : Equilibrium sorption capacities of different probe molecules often help to estimate or confirm the crystalline nature and the void volume of the microporous solids like zeolites. Table 3.3 summarizes equilibrium sorption capacities (at P/P_o = 0.8 , 298 K , 2 h) of water , n-hexane, cyclohexane, xylene isomers, n-butylamine (nBA) and tributylamine (TBA) for all the four zeolite samples. Although HAl(36)- and HGa(40)- MFI samples show almost comparable sorption capacities, the former shows slightly higher sorption capacities than the latter. The equilibrium sorption capacity for water decreases for Ga-isomorphs from 9.1 wt. % in HGa-ZSM-5(40) to 3.1 wt. % in HGa-ZSM-5(289). This is consistent[13] with the decrease in the hydrophilic character of the zeolite with the decrease in the framework gallium content. The sorption capacity of nonpolar cylindrical n-hexane molecule (kinetic diameter = 4.2 Å) seems to be least affected (11.0 ± 0.5 wt. %) with the change in SiO_2/Ga_2O_3 in the zeolite. The equilibrium sorption capacity of spherical cyclohexane molecule of the size (6.2 Å) comparable to the pore diameter, decreases with the increase in the SiO_2/Ga_2O_3 ratio. It was reported[14] earlier that the crystallite size

Table 3.3

Equilibrium sorption uptake* g/100g in different ZSM-5 zeolites

Sorbate	Sorbent			
	HGa-ZSM-5 (40)	HGa-ZSM-5 (97)	HGa-ZSM-5 (289)	HAl-ZSM-5 (36)
Water	9.14	8.13	3.09	10.06
n-hexane	10.00	11.01	11.50	11.10
cyclohexane	4.52	4.07	3.98	5.29
o-xylene	3.00	2.98	2.90	3.10
m-xylene	3.25	3.17	3.05	3.30
p-xylene	14.78	13.49	13.25	15.00
n-butylamine	12.00	12.10	13.26	12.80
tributylamine	0.75	0.65	0.60	0.90

* at 298 K, P/P_o = 0.8, 2 h.

increases with the increase in SiO_2/M_2O_3. Hence, due to longer diffusional path (trailing effect), the sorption capacity at a fixed time decreases with the increase in SiO_2/Ga_2O_3. Among the xylene isomers , the sorption capacity for para isomer (14 ± 1 wt. %) is much higher than the other two isomers (3.0 ± 0.2 wt. %). This shows the higher para selectivity of all the catalysts. The sorption capacity of a comparatively smaller basic polar molecule also decreases with the increase in SiO_2/Ga_2O_3 (decrease in gallium content). This is consistent with the fact that the number of acid centers decreases with the decrease in the framework gallium content. Tributylamine (kinetic diameter = 8.3 Å) uptake also is found to decrease with the increase SiO_2/Ga_2O_3 and hence with the increase in crystallite size. Since the size of TBA is larger than the 10 MR pore opening (5.5 Å) in MFI framework, it is sorbed only on the external surface.

3.3.5 n-Butylamine (nBA) sorption isotherms : Fig. 3.12 shows families of isotherms for the sorption of nBA in HAl-ZSM-5 and HGa-ZSM-5 samples in the temperature range of 323 to 523 K. It is seen from the Fig. 3.12 that except a few isotherms at higher temperature (523 K), most of them exhibit type I isotherms according to Kiselev's classification[15]. Almost 80 - 90 % of the total uptake takes place in a very narrow range of pressure (upto 5 Torr) after which there seems to be a gradual increase in the uptake with the pressure. nBA, being basic polar molecule initially may be interacting with the acid centers and then a very slow volume filling phenomenon may be operative on account

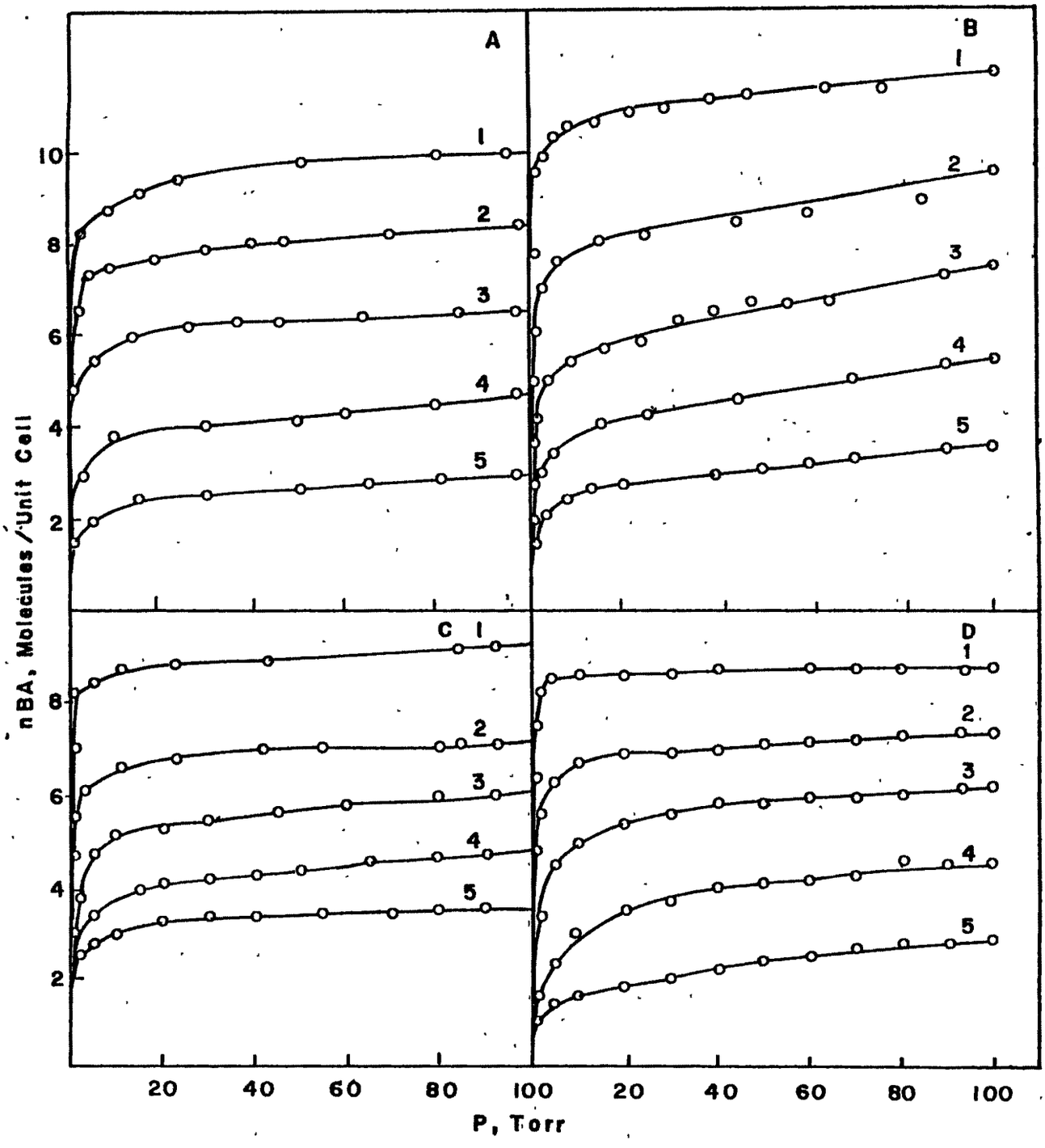

FIG.3.12: nBA SORPTION ISOTHERM IN (A) HGa-ZSM-5(40), (B) HAl-ZSM-5(36), (C) HGa-ZSM-5(97), (D) HGa-ZSM-5(289) AT (1) 323 K, (2) 373 K, (3) 423 K, (4) 473 K, (5) 523 K.

of its very moderate interactions with the silanol groups. Fig. 3.13A shows the typical dependence of sorption uptake on the concentrations of gallium in the MFI framework. At all the isotherm temperatures the nBA sorption uptake increases with the increase in gallium in the MFI framework. Similar observations were reported earlier[16] in case of different titanosilicates of MFI structure. A basic polar molecule like nBA is expected to interact with acidic protons, balancing the negative charge on the GaO_4^- tetrahedra. The decrease in the nBA uptake is rather sharper in the low gallium containing zeolites and is rather slower as the gallium concentration increases further. Fig. 3.13B shows the amount of nBA retained irreversibly during desorption by evacuation in vacuum (10^{-6}) as a function of desorption temperature. The Fig. 3.13B shows that the amount of nBA retained decreases sharply upto 423 K and then it decreases rather slowly at higher temperatures. The salient feature of Fig. 3.13B is the higher amount retained by HAl-ZSM-5(36) than that by HGa-ZSM-5(40). A considerably higher temperature is needed for the former zeolite than the latter one to achieve the same extent of nBA desorption. If the amount of nBA retained is assumed to be proportional, at least qualitatively, to the number of acid centers, then it clearly confirms[17] the earlier observations that acid sites in HAl-ZSM-5 possess higher strength than that of those in HGa-ZSM-5 zeolite with almost identical SiO_2/M_2O_3 (M = Al^{3+} or Ga^{3+}).

3.3.6 Application of sorption isotherm equations :

3.3.6 (A) Dubinin equation : An attempt is made here to test the

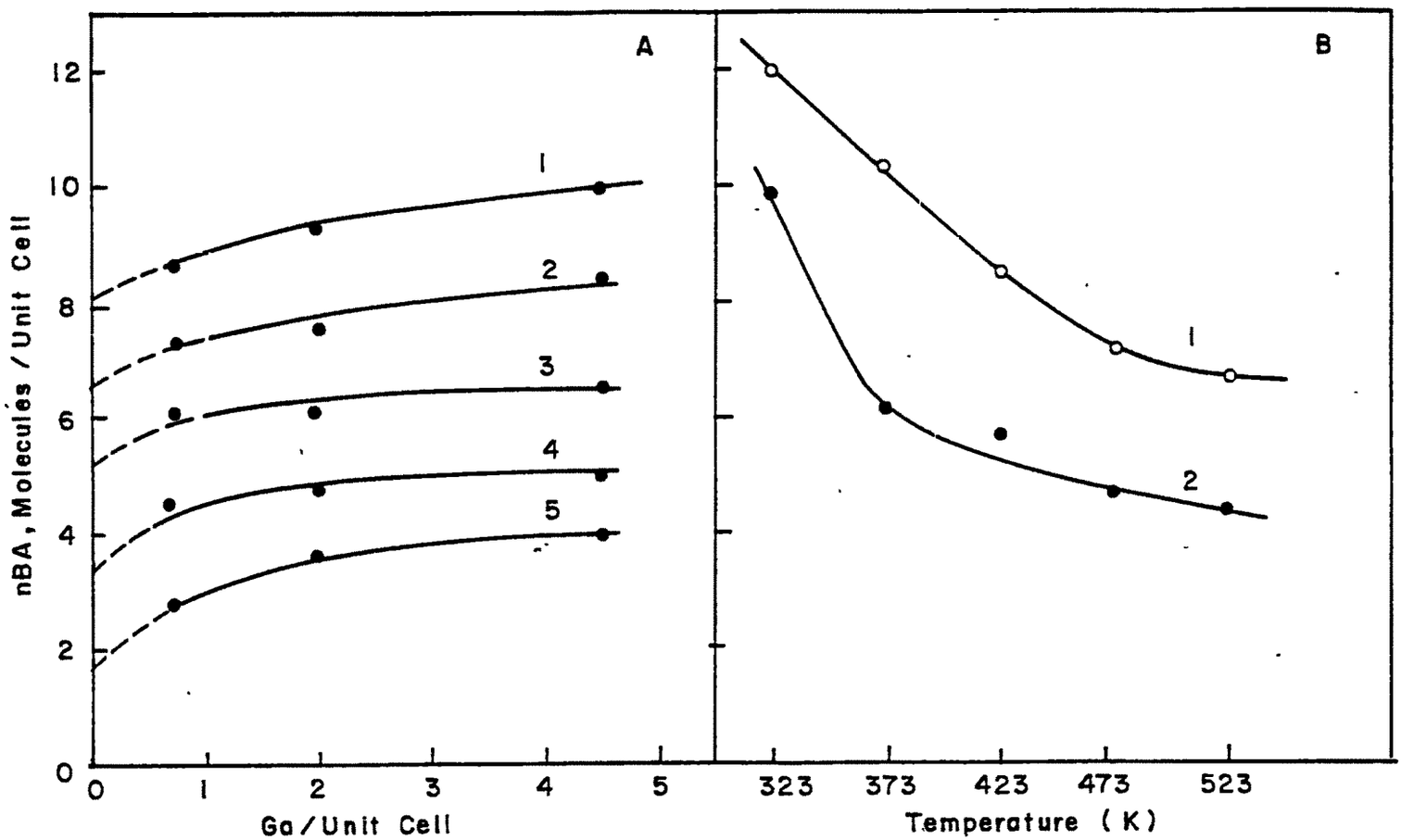

FIG. 3.13 : (A) nBA SORPTION UPTAKE AS A FUNCTION OF GALLIUM CONCENTRATION IN THE MFI FRAMEWORK. (B) RETENTION OF nBA DURING DESORPTION TEMPERATURE .

applicability of the Polanyi potential theory modified by Dubinin and Radushkevich[1] for nBA sorption in the different HGa-ZSM-5 zeolites and HAl-ZSM-5(36) over the temperature range 323 - 523K. The Dubinin-Radushkevich equation is expressed as :

$$\log W = \log W_o - \frac{B}{2.303\ \beta^2} \times \left(T \log \frac{P_o}{P}\right)^2 \qquad (1)$$

where W is the amount sorbed at equilibrium pressure P, W_o is the total sorption capacity, B is a constant independent of temperature and characteristic of the sorbent pore structure and β is the affinity coefficient. Dubinin plots so obtained exhibited excellent linearity and typical Dubinin plots are shown in Fig. 3.14, indicating the applicability of Dubinin-Radushkevich equation over the entire range of temperature (323 - 523 K). The saturation capacities and B/β^2 (β is the affinity coefficient) obtained from the intercept on the Y-axis and slopes of the linear plots, respectively, are tabulated in Table 3.4. The saturation capacities from Table 3.4 show close agreement with those obtained experimentally and thus indicated satisfactory representation of the nBA sorption data by Dubinin-Radushkevich equation based on the volume filling approach. The saturation capacity decreases with a decrease in the framework gallium content (an increase in SiO_2/Ga_2O_3 ratio). However, the saturation capacity increases with a decrease in sorption temperature. The decrease in the affinity coefficient 'β' (increase in B/β^2) with the increase in temperature indicated the reduced affinity of the sorption center towards the nBA

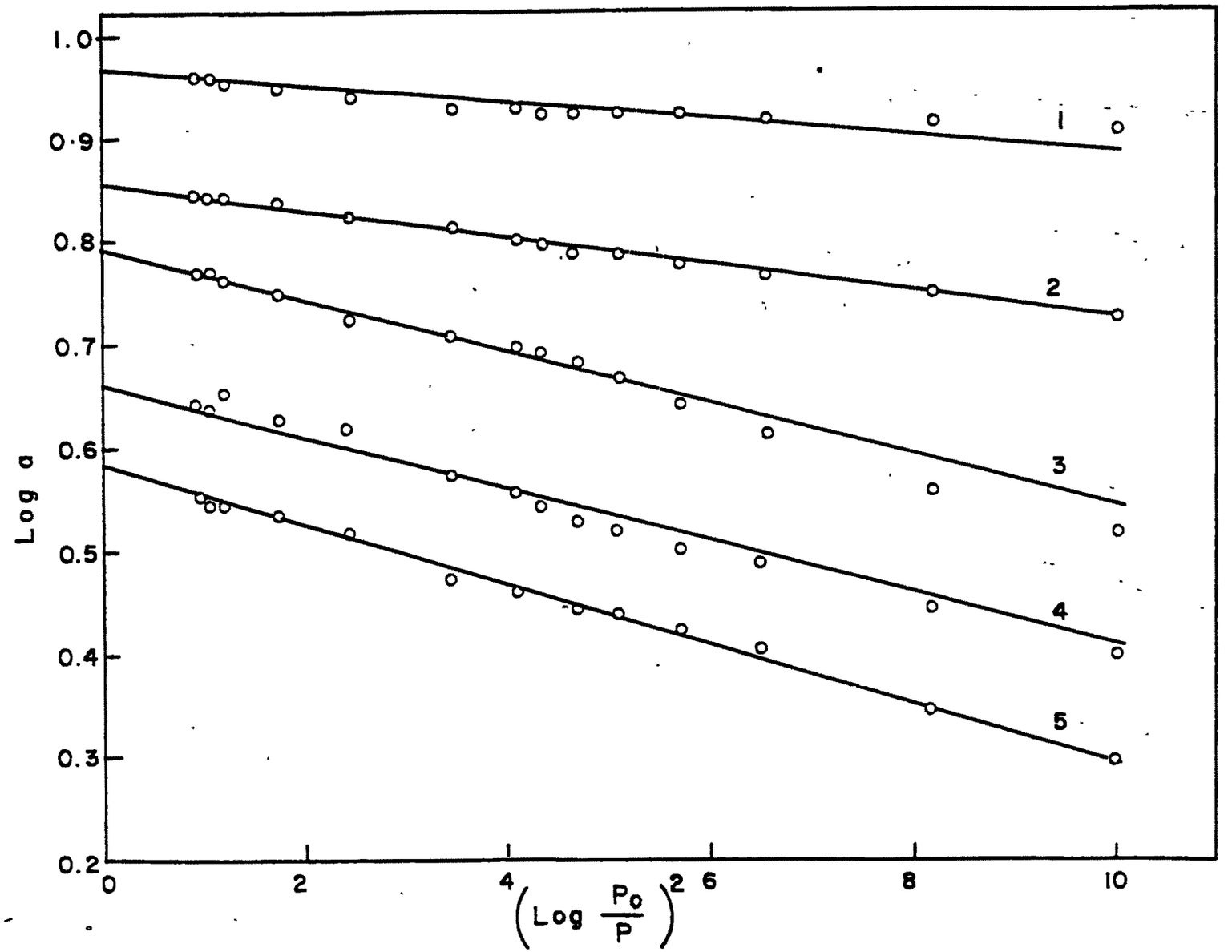

FIG. 3.14: DUBININ PLOTS FOR nBA SORPTION IN HGa-ZSM-5(97) (1) 323 K, (2) 373 K, (3) 423 K, (4) 473 K AND (5) 523 K.

Table 3.4

Saturation capacities and affinity coefficient of ZSM-5 zeolites

Zeolite	Temp. (K)	Saturation Capacities (molecules/U.C.)					B/β^2 X 10^2
		Experimental	Langmuir	BET	Freundlich	Dubinin	
HGa-ZSM-5 (36)	323	11.8	12.50	10.00	9.55	11.74	2.30
	373	9.3	8.93	7.89	6.46	9.33	5.07
	423	6.9	6.62	6.05	4.47	7.16	7.37
	473	5.4	5.00	4.63	2.75	5.62	10.36
	523	3.6	3.45	3.21	1.70	3.80	11.05
HGa-ZSM-5 (40)	323	10.2	10.00	9.09	7.76	10.35	2.10
	373	8.4	8.33	7.69	6.61	8.51	4.15
	423	6.4	6.25	5.88	4.37	6.68	5.53
	473	4.5	4.48	3.97	2.95	4.73	6.45
	523	2.9	2.88	2.60	1.32	3.16	7.37
HGa-ZSM-5 (97)	323	9.1	9.38	8.33	8.32	9.33	1.75
	373	7.0	7.50	6.40	5.75	7.16	2.88
	423	5.9	6.00	5.33	3.90	6.23	5.62
	473	4.7	4.54	4.16	2.88	4.62	5.76
	523	3.6	3.90	3.17	2.24	3.85	6.58
HGa-ZSM-5 (289)	323	8.7	8.75	8.18	8.32	8.71	0.76
	373	7.2	7.14	6.30	5.75	7.41	3.68
	423	6.1	5.88	5.00	3.63	6.68	8.75
	473	4.5	3.23	4.00	1.58	5.25	17.27
	523	2.8	1.85	1.88	1.05	3.63	28.78

molecule at higher temperatures. The affinity coefficient is maximum for HGa-ZSM-5(97) among the gallium isomorphs of MFI zeolites. It is, however, surprising that the affinity coefficient 'β' is lower for the HAl-ZSM-5(36) than that for HGa-ZSM-5(40) of almost the same SiO_2/M_2O_3 ratio.

3.3.6 (B) BET isotherm equation : The application of BET equation to the sorption of nBA in HAl-ZSM-5(36) and all the HGa-ZSM-5 zeolites yielded excellent linear plots and typical of them are shown in Fig. 3.15. The saturation capacities (monolayer capacities) obtained (Table 3.4) from the slope and the intercept of these linear plots are in reasonable agreement with those obtained from Dubinin-Radushkevich equation. The excellent linearity of these plots also confirms that the nBA sorption data in ZSM-5 zeolites can be satisfactorily described by BET model. Most of the BET plots pass through the origin without yielding an appreciable intercept on the ordinate. However, as the SiO_2/Ga_2O_3 ratio and the sorption temperature increases, BET plots yield a very small intercept on the ordinate. The constant C in the BET is related to the heat of sorption for the first layer. nBA sorption data in EU-1 zeolites[18] and CO_2 sorption data in LTL zeolites[19] also yielded linear BET plots. However, the BET approach showed only limited applicability to nBA sorption in titanosilicates of MFI[16] structure and both CO_2[19] and NH_3[9] sorption data could not be represented satisfactorily by the BET approach in cation exchanged Y zeolites.

3.3.6 (C) Langmuir sorption equation : When nBA Sorption data in Al- and Ga-ZSM-5 zeolites were fitted to Langmuir model,

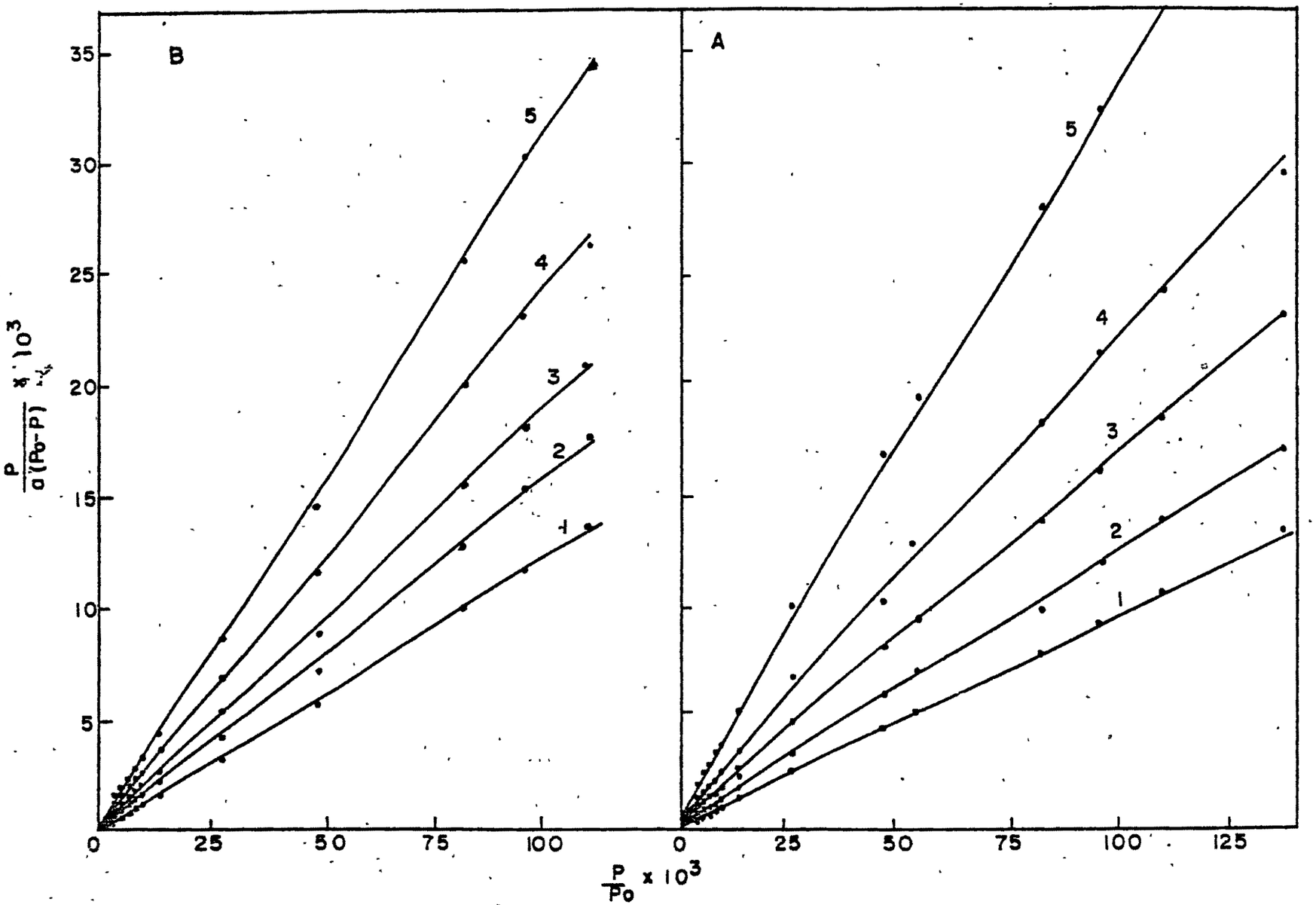

FIG. 3.15 : BET PLOTS FOR nBA SORPTION OF (A) HAl-ZSM-5(36) AND (B) HGa-ZSM-5(97) AT (1) 323 K, (2) 373 K, (3) 423 K, (4) 473 K AND (5) 523 K.

linear plots were obtained at all the temperature even upto 100 Torr of pressure. Typical linear plots are shown in Fig. 3.16. Monolayer capacities obtained from the reciprocal of the slopes of the linear plots are tabulated in Table 3.4 and they show fair agreement with those obtained experimentally, from Dubinin-Radushkevich and BET equations. Most of the linear plots pass through the origin and those at 523 K yield an intercept on the ordinate, suggesting a lower heat of sorption or weaker interaction between the sorbate molecules and sorption centers. The excellent linearity of the Langmuir plots suggests that nBA molecules are localized on the sorption center with 1:1 correspondence between the sorption center. nBA sorption in EU-1 zeolites[18], CO_2 sorption in LTL zeolites[19] and NH_3 sorption in cation exchanged Beta zeolites[20] , could satisfactorily be represented by Langmuir approach. A limited applicability was shown by Langmuir approach for the nBA sorption in titanosilicates molecular sieves of MFI structure. Although, the Langmuir approach represented nBA sorption in Fe^{3+} exchanged Y zeolites[21], it failed to represent CO_2[13] and NH_3[2] sorption in cation exchanged Y zeolites.

3.3.6 (D) Freundlich sorption equation : Recently, the Freundlich sorption equation satisfactorily represented nBA sorption in Fe^{3+} exchanged type Y zeolites[21] and CO_2 sorption in LTL zeolites[19]. When nBA sorption data in Al- and Ga-ZSM-5 zeolites were tried to fit into a Freundlich isotherm equation, linear plots were obtained over entire temperature range (323 - 523 K) even upto 100 Torr. The typical Freundlich plots are shown

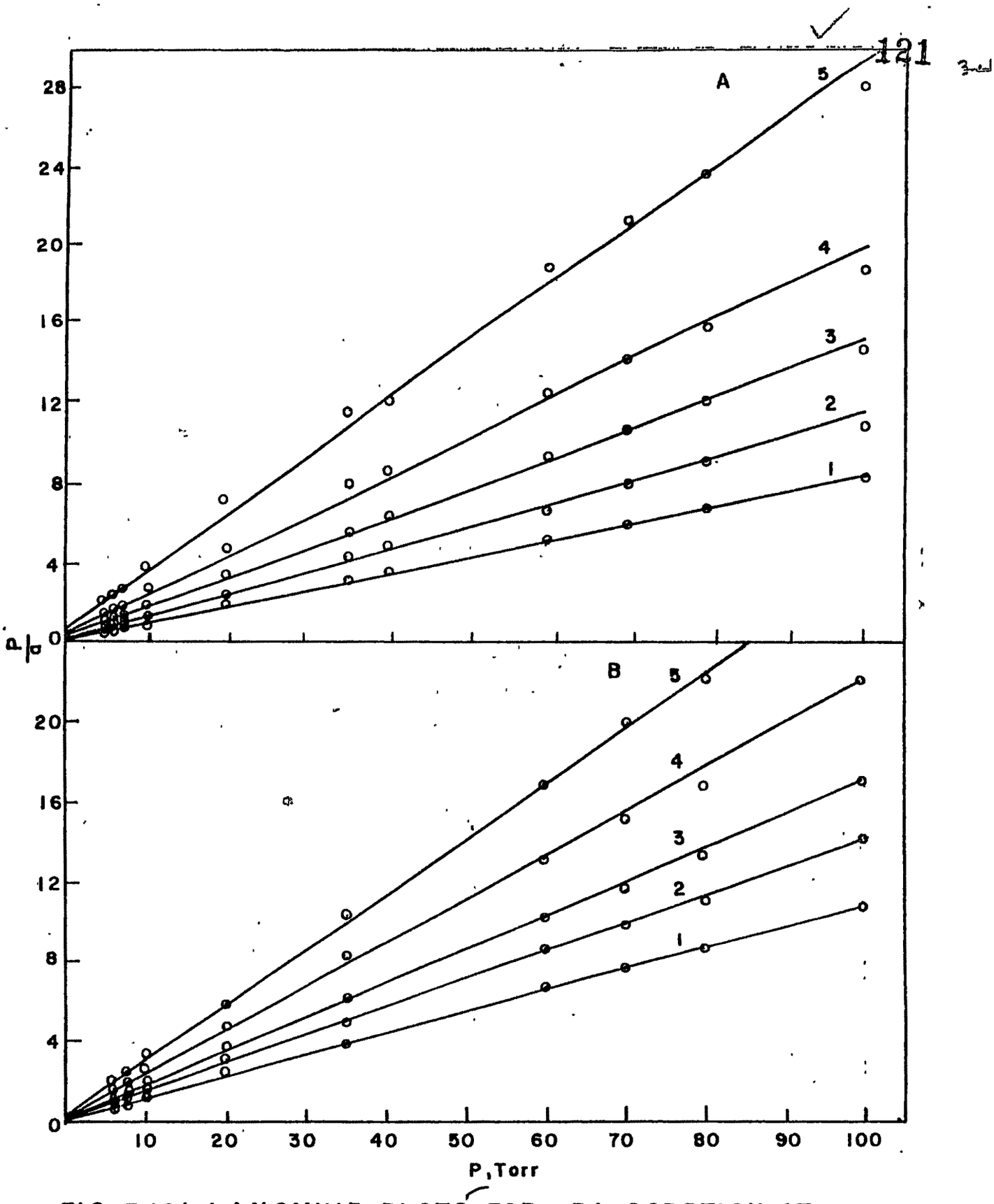

FIG. 3.16: LANGMUIR PLOTS FOR nBA SORPTION AT (A) HAl-ZSM-5(36) AND (B) HGa-ZSM-5(97) AT (1) 323 K, (2) 373 K, (3) 423 K, (4) 473 K, (5) 523 K.

in Fig. 3.17. The slope of these linear plots increased with the increase in the isotherm temperature and with the increase in SiO_2/Ga_2O_3 ratio. The excellent linearity of these plots, suggests two dimensional monolayer film of nBA molecules on the sorbent surface. Although linear plots were obtained, the sorption capacities, evaluated from the intercepts on the ordinate were found to be lower than those obtained experimentally. The Freundlich sorption model, however, failed to represent nBA sorption in EU-1 zeolites[18] and titanosilicates of the MFI structure[16].

3.3.6 (E) Sips equation and Koble- Corrigan equation : The Sips equation[22,23] based on the localized sorption with sorbate-sorbent interaction, takes care usually of any deviation from the Langmuir approach. If the sorption is assumed to be a chemical reaction between sorption centers and the sorbate molecules, the Langmuir equation results with a 1:1 correspond- ence between them, and if some tolerance is made for complicating factors, the Sips equation results. Although recently the Sips equation exhibited excellent applicability to CO_2[13] and NH_3[2] sorption in cation-exchanged Y zeolites, NH_3 sorption in cation-exchanged Beta zeolites[20] and nBA sorption in titanosilicates of the MFI structure,[16] it failed to represent the nBA sorption in Al- and Ga-ZSM-5 zeolites in the present studies.

Similarly, the Koble-Corrigan equations[23,24] based on the exact solution for the dissociative sorption of sorbate molecules on two active sites, could represent CO_2 sorption in cation exchanged Y zeolites[13]; but the same approach could not

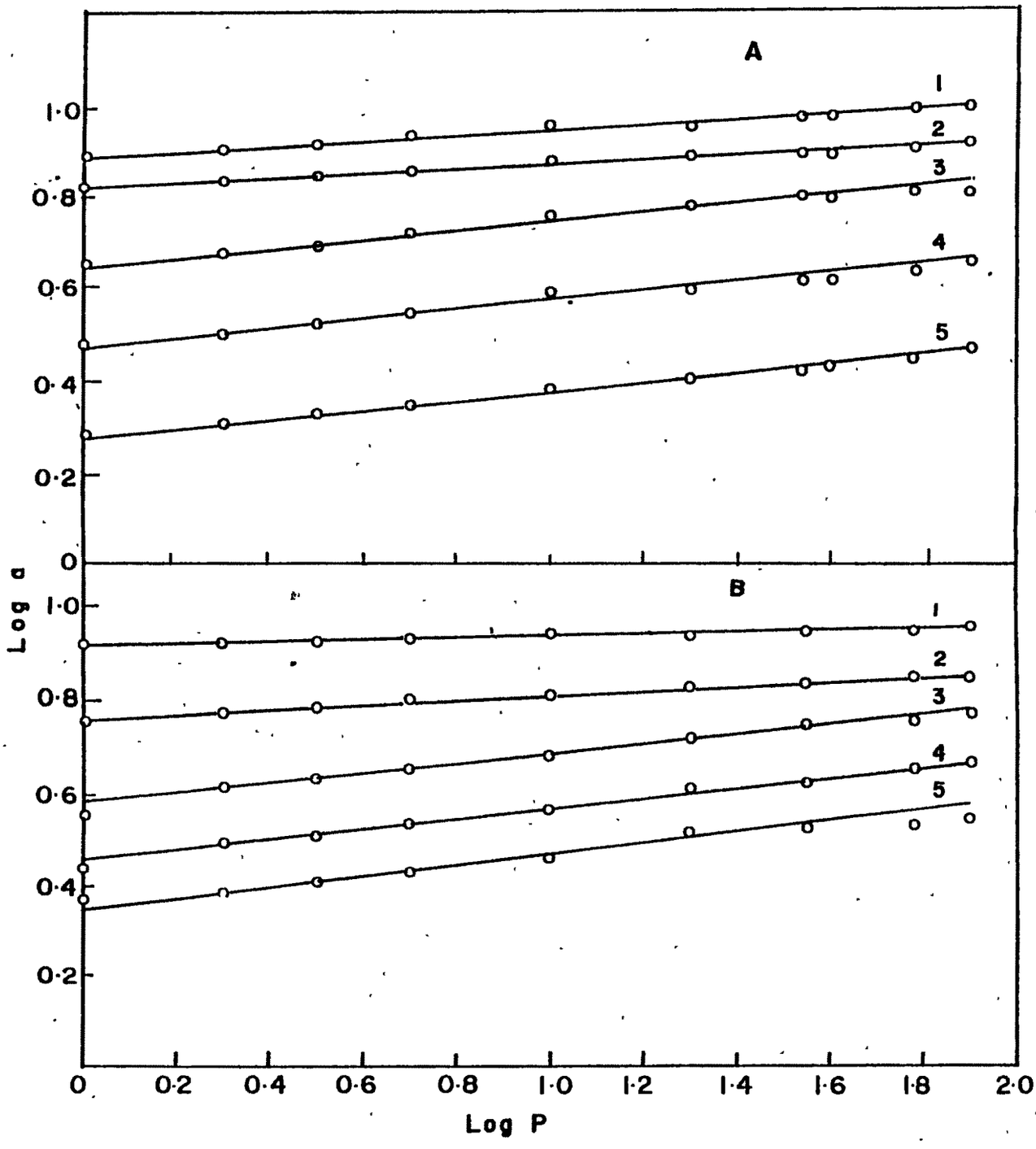

FIG. 3.17 : APPLICABILITY OF FREUNDLICH EQUATION FOR n BA SORPTION AT (1) 323 K, (2) 373 K, (3) 423 K, (4) 473 K AND (5) 523 K IN (A) HGa-ZSM-5(40) AND (B) HGa-ZSM-5 (97).

yield linear plots in the present study of nBA sorption and hence no meaningful conclusions could be drawn.

3.3.6 (F) Application of statistical models of Langmuir and Volmer : The statistical models of Langmuir and Volmer[25] derived initially for ideal systems are often applied[2,13,26] to real systems to yield information on the extent of deviations occurring in such systems on account of surface heterogeneity, multilayer formation and mutual interactions between sorbed molecules. In the present studies, however, plots of K_L, $\ln K_L$, K_V and $\ln K_V$ as a function of coverage (θ) did not yield linear plots, and hence, no useful information can be obtained regarding the state of the sorbed molecules.

3.3.6 (G) Chemical affinity and the selectivity of the sorbed phase : The decrease in the chemical potential takes place, when a gas is transferred reversibly and isothermally from a gas phase at a standard pressure P_o into an infinite amount of sorbent-sorbate mixture over an equilibrium pressure P. Neglecting the non-ideality of the sorbate, the chemical affinity may be expressed[25,27-29] as :

$$\Delta\mu = RT \ln (P/P_o) \qquad (3)$$

The value of $\Delta\mu$ may often be taken as the quantitative measure of the chemical affinity of the sorbate for the sorbent. Plots of $-\Delta\mu$ against the amount sorbed also serve as useful criteria for the comparison of the sorption affinities of a probe molecule in the lattices of different zeolites. Typical plots of $-\Delta\mu$ against the amount sorbed are shown in Fig. 3.18, for HAl-ZSM-5(36) and HGa-ZSM-5(40). The chemical affinity plots with

coverage were of the same nature for other zeolites also. Fig. 3.1ℊ shows that a drop in $-\Delta\mu$ with the coverage is rather sharper in HGa-ZSM-5(40) than that in HAl-ZSM-5(36). This indicates that the strength of the sorption centers in HAl-ZSM-5(36) is higher than that of HGa-ZSM-5(40). If acidic protons are assumed primarily to be the sorption centers, the above results support the literature[12] finding of lower strength of acid centers in HGa-ZSM-5 than that in HAl-ZSM-5. The Fig. 3.1ℊ also shows that at a fixed coverage, HAl-ZSM-5 shows higher chemical affinity than that in HGa-ZSM-5. As expected thermodynamically, the chemical affinity for nBA sorption decreases with the increase in the sorption temperature. The chemical affinity sequence in the mid-coverage region at 323 K was HAl-ZSM-5(36) > HGa-ZSM-5(40) > HGa-ZSM-5(97) > HGa-ZSM-5(289), but the same at 523 K was rather complicated. These curves also show that the drop in chemical affinity became rather sharp as the sorption temperature is increased.

3.3.6 (H) Isosteric heat (Q_{st}) of n-BA sorption : The isosteric heat (Q_{st}) of sorption is derived[25,27-29] by applying the Claussius-Clapeyron equation at constant sorbate loading using the relation :

$$-\Delta H^{-} = Q_{st} = R\,(T_2T_1 / T_2-T_1)\ln(P_2/P_1)$$

If Q_{st} is temperature-independent, the plots of ln P against 1/T at a fixed sorbate loading (isosters) are expected to be linear, In the present studies, the isosters were found to be fairly linear. Table 3.5 lists the values of isosteric heats obtained

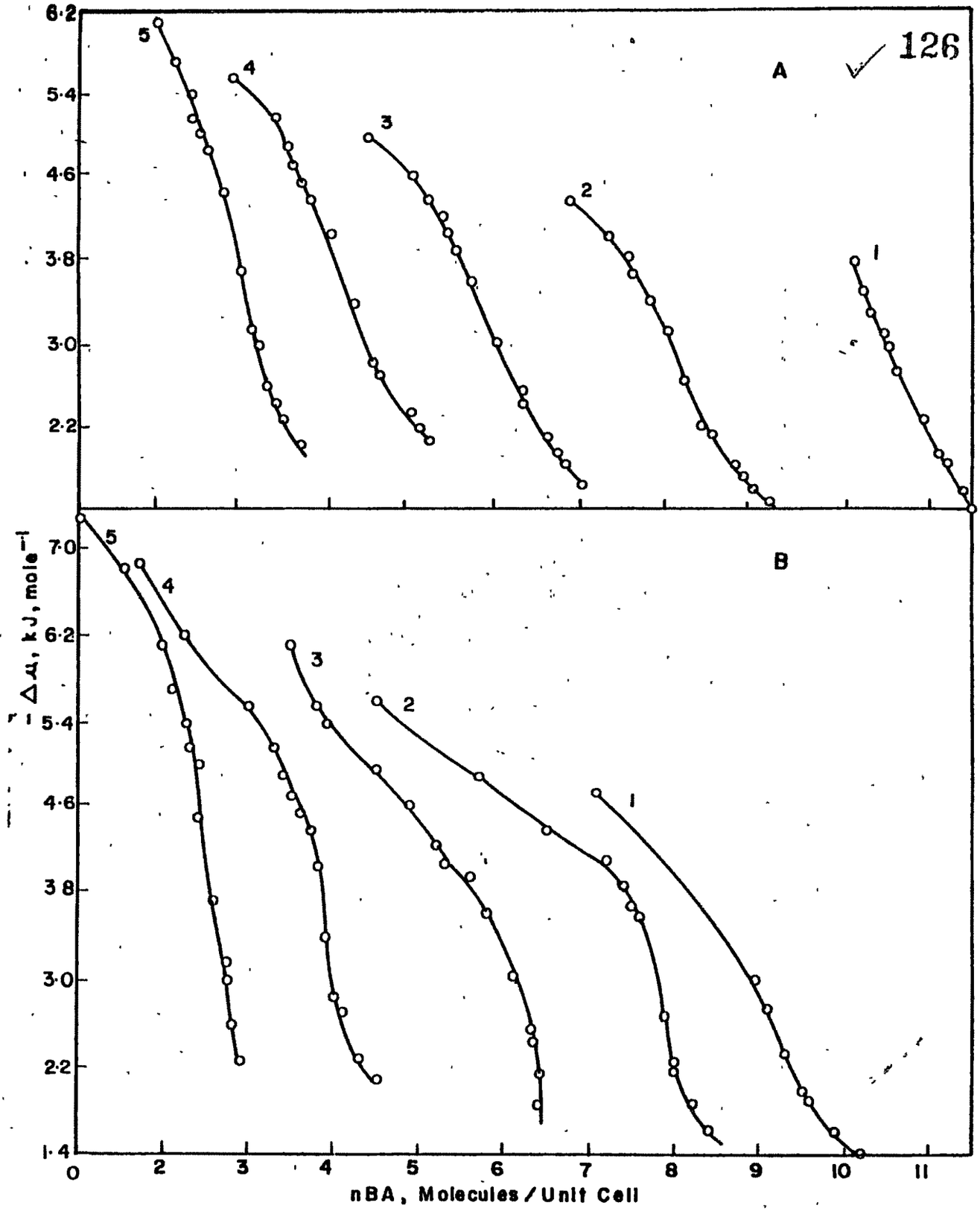

FIG. 3.18 : THE CHEMICAL AFFINITY PLOTS WITH THE COVERAGE FOR (A) HAl-ZSM-5 (36) AND (B) HGa-ZSM-5 (40) AT (1) 323 K, (2) 373 K, (3) 423 K, (4) 473 K AND (5) 523 K.

from the slopes of the linear isosters. The Table 3.5 shows that with the exception of HGa-ZSM-5(289), Q_{st} value increases with coverage. This shows that the nBA molecules interact strongly with sorption centers (acid sites) of increasing strength. The isosteric heat extrapolated to zero coverage is in the range of 34 - 24 kJ $mole^{-1}$ and follows the sequence HAl-ZSM-5(36) > HGa-ZSM-5(97) > HGa-ZSM-5(40) > HGa-ZSM-5(289). The sequence also indicates that among the gallium containing zeolites , HGa-ZSM-5(97) exhibits the highest Q_{st} value. It is known fact that, as isomorphous framework species substituting Si^{4+} in zeolite decreases, there is a decrease in the number of acid sites with an increase in the strength associated with each site. It seems therefore, probable that, the strength of acid site increases upto SiO_2/M_2O_3 = 97 and then it may decrease. The HGa-ZSM-5(289) shows lower value of Q_{st} than HGa-ZSM-5(97) and it also shows that in the higher coverage region Q_{st} decreases and then regains its original value. For such an indirect method as this, the experimental artifacts may influence Q_{st} values to some extent. In case of ammonia sorption in ZSM-5[30,31], the behaviour of Q_{st} was in the reverse order. Q_{st} first increased with the coverage and then decreased to level off. Sorbate-sorbent interaction usually prevails in the low coverage region and is expected to be appreciable in magnitude. The Q_{st} values in the mid-coverage region are a result of both sorbate-sorbent as well as sorbent-sorbent interactions, and depending upon the extent of contributions from each of them, humps in Q_{st} curves are observed[27]. In the higher coverage

Table 3.5

Isosteric heats kJ mole^{-1} (Q_{st}) of nBA sorption on ZSM-5 zeolites.

Zeolites	nBA molecules / unit cell										
	0.0	0.5	1.0	1.5	2.0	2.5	3.0	3.5	4.0	4.5	5.0
HAl-ZSM-5(36)	34.0	34.0	34.4	35.2	32.0	38.8	39.6	39.6	35.2	42.0	44.4
HGa-ZSM-5(40)	24.5	24.5	24.5	21.5	24.5	25.0	25.7	25.8	28.0	27.6	27.7
HGa-ZSM-5(97)	32.0	-	32.0	-	32.0	32.5	32.0	33.5	34.5	31.0	34.3
HGa-ZSM-5(289)	24.5	24.5	24.0	24.7	25.3	24.5	23.0	22.0	22.0	22.7	24.5

region, only sorbate- sorbate interactions are operative and usually Q_{st} values approach the the heat of liquefaction.

3.3.7 Infra red (IR) Spectroscopy : Fig. 3.19 shows the spectra of different pentasil zeolites in the region of fundamental vibrations of surface hydroxyl groups. The absorption peaks[32,33] are observed at 3740, 3725, 3699, 3607 and 3495 cm^{-1} for HAl-ZSM-5 (curve 1) at 3740, 3725, 3699, 3607, 3495 cm^{-1} for Ga impregnated HAl-ZSM-5 (curve 2), at 3740, 3720, 3690, 3619, 3607 cm^{-1} for HAlGa-ZSM-5 (curve 3) and at 3740, 3720, 3690, 3619 cm^{-1} for HGa-ZSM-5 (curve 4).The bands at 3740, 3720 cm^{-1} are assigned[32-34] to stretching vibrations of Si-OH groups (terminal and internal respectively) and a band at ~ 3690 cm^{-1} is assigned to extra lattice Al or Ga. The bands at 3607 and 3619 cm^{-1} are assigned[34] to bridging hydroxyl groups Al-O-Si and Ga-O-Si respectively. The broad band seen in curve 3 is because of the overlapping bands of bridging hydroxyl groups of Al and Ga. The band of bridging hydroxyl group to Ga appears as a shoulder because of the lower concentration of Ga as compared to Al. The broad band at ~ 3490 cm^{-1} is assigned due to hydrogen bonded hydroxyl groups[35].

FTIR spectroscopic study of pyridine adsorption is widely used for the determination of acid strength distribution of catalysts. Fig. 3.20 (curves 1-4) shows the infra-red spectra of pyridine adsorbed on HAlGa-ZSM-5 and Ga impregnated HAl-ZSM-5 at 373 K and 423 K in the 1400 to 1700 cm^{-1} region. Absorption bands due to adsorbed pyridine were reported[35-36] at 1635, 1620, 1598, 1544, 1490, 1454, 1445 cm^{-1}. The spectral bands at 1635 and

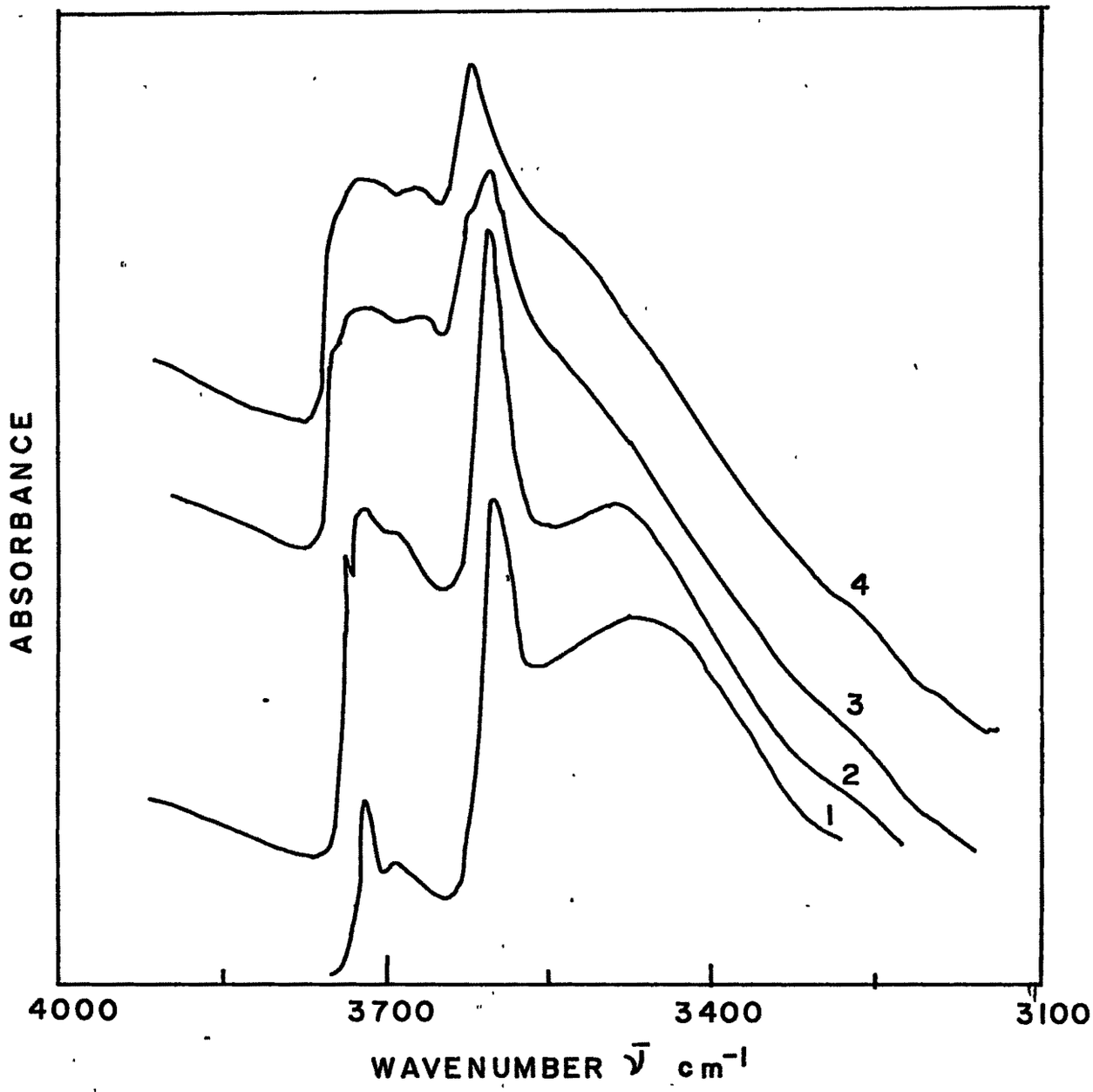

FIG. 3.19 : IR SPECTRA OF DIFFERENT PENTASIL (MFI) ZEOLITES IN THE HYDROXYL REGION. (1) HAl-ZSM-5 (85), (2) 2% Ga_2O_3 IMPREG. HAl-ZSM-5, (3) HAlGa-ZSM-5 (40) AND (4) HGa-ZSM-5 (97).

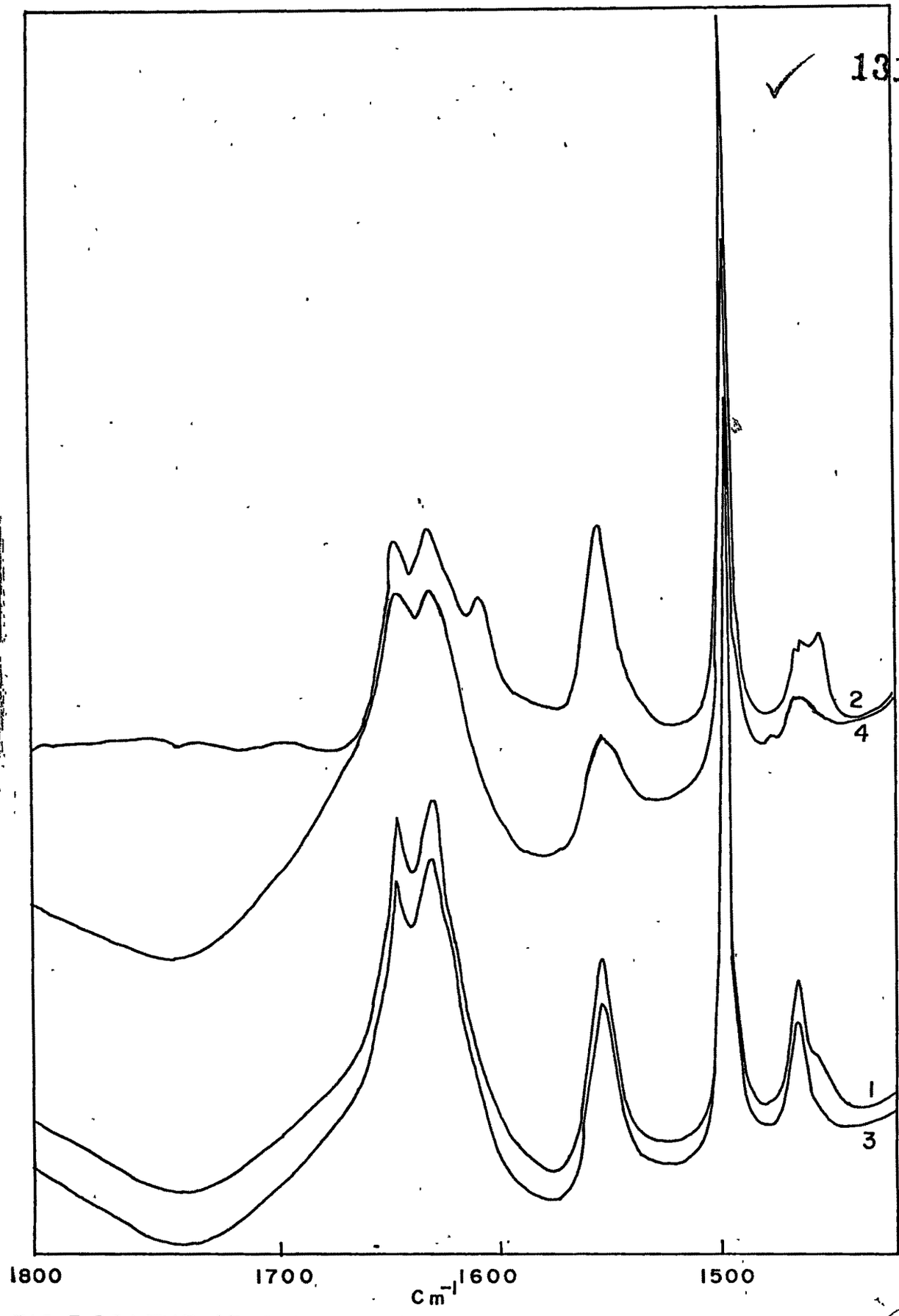

FIG.3.20: THE IR SPECTRA OF PYRIDINE ADSORBED AT 373 K ON (1) HAlGa-ZSM-5(40) AND(2) 2% Ga_2O_3 IMPREG. HAL-ZSM-5. THE IR SPECTRA OF PYRIDINE DESORBED AT 423 K FROM (3) HAlGa-ZSM-5(40) AND (4) 2% Ga_2O_3 IMPREG. HAl-ZSM-5 RESPECTIVELY.

1544 cm^{-1} were attributed[35-36] to the Bronsted acid sites i.e. due to the vibrations of pyridinium ions (N^+-H stretching vibration). The spectral bands around 1620, 1490, 1450 cm^{-1} were assigned[35-36] to pyridine molecules co-ordinated to Lewis acid sites. The bands at 1445 and 1598 cm^{-1} are also present which are due to hydrogen bonding. The intensity of absorption of all the peaks for both HAlGa-ZSM-5 and Ga impregnated HAl-ZSM-5 is found to decrease when the catalyst was evacuated at 423 K. From the spectra it can be noted that relative concentrations of Lewis acid sites compared to Bronsted acid sites on Ga impregnated HAl-ZSM-5 is higher than that on HAlGa-ZSM-5 samples. Thus FTIR study supports the presence of Ga in the tetrahedral framework of pentasil zeolites.

Fig. 3.21 gives the framework IR spectra by different heat treated Ga-ZSM-5 samples. Curve 1 corresponding to Ga-ZSM-5 heated at 1173 K for 2h gives IR spectra typically of ZSM-5[32-39]. From the figure, it is seen that as the temperature of heat treatment increases, the IR band at 550 cm^{-1}, characteristic of double 5-membered[32-39] (related to crystallinity of the sample) and a peak at 722 cm^{-1} (due to tetrahedral asymmetric stretching vibration) decreases in intensity. Both the peaks vanish for the sample treated at 1393 K (curve 4). Similarly, as the temperature of the heat treatment increases, the peak at 618 cm^{-1} increases in intensity and becomes much sharper in curve 4. A peak[32-39] at 460 cm^{-1} due to pore opening[32-39] becomes broad and shifts to higher frequency in curve 4. Curve 4 corresponds to the framework IR spectra of cristoballite. These observations support

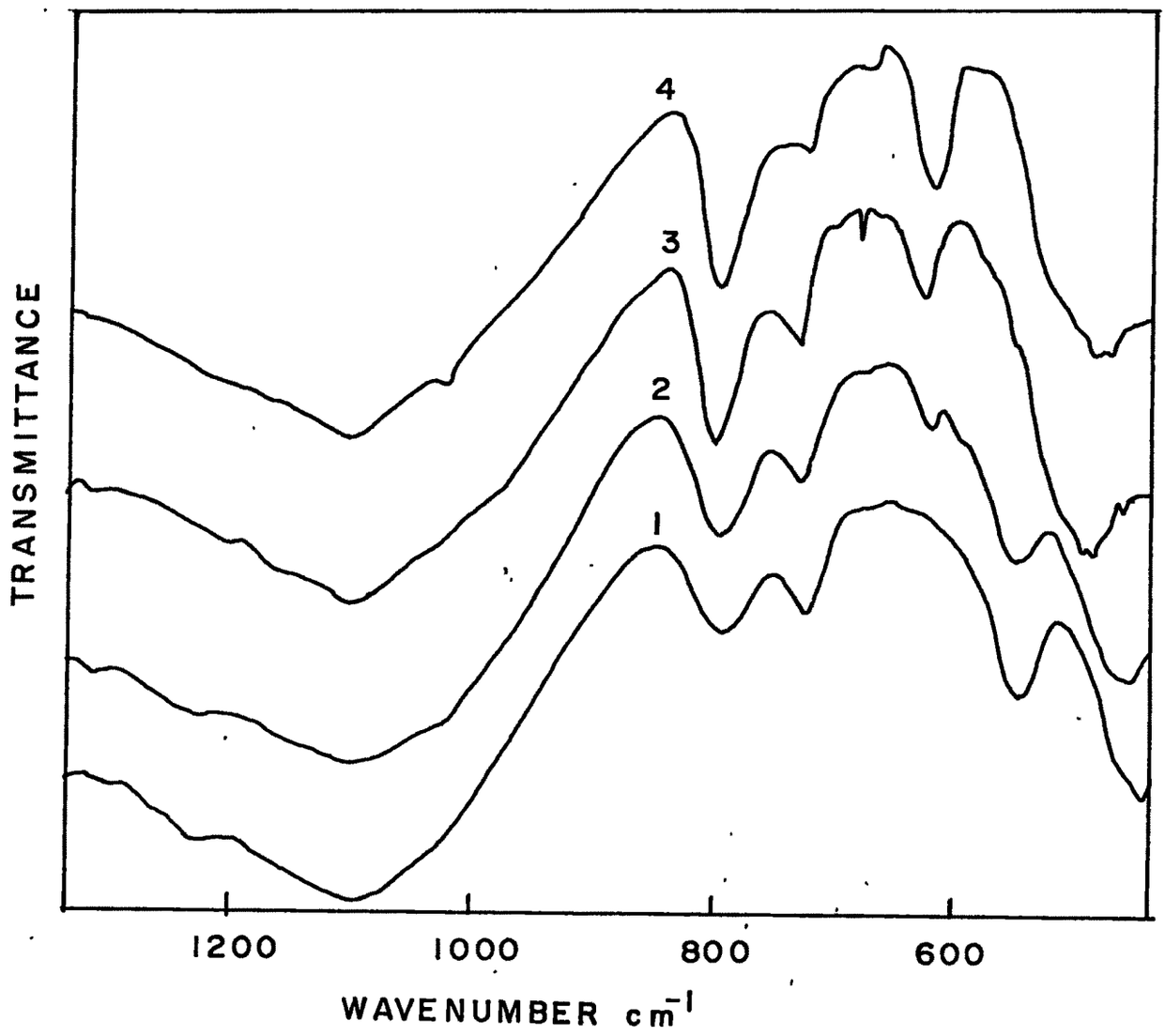

FIG. 3.21: INFLUENCE OF CALCINATION TEMPERATURE ON THE IR SPECTRA AT (1) 1173 K, (2) 1248 K, (3) 1298 K AND (4) 1393 K FOR THE PENTASIL (MFI) GALLOSILICATE OBTAINED FROM SYSTEM III.

the results obtained from XRD.

3.3.8 X-ray Photoelectron spectroscopy (XPS) : XPS has been extensively used in the study the external layer of zeolite surfaces[40-45]. The presence of aluminum , gallium or any other substituted trivalent cation in the zeolite framework modifies the acidic properties of zeolite. Therefore the study of actual distribution of substituted trivalent cation at the surface of the zeolite has attracted greater attention. The surface composition of the Ga^{3+} substituted pentasil zeolite was studied systematically by XPS. The XPS measurements were performed as described earlier. The intensity of various XPS bands was determined using linear background subtraction. All the XPS bands for $Si2p_{3/2}$, $Ga2p_{3/2}$, O1s were found symmetric. The atomic concentration ratio in outer layer designated as $(Si/Ga)_S$ was estimated for the corresponding XPS peak area using the relation[45],

$$(x/M)_S = A_x/A_M \cdot r_M/r_x \cdot (E_{Kx}/E_{KM})^{0.71}$$

where x stands for Si and M stands for Ga. A, r, E_k are the normalized peak area, the effective ionization cross section, and the photoelectron kinetic energy respectively. Cross section values were used from Scofield[45].

The bulk atomic concentration ratio designated as $(Si/Ga)_B$ was calculated from chemical analysis. The chemical composition expressed by the bulk atomic ratio $(Si/Ga)_B$ and the surface atomic ratio $(Si/Ga)_S$ calculated from the XPS intensity ratio of the samples studies are given in Table 3.6. From the $(Si/Ga)_S$

ratio in Table 3.6, it can be concluded that the surface of the samples is enriched with Si.

Table 3.6

Bulk and surface characteristic of pentasil gallosilicates.

System	(Si/Ga)B	$(Si/Ga)_S$
I	20.19	64.88
II	48.38	100.00
III	144.47	-

The Binding energies (B.E) for and $Si2p_{3/2}$, $Ga2p_{3/2}$ O1s tabulated in Table 3.7 for pentasil (MFI) gallosilicates agree well with those of reported[46,47]. The presence of trivalent Ga in the lattice framework can be confirmed by XPS. The XPS spectra of $Si2p_{3/2}$, $Ga2p_{3/2}$, O1s for Ga-ZSM-5 obtained from system I is

Table 3.7

Binding energies of various components present in Ga-ZSM-5.

System	Si2p	$Ga2p_{3/2}$	O1s
	B.E[b]	B.E	B.E
I	103.7	1118.8	532.44
II	103.6	1118.9	532.42
III	103.3	-	533.12

b B.E values are in eV.

given in Fig. 3.22. Irrespective of the ratio only one O1s peak at 532.6 eV is observed due to zeolite lattice oxygen. The shoulder peak around 530.1 eV reported[3] to be due to the oxygen associated with extra-lattice oxidic trivalent species was found absent in this sample.

3.3.9 ^{29}Si MASNMR : A study using ^{29}Si MASNMR (Fig. 3.23) of three different samples (a) pure silicalite(> 3000); (b) Ga-ZSM-5 (289) and (c) Ga-ZSM-5(40), showed two types of Si ordering in as-synthesized gallosilicate. The chemical shift value of about -103 ppm, corresponds to Si(1T) environments and a large signal at about -112 ppm corresponds to Si(0T) atoms. Hence, the signal at δ = -103 ppm can be attributed to Si atoms having Ga atoms in their second co-ordination sphere. The peaks marked with an asterisk (*) are due to the spinning side-bands. The apparent line intensity changes were found to be consistent[48] with the Ga content (SiO_2/Ga_2O_3) of these gallosilicates.

Fig. 3.24 exhibits ^{29}Si MAS NMR spectra of Ga-ZSM-5(97) with different heat treatments. Curve 1 for Ga-ZSM-5 heated at 1073 K shows two different Si^{4+} environments, Si(1Ga) and Si(0Ga) corresponding to a chemical shift of - 104.6 and -112.3 ppm. These data are in close agreement with the literature[49-52]. Curve 2 for Ga-ZSM-5 heated at 1248 k shows only single silicon environment corresponding to a chemical shift at -113.0 ppm. A shoulder band due to Si(1Ga) around -105 ppm disappears in this sample. It seems therefore that on calcinations at 1248 K degalliation of Ga-ZSM-5 takes place and perhaps the resultant product may be similar to silicalite-1. As the heat treatment

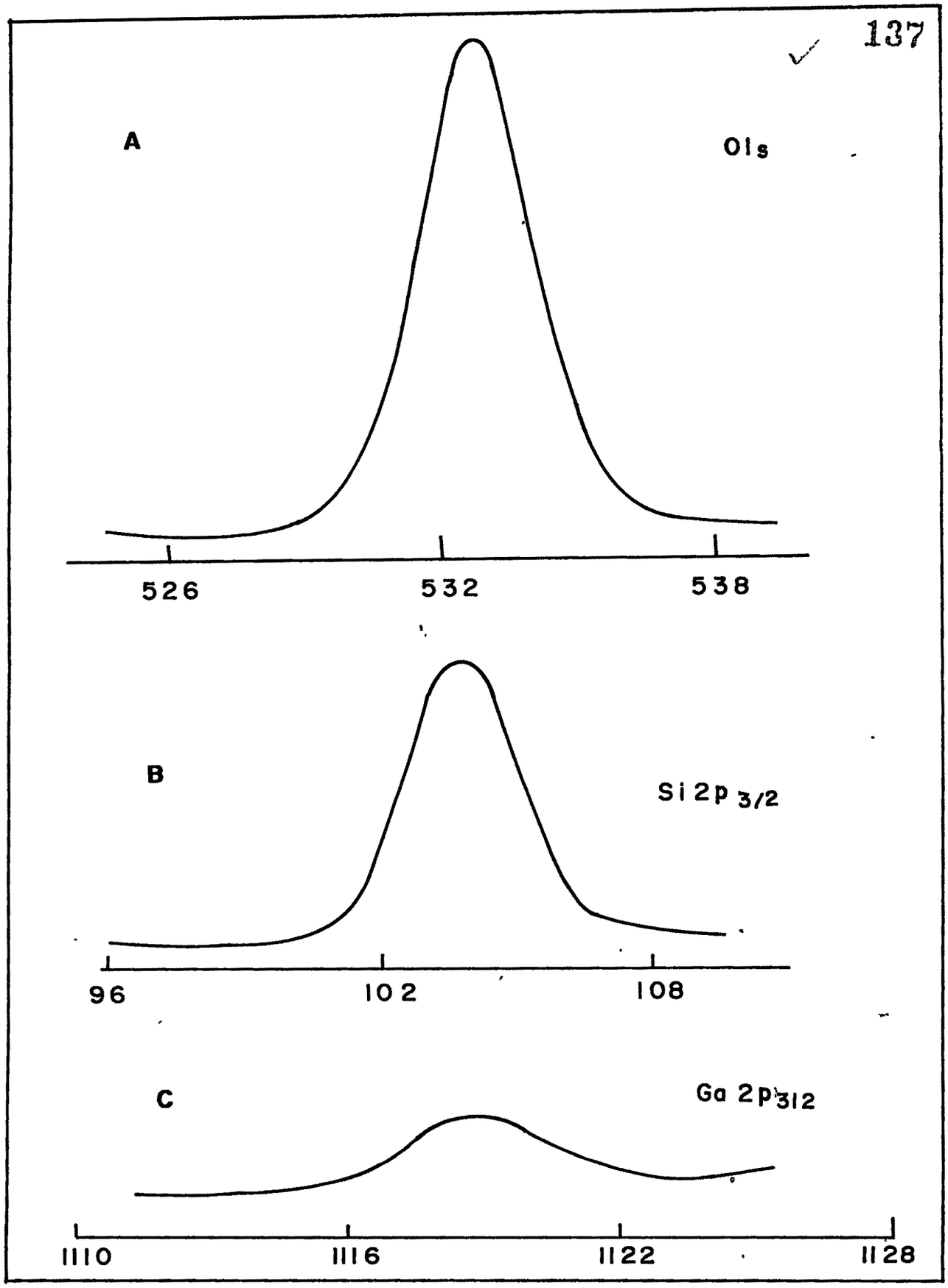

BINDING ENERGY (eV)

FIG. 3.22 : XPS SPECTRA OF (A) O1s, (B) $Si2p_{3/2}$ AND (C) $Ga2p_{3/2}$ OF Ga–ZSM–5 (40).

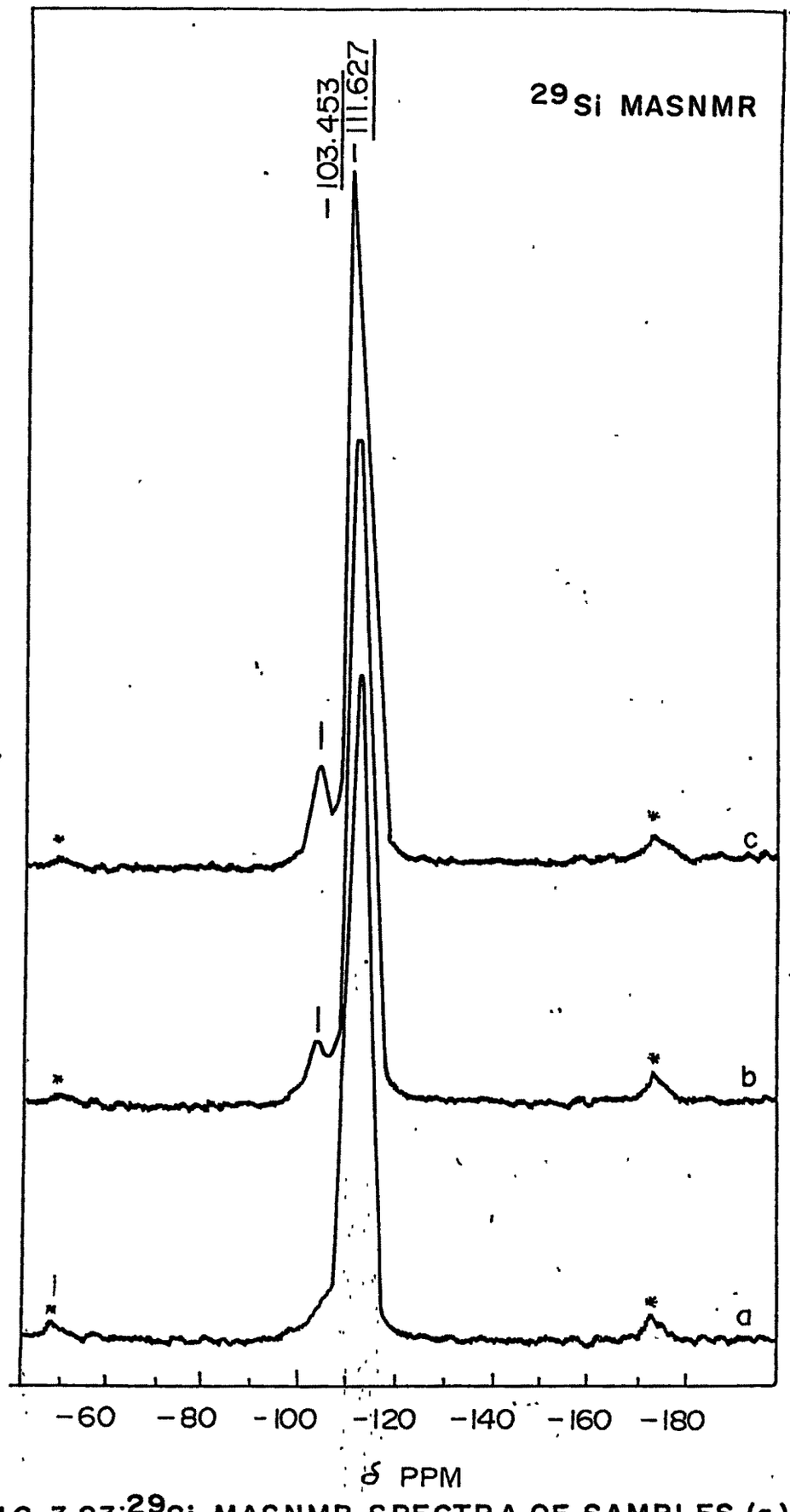

FIG. 3.23: ^{29}Si MASNMR SPECTRA OF SAMPLES (a) SILICALITE (>3000); (b) Ga-ZSM-5 (289) AND (c) Ga-ZSM-5 (40). THE SHIFTS ARE GIVEN RELATIVE TO TMS.

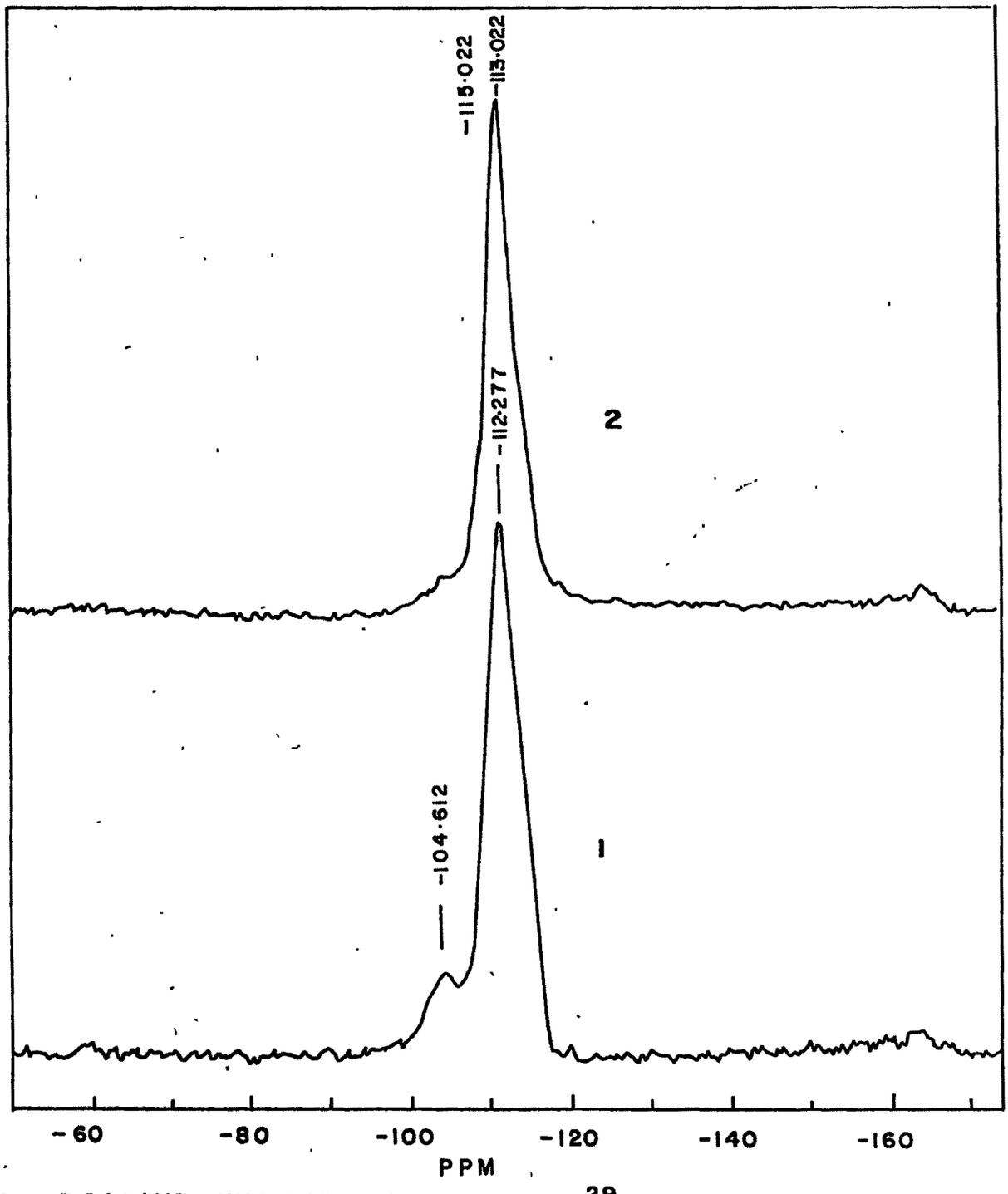

FIG. 3.24 : INFLUENCE OF TEMPERATURE ON ^{29}Si MASNMR OF PENTASIL(MFI) GALLOSILICATE OBTAINED FROM SYSTEM II 1) 1073K, 2) 1248K.

temperature of the peak due to Si(OGa) shifts gradually to a higher chemical shift from -113.0 to -109.5 ppm. Cristoballite exhibits only one environment, Si(OAl) for silicon. Moreover, cristoballite is a more stable phase than ZSM-5 and shifting of Si(OAl) environment to higher chemical shift seems to be concurrent with it.

3.4 REFERENCES

1. Dubinin,M.M. and Radushkevich,L.V., Proc. Acad. Sci., USSR , **55**, 327 (1974).
2. Shiralkar,V.P. and Kulkarni,S.B., J. Colloid and Interface Sci., **108**, 1 (1985).
3. Richter, K. and Peplinski, B., J. Electron. Spectrosc. Relat. Phenom., **13** 69 (1978).
4. Erdem,A. and Sand, L.B., J. Catal.,**60** , 241 (1979).
5. Wu. E.L., Lawton, S.L., Olson,D.H. Rohrman, Jr., A.C. and Kokotailo, G.T., J. Phys. Chem., **83**, 21, 2777 (1979).
6. Perego, G., Bellussi, G., Corno, C., Taramasso, M., Buonomo, F. and Esposite, A., New Development in Zeolite Science and Technology, Murakami, Y etal., (Eds), Elsevier, Amsterdam, P.129, (1986).
7. Taramasso, M., Perego, G. and Notari, B., U.S. Pat. 4,410,501 (1983).
8. Kuhl,G.B. J.Inorg. Nucl. Chem. **33**, 3261 (1971).
9. Simmons, D.K., Szostak, R. and Agrawal, P.K., J. Catal. **106**, 287 (1987).
10. Shiralkar,V.P. and Kulkarni,S.B., Ind. J. Chem., **16A**, 665 (1978).
11. Habgood, H.W. Can. J. Chem. **36**, 1384 (1958).
12. Awate, S.V., Joshi, P.N., Shiralkar, V.P. and Kotasthane, A.N., J. Incl. Phenon. & Mol. Recogn., **13**, 207 (1992).
13. Shiralkar,V.P. and Kulkarni,S.B., Zeolites, **4**, 329 (1984).
14. Kotasthane, A.N.; Shiralkar,V.P.; Hegde, S.G. and Kulkarni,

S.B., Zeolites, 6, 253 (1986).

15. Kiselev,A.V., Discuss. Faraday Soc., 40, 205 (1965).
16. Mirajkar,S.P., Thangraj,A. and Shiralkar,V.P., J. Phys.Chem., 94, 3073 (1992).
17. Eapen, M.J., Reddy, K.S.N., Joshi,P.N. and Shiralkar, V.P., J. Incl. Phenon. & Mol. Recogn., 14, 119 (1993).
18. Rao,G.N., Joshi,P.N., Kotasthane,A.N. and Shiralkar,V.P., J. Phys. Chem., 94, 8589 (1990).
19. Joshi, P.N. and Shiralkar,V.P., J. Phys. Chem., 97, 619 (1993).
20. Reddy,K.S.N., Eapen,M.J., Soni, H.S. and Shiralkar,V.P., J. Phys. Chem., 96, 7923 (1992).
21. Kulkarni,S.J. and Kulkarni,S.B., Ind. J. Chem., 18A, 6 (1989).
22. Sips,R.J., Chem. Phys., 16, 491 (1948).
23. Coughlan,B. and Larkin,P.M., Proc. Royal Irish. Acad. Inst. Chem., Centenary Issue, 383 (1977).
24. Koble,R.A. and Corrigan,T.E.,Ind. Eng. Chem., 44, 383 (1952).
25. Barrer, R.M. and Coughlan,B.,`Molecular Sieves' Soc. Chem. Ind. London , 1968 , pp. 141,233,241.
26. Coughlan, B. and McEntee, J.J., Proc. Roy. Irish Acad., 76B, 473 (1976).
27. Coughlan, B. and Kilmartin, S.J., J. Chem. Soc. Faraday Trans. I, 71, 1809 & 1818 (1975).
28. Shiralkar,V.P. and Kulkarni,S.B., Zeolites, 5, 37 (1985).
29. Shiralkar,V.P. and Kulkarni,S.B., J. Colloid and Interface Sci., 109, 115 (1986).

30. Tsutsumi,K., Hong Quikoh, Hagiwara, S. and Takahashi, H., Bull. Chem. Soc. Japan, **48**, 3576 (1975).

31. Masuda,T., Taniguchi,H., Tsutsumi, K and Takahashi, H., Bull. Chem. Soc. Japan , **51**, 1965 (1978).

32. Topsoe,N.Y; Pedersen,K; Derouane, E.G. J.Catal. **70**, 41(1981).

33. Jacobs,P.A.; von Ballmoos,R. J.Phys.Chem., **86**, 3050(1982).

34. Cynthia, T.W. and Clarence, D.C., J.Phys.Chem., **89**, 1569-1571 (1985).

35. Vedrine, J.C. et al. in proceedings of the VIth Int. Zeol. Conf. (Eds. D. Olson etal) Butterworths, Guildford UK 497, (1984).

36. Flanigen, E.M. `Zeolite Chemistry and Catalysis', (Ed. J. A. Rabol) Adv. Chem. Ser. Ch.2, 171 (1976).

37. Ballmoos, R. von., Ph.D Thesis, E.T.H. Zurich, 1981.

38. Jacobs, P.A., Beyer, H.K. and Valyon, J., Zeolites,**1**, 161 (1981).

39. Coudurier, G., Naccache, C. and Vedrine, J.C., J. Chem. Soc., Chem. Comm. 1413 (1913).

40. Kerr, G.T., Adv. Chem. Ser., **121**, 219 (1973).

41. Temper, F., Delafosse, D. and Contoux, J.P., ACS Symp. Ser., **40**, 76 (1977).

42. Vedrine, J.C., Dufoux, M., Naccache, C. and Imelik, B., J. Chem. Soc. Faraday Trans. I, **74**, 440 (1972).

43. Kulkarni, S.J., Badrinarayan, S. and kulkarni, S.B., J. Catal., **75**, 423 (1982).

44. von Ballmoos, R. and Meier, W.M., Nature,**289**, 782 (1981).

45. Scofield, J.H., J. Electron. Spectrosc. Relat. Phenom., **8**,

129 (1976).

46. Vedrine, J.C., Auroux, A., Bolis, A., Dejaifve, P., Naccache,C., Wierzchowski, P., Derouane, E.G., Nagy, J.B., Gilson, J.P,, Van Hoff, J.H.C., Van der Berg, J.P. and Wolthuizen, J., J. Catal., 59, 248 (1979).
47. Badrinarayan, S., Hegde,S.G., Balkrishnan, I., Kulkarni, S.B., Ratnasamy, P., J. Catal., 71, 439 (1981).
48. Mastikhin, V.M. and Zamaraev, K.I., Z. Phys. Chem. Neue. Floge. 152, 59 (1987).
49. Thomas, J.M., Klinowski, J., J.Adv. Catal., 33, 199 (1985).
50. Klinowski, J., Prog. NMR Spectrosc. 16, 237 (1984).
51. Jarman, R.H., Jacobson, A.J., Melchlor, M.T., J. Phy. Chem., 88, 5748 (1984).
52. Thomas, J.M. and Liu, Xin-Sheng., J. Phy. Chem., 90 (No.20), 4846 (1986).

****

Chapter 4

CATALYTIC EVALUATION OF MFI TYPE ZEOLITES

****

CONTENTS

4.1 INTRODUCTION

It is well known that the acidic zeolites catalyze the hydrocarbon conversion reactions such as cracking, isomerization, alkylation and disproportionation,[1-13] on account of variation in the strength of acid sites. ZSM-5 class of catalysts are proven to be advantageous over the other zeolites in these reactions due to their unusual physico-chemical properties. A direct correlation with the activity has been reported in case of aluminosilicate zeolite[8].

Aromatic reactions such as isomerization of xylenes, disproportionation and methylation of toluene are industrially important reactions. In this chapter, we report the catalytic activity of gallosilicates with pentasil (MFI) framework structure in the hydrocarbon conversion reactions wherein p-xylene is the product of interest. A comparison of its catalytic behavior with Fe and Al analogs is also made. The bifunctional nature of the zeolite in aromatization reactions like n-hexane conversion is also discussed.

The importance of aromatics is well known as fundamental building blocks and Octane boosters in gasoline. In order to increase the aromatic content, naphtha reforming is practised industrially[14-19], by converting the heavy naphtha containing C_7-C_8 paraffins) to BTX aromatics. However, conversions of lower paraffins (C_2-C_6) to aromatics is more difficult and is equally important. Several authors[20-23] have studied the aromatization using zeolites. Kanai and Kawata[24] have reported the aromatization of n-hexane over modified zeolites whereas Ono and

coworkers[20.25] have studied the conversion of lower paraffins and olefins to aromatics using zinc and gallium containing zeolites. The formation of aromatics by dehydrogenation followed by cyclization of lower paraffins, has been well documented[26]. A bifunctional mechanism was envisaged in the literature[27]. we report the influence of gallium in the framework and nonframework positions and their concentration on the aromatization of n-hexane.

4.2 EXPERIMENTAL

Synthesis and characterization of the samples used in this study were discussed in detail in Chapter II, Section 2.5.1. The powdered catalysts are pressed and pelleted to 10-20 mesh. All the reactions were carried out at atmospheric pressure in a fixed bed, downflow, integral reactor shown in Fig. 4.1. About 2 g. of the catalyst was positioned in a cylindrical, silica reactor (1.5 X 40 cm) provided with a thermowell at the center. The thermowell top and the catalyst bed upper surface in the reactor were at the same level. The reactor was placed in the constant temperature zone of an electrically heated furnace. The reactor was connected to the product receiver through a coiled condenser having cold (278 K) water circulation. The feed unit consisting of a Sage syringe pump equipped with 100 ml syringe was connected to the top of the reactor. The zone above the catalyst bed is filled with inert porcelain beads to serve as preheater. For the all the reactions, the catalyst was activated overnight in air at 823 K. For the n-hexane aromatization reaction, the temperature of the reactor was brought down to about 373 K in inert atmosphere of

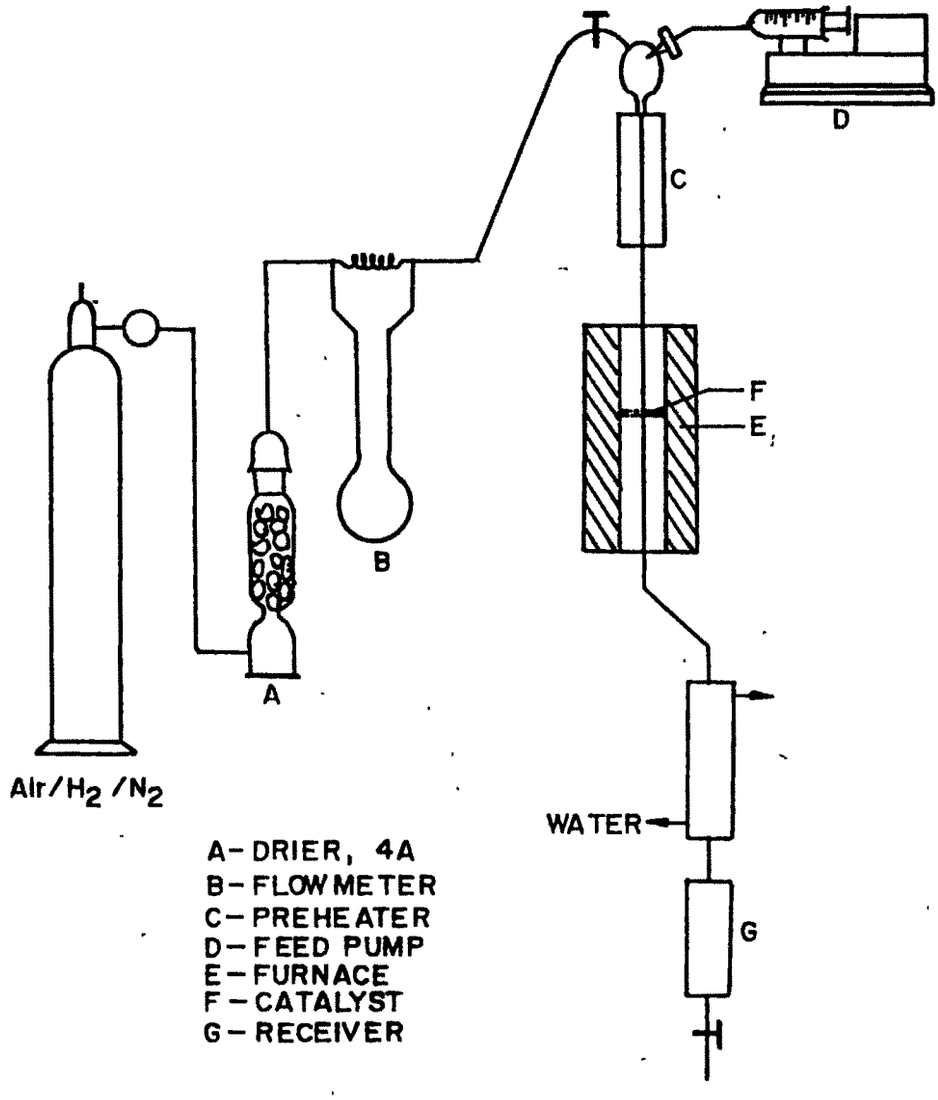

Fig. 4.1 Fixed bed, down-flow reactor used in this study.

nitrogen. Then the reactor temperature was raised to the reaction temperature in presence of hydrogen flow (flow rate 70 ml/min) and the reaction was started by passing the reactant (nC_6) at desired rate. For other reactions, after activating the catalyst at 823 K, nitrogen was passed for 15 minutes and the reaction was carried out after attaining the desired temperature. The products were collected at regular intervals and the mass balance was calculated from the analysis of liquid and gaseous products. The gaseous and liquid products of n-hexane aromatization were analyzed using a capillary column of 50 meters length and 0.25 mm diameter having silicon gum as the stationary phase. The capillary is connected to Shimadzu GC 1RA model. For other reactions, the liquid products were analyzed on a Bentone-34/DIDP (Di-isodecyl phthalate) column fitted to a Shimadzu GC having FID detector. Gaseous products were analyzed in a PORAPAK column. The results tabulated are from the mass balance studies.

4.3 RESULTS AND DISCUSSION

The unit cell compositions of the catalysts used in the present hydrocarbon conversion reaction studies are tabulated in Table 4.1. n-Hexane (99.6%), o-xylene (99.9%), toluene (99.8%) and methanol (99.9%) were used as reactants in the present studies.

4.3.1 Aromatization of n-hexane : Table 4.2 shows the influence of temperature on the product distribution of aromatization of n-hexane over A : HAlGa-ZSM-5(40); B : 2 % Ga_2O_3 impreg. on HAl-ZSM-5(85) and C : HGa-ZSM-5(97) whereas R = SiO_2/M_2O_3 (M = Al and/or Ga). It is seen that the formation of gaseous products and

Table 4.1

Unit cell compositions of the catalysts.

No.	Catalyst	Unit cell composition
1.	HGa-ZSM-5(40)	$H_{4.50}Na_{0.03}[(GaO_2)_{4.53}(SiO_2)_{91.47}]$
2.	HGa-ZSM-5(97)	$H_{1.86}Na_{0.08}[(GaO_2)_{1.94}(SiO_2)_{93.86})]$
3.	HGa-ZSM-5(289)	$H_{0.65}Na_{0.01}[(GaO_2)_{0.66}(SiO_2)_{95.35}]$
4.	HAlGa-ZSM-5(40)	$H_{4.50}Na_{0.02}[(GaO_2)_{2.26}(AlO_2)_{2.26}(SiO_2)_{91.48}]$
5.	HAl-ZSM-5(85)	$H_{2.12}Na_{0.08}[(AlO_2)_{2.20}(SiO_2)_{93.80}]$
6.	HFe-ZSM-5(80)	$H_{2.27}Na_{0.08}[(FeO_2)_{2.35}(SiO_2)_{93.60}]$
7.	Silicalite (>3000)	$Si_{96}O_{192}$
8.	2% Ga_2O_3 impreg. HAl-ZSM-5	2% $Ga_2O_3\{H_{2.12}Na_{0.08}[(AlO_2)_{2.20}(SiO_2)_{93.80}]\}$
9.	3.83% Ga_2O_3 impreg.silicalite	3.83% $Ga_2O_3\{Si_{96}O_{192}\}$

Table 4.2

Influence of temperature on the product distribution of aromatization of n-hexane

Reaction temperature :

Temperature range : 743 - 793 K
Pressure : atmospheric
WHSV : 2.64 h^{-1}
H_2/HC (mole) : 4
Feed : n-hexane (99.6 %)

Temp. & catalyst / Parameter	793 k			773 K			743 k		
	A*	B#	C@	A	B	C	A	B	C
C_1	15.4	5.8	2.6	13.0	4.5	9.1	7.6	3.1	7.4
C_2+C_2 =	14.4	13.8	10.6	10.0	9.1	21.8	7.1	7.7	17.8
C_3+C_3 =	16.4	35.5	23.7	32.5	32.9	9.6	30.2	38.3	10.9
iC_4	0.6	4.2	6.6	3.5	5.5	2.0	9.2	10.8	1.7
nC_4	1.2	5.0	4.4	3.3	5.9	4.2	7.9	8.3	4.7
Total aromatics	34.7	30.5	16.1	29.9	25.5	15.2	25.6	21.3	11.5
Sel* BTX	33.4	27.7	11.4	26.4	24.0	11.6	22.1	18.0	6.3
% Conv.	99.4	97.6	73.9	97.9	97.3	71.8	99.8	93.9	58.7

* A : SiO_2/Ga_2O_3 = 80
\# B : 2 % Ga_2O_3 impreg. HAl-ZSM-5
@ C : SiO_2/Ga_2O_3 = 97
Sel.: Selectivity

the selectivity to aromatics is increases with temperature. For all the catalysts, the conversion increased with the increase in the reaction temperature. However, the following trend was observed in the conversion of n-hexane at all temperatures. HAlGa-ZSM-5 (100 %) > 2 % Ga_2O_3 impreg. HAl-ZSM-5 (93 %) > HGa-ZSM-5 (58 - 74 %).

The enhanced formation of isoparaffins on HAlGa-ZSM-5 and 2 % Ga_2O_3 impregnated on HAl-ZSM-5 at low temperature indicates that cyclization is favored at lower temperature. But HGa-ZSM-5 shows higher isoparaffins at higher temperatures.

HAlGa-ZSM-5 and Ga_2O_3 impregnated HAl-ZSM-5 show higher conversion as well as higher aromatics in the products as compared to HGa-ZSM-5. This may be partly explained on the basis of the acidic strength of the catalysts and the site occupancy and the concentration of the gallium. The Al containing catalysts being more acidic, favors the cracking reactions. All catalysts showed an increase in formation of aromatics at higher temperature. Table 4.3 indicates the influence of space velocity on n-hexane conversions over these catalysts. In all cases higher space velocity favors the higher selectivity to aromatics inspite of lower conversions. At lower space velocity, cracking of n-hexane is favored leading to the formation of C_1-C_3 paraffins and olefins. In all three catalysts the formation of gaseous products (C_1-C_3) remains almost constant, irrespective of space velocity depending on the zeolite. Al containing catalysts indicate higher formation of C_1-C_3 products than for pure gallosilicate. Similarly, selectivity towards aromatics is higher in Al-

Table 4.3

Influence of $WHSV^{-1}$ on the product distribution (wt.%) of aromatization of n-hexane

Reaction temperature :

Temperature range : 793 K
Pressure : atmospheric
H_2/HC (mole) : 4
Feed : n-hexane (99.6 %)

WHSV h^{-1} & catalyst	2.64			3.30			4.95		
Parameter	A*	B#	C@	A	B	C	A	B	C
C_1	15.4	5.8	2.6	7.2	5.4	13.0	3.3	3.3	10.0
C_2+C_2 =	14.4	13.8	10.6	5.9	13.2	25.3	6.9	10.2	20.7
C_3+C_3 =	16.4	35.5	23.7	19.0	38.2	7.1	16.5	35.5	7.0
iC_4	0.6	4.2	6.6	1.1	5.1	2.2	3.9	6.1	1.3
nC_4	1.2	5.0	4.4	2.0	5.9	5.7	4.9	6.3	3.8
Σ C_1-C_4	48.0	64.4	47.8	35.2	67.9	53.4	35.4	6.4	42.8
iC_4/nC_4	0.5	0.8	1.5	0.6	0.9	0.4	0.8	1.0	0.3
BTX	33.6	28.3	15.4	29.4	24.1	19.1	44.6	25.7	14.9
Total aromatics	34.7	30.5	16.1	32.9	25.2	20.3	44.6	27.9	16.0
Sel* BTX	33.4	27.7	11.4	29.0	23.3	14.8	37.2	24.2	9.6
% Conv.	99.4	97.6	73.9	98.9	96.8	77.3	83.3	94.3	64.5

* A : SiO_2/Ga_2O_3 = 80
# B : 2 % Ga_2O_3 impreg. HAl-ZSM-5
@ C : SiO_2/Ga_2O_3 = 97
Sel.: Selectivity

containing catalysts. Only HGa-ZSM-5 shows lower aromatics than both the HAlGa-ZSM-5 and 2 % Ga_2O_3 impreg. HAl-ZSM-5. This suggests that the acid function of the zeolite and Ga is facilitating the bifunctional reaction of n-hexane. It was reported[2,28-29] that the aromatization of n-hexane over Ga_2O_3 supported ZSM-5 is a bifunctional process in which aromatization reaction is catalyzed by Ga species. Therefore, in case of gallium impregnated HAl-ZSM-5, the yield of aromatics increased with the decrease in acidity of the zeolites. Fig. 4.2. indicates the distribution of benzene, toluene and xylenes over these three catalysts at 793 K and WHSV = 2.64 h^{-1}. The formation of xylene is very low and hence the ratio of xylene to benzene is higher indicating the dealkylation of xylenes in acidic zeolites like HAlGa-ZSM-5 and Ga impregnated HAl-ZSM-5.

4.3.2 Isomerization of o-xylene : The catalysts used in this study are HGa-ZSM-5 (40, 97, 289), HAl-ZSM-5(85), HFe-ZSM-5(80), silicalite (>3000) and 3.83 % impreg. silicalite. The reaction was studied in detail as a function of reaction temperature, SiO_2/Ga_2O_3 mole ratio and space velocity. This reaction was carried out at comparatively low temperature to minimize side reactions.

Influence of temperature : The influence of temperature on the product distribution of isomerization of o-xylene over HGa-ZSM-5 (97) is shown in Table 4.4. An increase in o-xylene conversion is observed with the increase in the reaction temperature, but the selectivity to isomerization is nearly constant over the temperature range 523-673 K. At lower temperature p-xylene

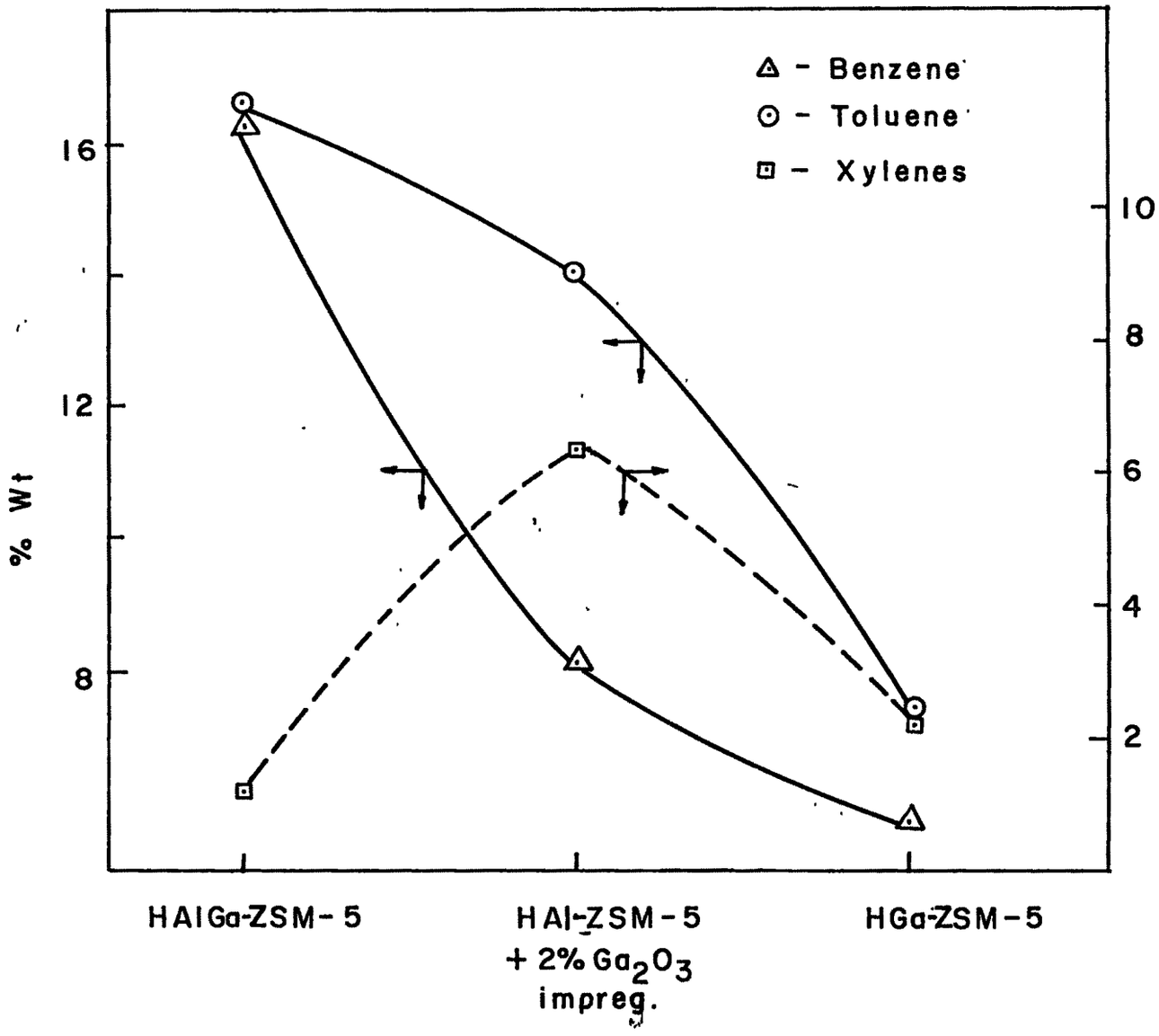

FIG. 4.2: DISTRIBUTION OF BENZENE, TOLUENE AND XYLENES OVER HAlGa-ZSM-5 (40), 2% Ga_2O_3 IMPREG. HAl-ZSM-5 AND HGa-ZSM-5(97) AT 793 K AND WHSV = 2·64 h^{-1}.

Table 4.4

Influence of Temperature on the product distribution in isomerization of o-xylene over HGa-ZSM-5(97).

Reaction conditions :

Temperature range : 523 - 673 K
Pressure : atmosphere
WHSV[a] : 10 h^{-1}
Feed : o-xylene

Parameter	Temperature (K)			
	523	573	623	673
Conversion (%w/w)	26.0	59.0	63.9	68.3
Products (%w/w)				
Aliphatics	0.1	0.2	0.4	0.1
Benzene	0.1	-	0.1	0.1
Toluene	0.1	0.2	1.4	3.0
Ethyl Benzene	0.1	0.1	0.1	0.1
p-Xylene	6.8	17.3	19.1	19.1
m-Xylene	18.8	40.8	41.2	43.1
o-Xylene	74.0	41.0	36.3	31.7
1,3,5 TMB[b]	0.1	0.1	0.1	0.1
1,2,4 TMB	0.1	0.2	1.3	2.4
1,2,3 TMB	0.0	0.1	0.0	0.1
Sel. isom.[c]	98.4	98.5	94.6	91.0
Para/(p+m xylenes)	0.3	0.3	0.3	0.3

a = Weight Hourly Space Velocity. b = Trimethylbenzene.
c= [(para+meta) xylenes/ o-xylene converted] X 100.

selectivity is higher than the equilibrium value, whereas at high temperature, tri-methyl benzenes are noticed. The observed para selectivity is attributed to the high diffusivity of p-xylene. Negligible amounts of secondary products viz. toluene and trimethylbenzene(TMB), suggest lower dealkylation to toluene or disproportionation to TMB. The lower disproportionation is associated with the reactant or product shape selectivity of pentasil zeolites.

Influence of space velocity : Space velocity has a marked influence on the isomerization of o-xylene. Fig 4.3 illustrates the correlation between p-xylene selectivity and space velocity as a function of o-xylene conversion over HGa-ZSM-5(97) catalyst. Lower para selectivity and o-xylene conversion is observed at higher space velocity. At all conversions levels the selectivity to p-xylene is constant. The selectivity to isomerization remains almost constant over space velocities ranging from 4 to 36 h^{-1}. Thus the p-selectivity seems to be dependent on diffusivity rather than on the conversion.

Influence of SiO_2/Ga_2O_3 ratio : With increasing SiO_2/Ga_2O_3 ratio, decrease in the conversion of o-xylene and an increase in the concentration of para isomer in the product is noticed (Table 4.5). The acidic nature of the zeolite is dependent on the framework composition, wherein, the proton associates with the excess charge balancing. Lower number of charge balancing protons, possess lower number of acid sites. The observed conversions are thus in agreement with the SiO_2/Ga_2O_3 ratio of the zeolite. This is in part due to the decrease in acidity of

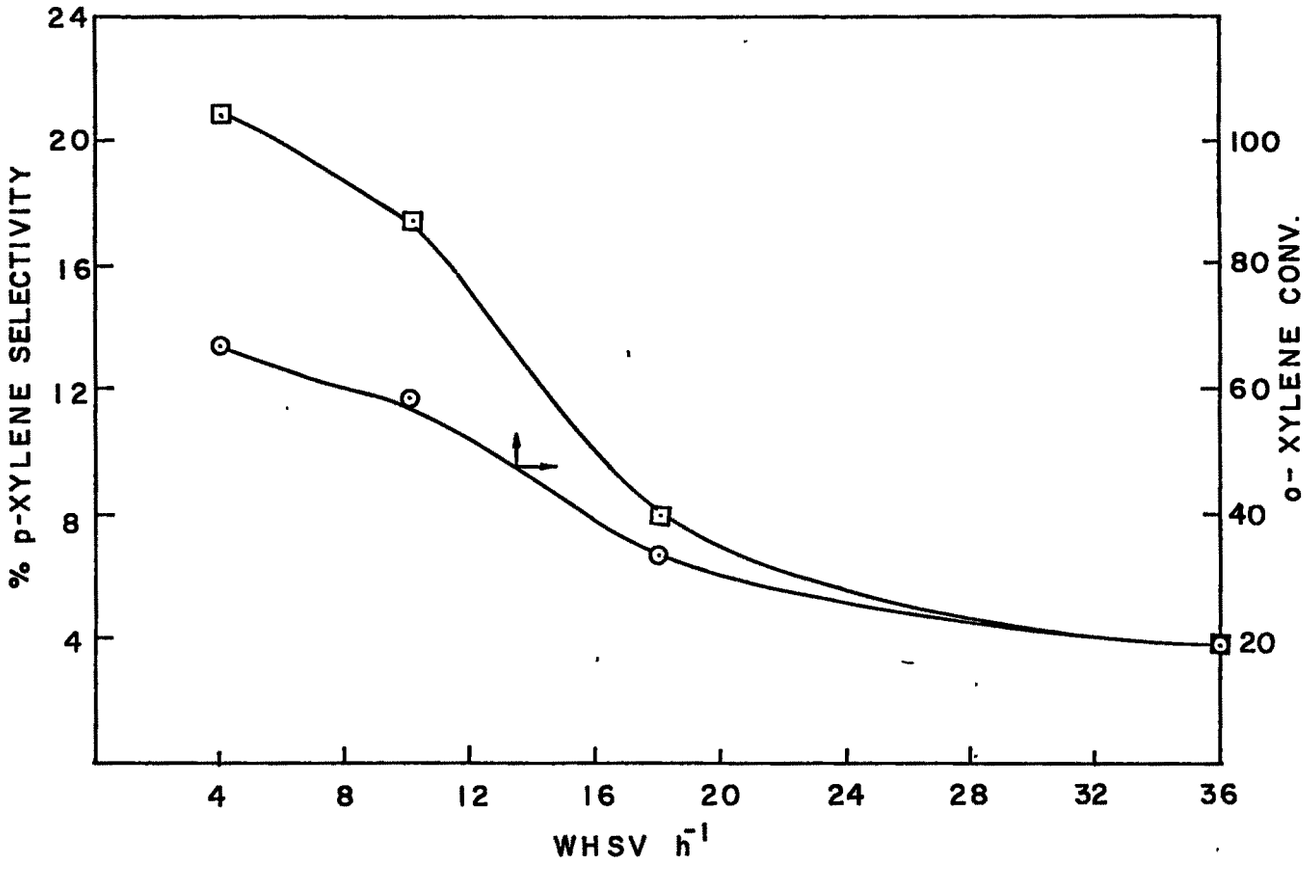

FIG. 4.3 : p-XYLENE SELECTIVITY AND SPACE VELOCITY Vs. % CONVERSION OF o- XYLENE OVER HGa-ZSM-5 (97) AT 623 K.

Table 4.5

Influence of SiO_2/Ga_2O_3 ratio in HGa-ZSM-5 on the product distribution of isomerization of o-xylene.

Reaction conditions :

Temperature : 623 K
Pressure : atmospheric
WHSV[a] : 10 h^{-1}
Feed : o-xylene

Parameter	SiO_2/Ga_2O_3 ratio		
	40	97	289
Conversion (%w/w)	70.2	68.3	63.2
Products (%w/w) Aliphatics	-	0.1	0.5
Benzene	0.3	0.1	0.2
Toluene	3.3	3.0	1.0
Ethyl Benzene	0.0	0.1	0.1
p-Xylene	18.7	18.1	16.3
m-Xylene	44.8	43.1	43.9
o-Xylene	29.8	31.7	36.8
1,3,5 TMB[b]	0.3	0.1	0.1
1,2,4 TMB	1.9	2.4	0.1
1,2,3 TMB	0.2	0.1	0.2
% Sel.isom.[c]	90.4	91.0	95.4
Para/(p+m xylenes)	0.3	0.3	0.3

a,b c Refer Table 4.4

the samples with increase in SiO_2/Ga_2O_3 ratio. Also an increase in crystallite size may slow down the diffusion of o-xylene molecules into the channels which may also contribute to the decrease in activity[30]. The observed para selectivity over a zeolite with higher SiO_2/Ga_2O_3 ratio is at lower conversions. This is probably more related to the change in the crystallite size rather than acidity or the conversion. According to Wei[31], Theodrou[32] the para selectivity is proportional to the length of diffusion path, which is more for larger crystallites. The crystallite size increases with increase in SiO_2/Ga_2O_3 ratio (2, 3, 4 μm for R = 40, 97, 289 respectively). This is in agreement with the earlier reports[31,32]. Further, at all the conversion levels for gallosilicates with different SiO_2/Ga_2O_3 ratio, the selectivity to isomerization is constant.

Influence of catalyst composition : The comparison of the catalytic activity for o-xylene isomerization over silicalite, Ga_2O_3 impregnated silicalite, HAl-ZSM-5(85), HGa-ZSM-5(97), HFe-ZSM-5(80) is made in Table 4.6. The lower conversion of xylene for silicalite is due to the lower acidity associated with it. Similarly in the Ga_2O_3 impregnated silicalite, there was no increase in the acidity and accordingly the conversion was not very high. This shows that Bronsted acid sites are required for this reaction. Conversion for Al-, Ga- and Fe- analogs of pentasil (MFI) are in the order HAl-ZSM-5 > HGa-ZSM-5 > HFe-ZSM-5. Thus acidity is contributed only by framework Ga^{3+} ions rather than the extraframework gallium. From sorption studies, it was revealed that the channel tortuosity and pore

Table 4.6

Product distribution of isomerization of o-xylene over different catalysts

Reaction conditions :

Temperature : 623 K
Pressure : atmospheric
WHSV[a] : 10 h^{-1}
Feed : o-xylene

Parameter	Zeolite (MFI) type				
	A*	B*	C*	D*	E*
Conversion (%w/w)	2.5	2.4	59.2	68.3	71.7
Products (%w/w)					
Aliphatics	0.6	0.6	0.1	0.1	0.1
Benzene	-	-	0.0	0.1	0.3
Toluene	0.4	-	1.5	3.0	1.0
Ethyl Benzene	0.1	0.1	0.0	0.1	0.0
p-Xylene	0.1	0.1	15.0	19.1	22.6
m-Xylene	1.4	1.4	40.0	43.1	47.5
o-Xylene	97.5	97.6	40.8	31.7	28.4
1,3,5 TMB[b]	-	0.2	0.1	0.1	0.1
1,2,4 TMB	-	0.1	1.2	2.4	0.1
1,2,3 TMB	-	-	0.1	0.1	0.1
% Sel.isom.[c]	62.2	61.8	92.9	91.0	97.7
Para/(p+m xylenes)	0.2	0.1	0.3	0.3	0.3

A* = silicalite (>3000)
B* = 3.83 % Ga_2O_3 impreg.silicalite
C* = HFe-ZSM-5(80)
D* = HGa-ZSM-5(97)
E* = HAl-ZSM-5(85)
a,b,c Refer Table 4.4

mouth diameter remains unaltered after Ga_2O_3 impregnation. Thus the observed para selectivity is related to sorption properties. The selectivity to isomerization is less for silicalite and Ga_2O_3 impregnated silicalite.

4.3.3 Disproportionation of toluene : In toluene disproportionation the main reaction is the formation of xylenes and benzene. Depending on the temperature, acidity and nature of the catalyst dealkylation of toluene to benzene and disproportionation of xylenes to trimethylbenzene is also favored. Kaeding and coworkers[6,33] indicated that over unmodified pentasil zeolites, xylene isomers were formed in the products and the benzene to xylene ratios varied from 1.8 to 1.0 depending on the reaction conditions and the silica to alumina ratio of the zeolite. By modification with phosphorous, para selectivity to the extent of 90 % was achieved[6,33].

The present study compares the catalytic activity of HAl-ZSM-5(85), HGa-ZSM-5(97) and HFe-ZSM-5(80) at different temperatures. Fig. 4.4 illustrates the influence of temperature in the range 713 - 833 K, at atmospheric pressure, WHSV = 4 h^{-1} and toluene to hydrogen ratio 1 : 2 molar. All the three catalysts show increase in conversion with the reaction temperature. The conversion for this reaction decreases in the order HAl-ZSM-5 > HGa-ZSM-5 > HFe-ZSM-5 which is in accordance with the acid strength associated with the site. The mole ratio of B/X in the product for all these catalysts increases with temperature indicating that side reactions are favored at higher temperatures. The order of B/X ratio for these catalysts is

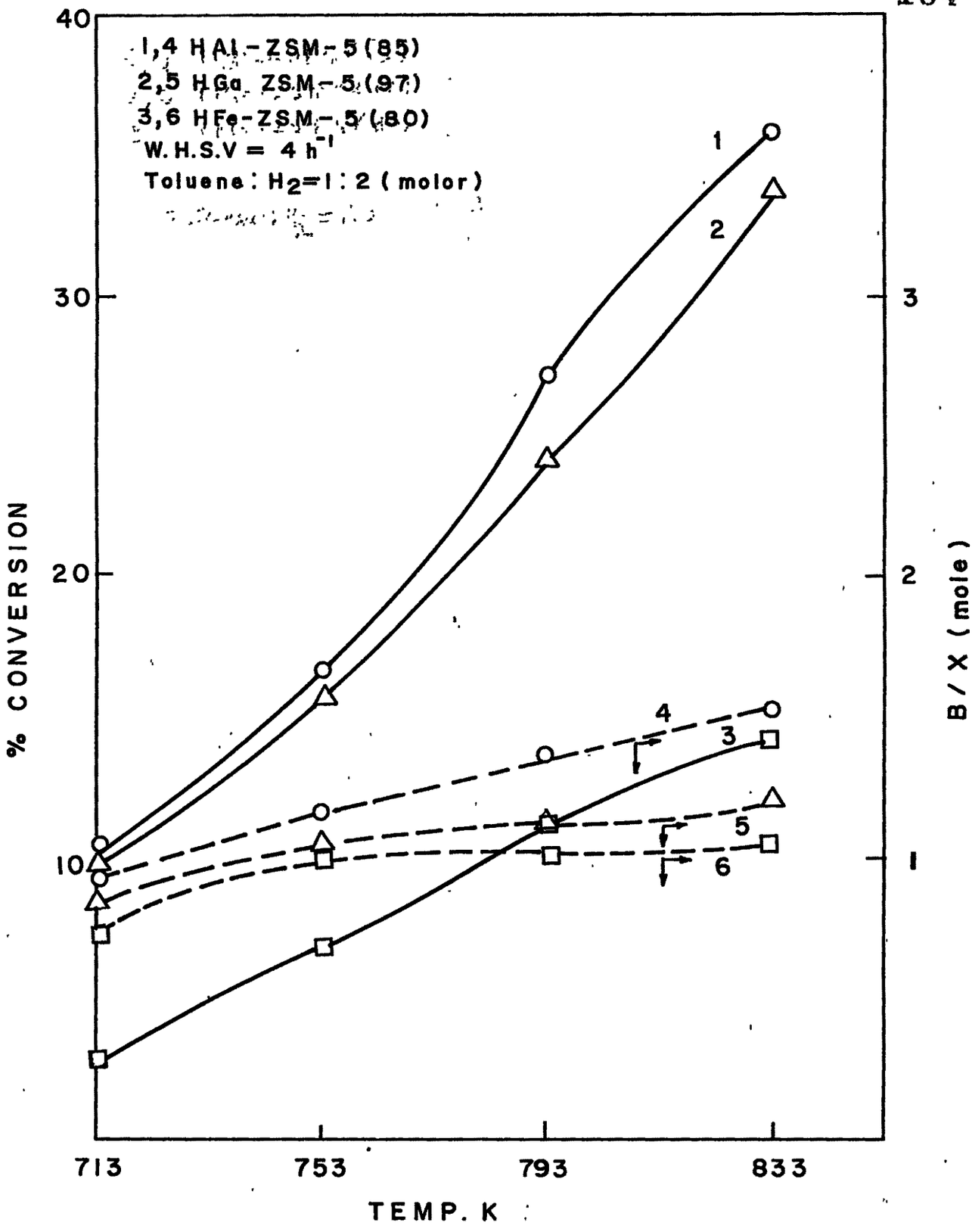

FIG. 4.4 : DISPROPORTIONATION OF TOLUENE OVER Al-, Ga-, AND Fe- ANALOGS OF PENTASIL (MFI) ZEOLITE EFFECT OF TEMPERATURE ON (a) % CONVERSION AND (b) B/X RATIO.

also HAl-ZSM-5 > HGa-ZSM-5 > HFe-ZSM-5. The formation of benzene and TMBs (0.1 - 0.3 %) suggests both disproportionation of xylene and dealkylation of toluene occur simultaneously along with toluene disproportionation.

Larger particle size[9,34], blockage of the channels during diffusion of the products[35] and lower acidity of the catalyst favors the p-selectivity in the disproportionation of toluene. Fig. 4.5 depicts the comparison of p-xylene selectivity in xylenes of Al-, Ga- and Fe- analog of pentasil (MFI) catalysts at different temperatures. It is observed that p-selectivity increases with temperature and follows the order HFe-ZSM-5 > HGa-ZSM-5 > HAl-ZSM-5. The higher particle size, the lower acidity and blocking of the channels due to the deposition of iron oxide during the diffusion of the reaction products favors the higher p-selectivity of HFe-ZSM-5. The lower p-xylene selectivity of HGa-ZSM-5 compared HFe-ZSM-5 may be due to smaller crystallite size, lower acidity and more open channels during reaction temperature. So it shows lower p-selectivity than HFe-ZSM-5. HAl-ZSM-5 being more acidic and more stable, formation and diffusion of other isomers of xylene also takes place and hence the p-selectivity is lower than Fe- and Ga- analog of ZSM-5.

The results obtained while studying the influence of time on stream (TOS) of the feed and space velocity on disproportionation of toluene over HGa-ZSM-5(97) is summarized in Table 4.7. % Conversion decreases and p-selectivity increases with increase in space velocity and TOS. Mole ratio of benzene/xylene is found to decrease with increase in the space velocity and TOS. The

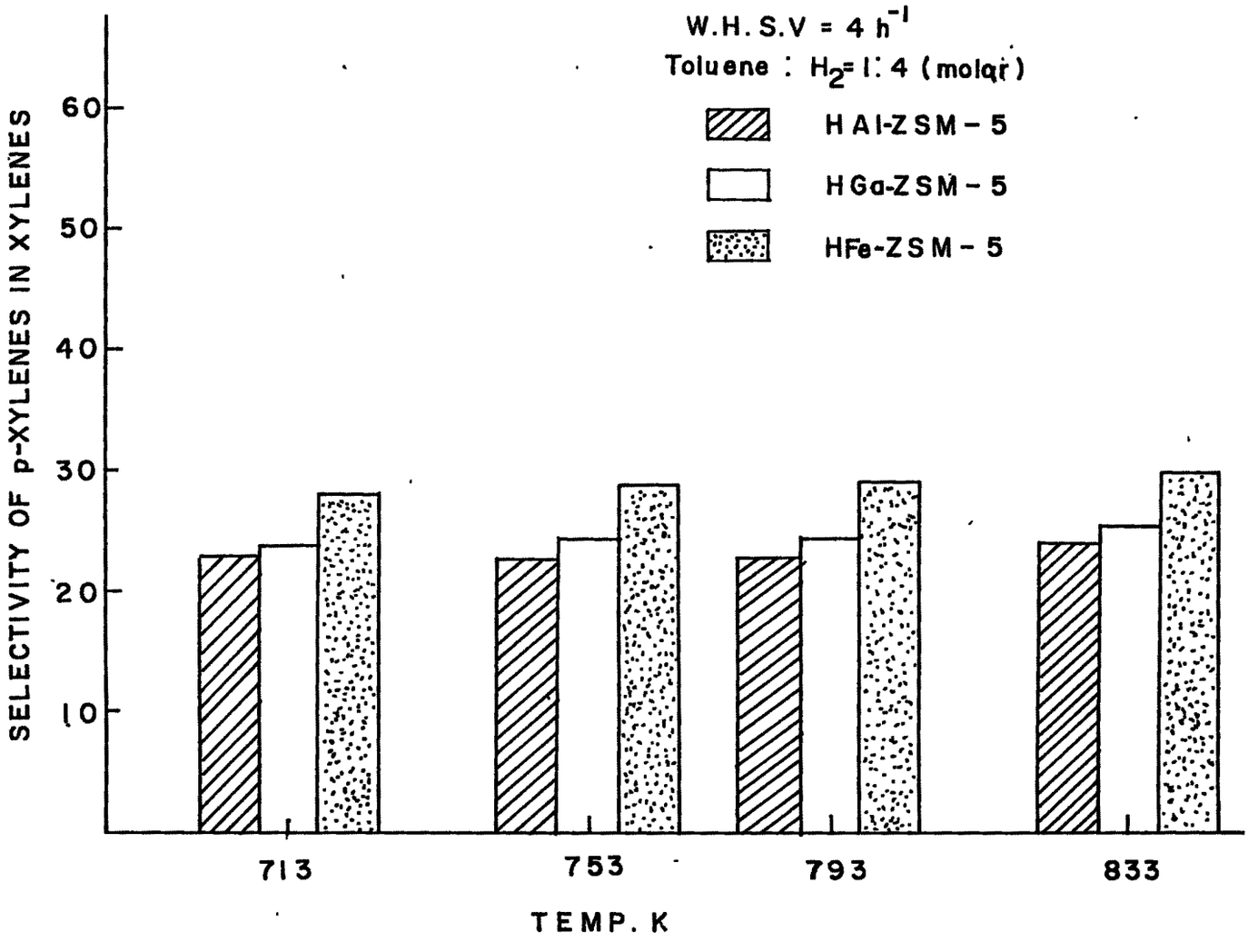

FIG.4.5: SELECTIVITY OF p-XYLENE IN XYLENES FOR Al-, Ga-, AND Fe-ANALOGS OF PENTASIL (MFI) AT DIFFERENT TEMPERATURES.

Table 4.7

Influence of Time on stream (TOS) and space velocity (WHSV[a] h^{-1}) on disproportionation of toluene over HGa-ZSM-5(97).

Reaction conditions :

Temperature : 763 K Pressure : atmospheric
Feed : Toluene : Hydrogen (1:4 molar) WHSV[a] : 4 h^{-1}

Parameter	Time					
	1	2	4	8	12	16
Conversion %w/w	24.4	18.8	15.6	9.8	4.1	2.2
	-	(33.0)	(24.4)	(15.5)	-	(14.9)
Products %w/w						
Aliphatics	0.1	0.1	0.1	0.1	0.1	0.1
	-	(0.1)	(0.1)	(0.1)	-	(0.1)
Benzene	11.8	8.5	7.2	4.6	1.9	0.8
	-	(16.2)	(11.8)	(7.2)	-	(7.0)
Toluene	75.6	81.2	84.4	90.2	95.9	97.8
	-	(67.0)	(75.6)	(84.5)	-	(85.1)
Ethyl-benzene	0.1	0.1	-	-	-	-
	-	(-)	(0.1)	(-)	-	(-)
p-Xylene	2.9	2.4	2.0	1.2	0.6	0.3
	-	(4.1)	(2.9)	(2.1)	-	(1.9)
m-Xylene	6.1	4.9	4.1	2.4	1.2	0.6
	-	(7.7)	(6.1)	(3.9)	-	(3.6)
o-Xylene	2.8	2.2	1.9	1.1	0.5	0.2
	-	(4.6)	(2.8)	(2.1)	-	(1.9)
1,3,5-TMB[b]	0.1	0.1	-	-	-	-
	-	(-)	(-)	(-)	-	(-)
1,2,4-TMB	0.2	0.1	0.1	0.1	-	-
	-	(0.3)	(0.2)	(0.1)	-	(0.1)
1,2,3-TMB	0.1	0.1	-	-	-	-
	-	(-)	(0.1)	(-)	-	(-)
Xylenes %						
Para	24.9	25.2	25.0	25.5	26.1	27.3
	-	(25.0)	(24.9)	(26.0)	-	(25.6)
Meta	51.5	51.5	51.2	51.0	54.0	56.0
	-	(46.9)	(51.5)	(48.0)	-	(48.6)
Ortho	23.5	23.1	23.8	23.4	23.0	22.0
	-	(28.0)	(23.5)	(26.0)	-	(25.6)
benzene/xylenes	1.4	1.3	1.2	1.2	1.2	1.1
	-	(1.3)	(1.3)	(1.2)	-	(1.2)

a,b Refer Table 4.4
Figures in brackets are of WHSV h^{-1} and without brackets are of TOS in hours.

formation of benzene due to dealkylation is found to decrease with increase in space velocity and TOS.

4.3.4 Methylation of toluene : Catalytic performance and the selectivity to p-xylene in this reaction is tested for HAl-ZSM-5(85), HGa-ZSM-5(97) and HFe-ZSM-5 (80). A mole ratio of 3.5 : 1 of toluene : methanol was selected. This being an electrophilic reaction, the products are mostly o- and p- xylenes. m-Xylene and C_9 aromatic products are formed by secondary reactions such as isomerization and successive alkylations. The results of methylation of toluene at different reaction temperatures for Al, Ga- and Fe- analog of pentasil (MFI) zeolites are shown in Fig. 4.6. It indicates that higher temperature favors the alkylation. The sequence observed in the % conversion is HAl-ZSM-5 > HGa-ZSM-5 > HFe-ZSM-5 which demonstrates the relationship between conversion and the strength of the acidity of the catalyst. Methanol conversion is complete in the temperature range 673 - 763 k. Among the xylenes, p-xylene is in equilibrium value for both Al- and Ga- analogs whereas for HFe-ZSM-5, it is higher upto 40 %. The order of p-selectivity observed is as HFe-ZSM-5 > HGa-ZSM-5 > HAl-ZSM-5. According to Yashima et al.[36], the primary product in alkylation over HAl-ZSM-5 is p-xylene which later isomerize on strong acid sites to yield the other isomers. For HGa-ZSM-5 and HAl-ZSM-5, p-selectivity decreases slightly at higher temperature probably because of diffusional effects, higher temperatures favoring faster diffusion of the other isomers. Among the trimethylbenzenes, 1,2,4 is predominant (1.0 -1.2%) suggesting the shape selective nature of medium pore

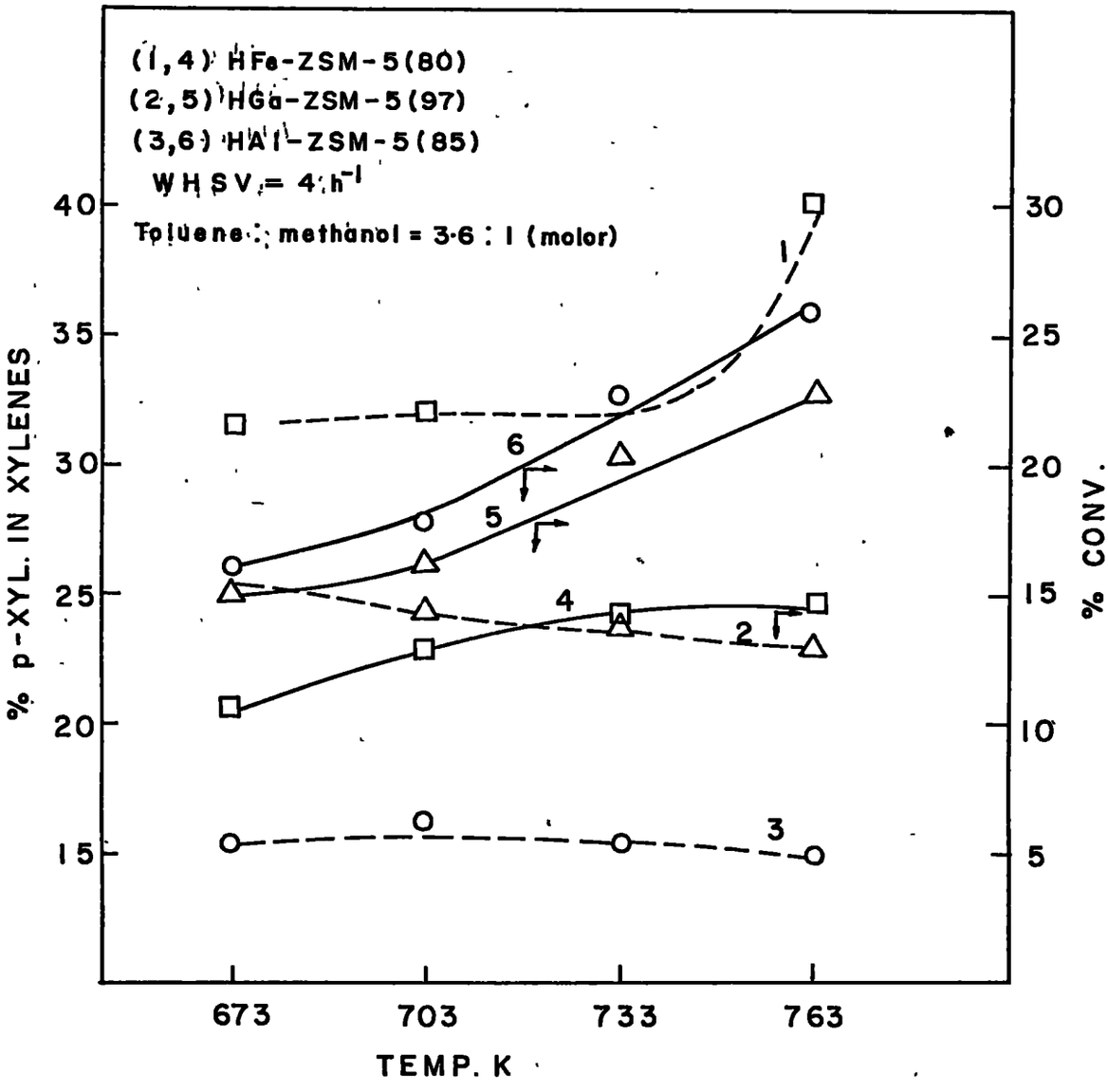

FIG. 4.6 : INFLUENCE OF TEMPERATURE ON METHYLATION OF TOLUENE OVER Al-, Ga-, AND Fe-. ANALOGS OF PENTASIL (MFI) ZEOLITES ON (a) p-XYLENE SELECTIVITY AND (b) % CONVERSION.

zeolites. Benzene formation increases with the increase in temperature due to disproportionation and dealkylation of the alkylbenzenes.

Table 4.8 summarizes the results influence of time on stream (TOS) of the feed and space velocity on methylation of toluene over HGa-ZSM-5 catalyst. The figures indicated in the brackets are of space velocities. It is observed that conversion decreases and p-selectivity increases with increase in TOS and the space velocity. The increase in the p-selectivity is due to the reduction in effective channel size due to the internal coking[33] or partial blocking of the channel opening by external coke deposit[35]. Higher concentration of 1,2,4 tri-methyl benzene among all TMB isomers indicate the predominance of transition shape selectivity.

Table 4.8

Influence of time on stream (TOS) and space velocity (WHSV h^{-1}) on methylation of toluene over HGa-ZSM-5(97).

Reaction conditions :

Temperature : 763 K **Pressure : atmospheric**
Feed : Toluene : methanol (3.6 : 1 molar) **WHSV[a] : 4 h^{-1}**

Parameter	Time						
	1	2	4	8	10	12	16
Conversion %w/w	24.2	21.4	13.8	9.7	-	8.4	7.8
	-	(33.5)	(26.3)	(22.1)	(19.6)	-	-
Products %w/w							
Aliphatics	0.2	0.2	0.2	0.2	-	0.1	0.1
	-	(0.1)	(0.2)	(0.2)	(0.3)	(0.1)	(0.1)
Benzene	4.4	2.8	1.5	0.8	-	0.6	0.5
	-	(9.0)	(4.4)	(3.1)	(2.3)	-	-
Toluene	73.1	76.8	83.1	86.2	-	88.4	88.9
	-	(66.5)	(73.7)	(77.9)	(80.4)	-	-
Ethyl-benzene	0.1	0.1	0.1	0.1	-	-	-
	-	(0.1)	(0.1)	(0.2)	(0.1)	-	-
p-Xylene	4.0	3.9	3.0	2.4	-	2.0	1.9
	-	(5.3)	(4.8)	(4.3)	(4.2)	-	-
m-Xylene	10.3	8.9	6.9	5.4	-	4.6	4.3
	-	(12.1)	(10.2)	(8.9)	(8.4)	-	-
o-Xylene	4.7	4.3	2.9	2.1	-	1.6	1.4
	-	(5.4)	(4.7)	(4.1)	(3.9)	-	-
p-Ethyltoluene	0.8	0.8	0.7	0.8	-	0.6	0.5
	-	(0.2)	(0.2)	(0.4)	(0.6)	-	-
m-Ethyltoluene	0.2	0.2	0.4	0.3	-	0.2	0.2
	-	(0.1)	(0.4)	(0.1)	(0.1)	-	-
1,3,5 TMB[b]	0.1	0.1	-	-	-	-	-
	-	(0.1)	(0.1)	(0.1)	(0.1)	-	-
1,2,4 TMB	1.0	1.1	1.2	1.3	-	1.1	0.9
	-	(1.0)	(1.0)	(1.7)	(1.0)	-	-
1,2,3 TMB	0.1	0.2	0.5	0.6	-	0.4	0.3
	-	(0.2)	(0.1)	-	(0.2)	-	-
Xylenes %w/w							
Para	21.0	22.4	23.4	24.2	-	24.4	25.0
	-	(23.1)	(24.3)	(24.8)	(25.4)	-	-
Meta	51.7	51.1	53.9	55.6	-	57.5	58.9
	-	(53.1)	(51.4)	(38.9)	(36.6)	-	-
Ortho	23.6	24.7	22.6	21.6	-	20.0	19.1
	-	(23.8)	(23.7)	(17.9)	(17.2)	-	-

a,b Refer Table 4.4
Figures in brackets are of WHSV h^{-1} and without brackets are of TOS in hours.

4.4 REFERENCES

1. Simmons, D.K., Szostak, R., Agarwal, P.K., Thomas, T.L., J. Catal. **106**, 287 (1987).
2. Rastelli, H., Lok, B.M., Duisman, J.A., Earls, D.E. and Mullhaupt, J.T., Canad. J. Chem. Eng. **60**, 44 (1982).
3. Young, L.B., Butter, S.A. and Kaeding, W.W., J. Catal., **76**, 418 (1982).
4. Haag, W.O., Olson, D.H. and Weisz, P.B., `Chemistry for the future' (Ed. Grunewald,H.) Pergamon press oxford and N.Y. 327 (1984).
5. Csicsery, S.M., `Zeolites', **4**, 202 (1984).
6. Kaeding, W.W.,Chu, C., Young, L.B. and Butter, S.A., J.Catal. **69**, 392 (1981).
7. Nayak, V.S. and Chowdhary, V.R., Appl. Cat., **4**, 333 (1982).
8. Jacobs, P.A., `Carboniogenic Activity of Zeolites', Elsevier Scientific Publishing Co., Amsterdam, Oxford, N.Y., Chapter II, p.253, 168 (1977).
9. Chen, N.Y., Kaeding, W.W. and Dwyer, F.G., J. Chem. Soc., **101**, 6783 (1979).
10. Butter, S.A., U.S., Patent, 4007231 assigned to Mobil Oil Corp. (1977); Haag, W.D., Olson, D.H., U.S. Patent 3856871 assigned to Mobil Oil Corp. (1974); Morrison, R.A., U.S. Patent 3856872 assigned to Mobil Oil Corp. (1974).
11. Derewinski, M., Haber, J., Ptaszynski, J., Shiralkar, V.P. and Dzwigaj, S. in `Structure and Reactivity of Modified Zeolites', (Ed. Jacobs, P.A.), Elsevier Science Publishers, Amsterdam (1984).

12. Beltrame, B., Beltrame, P.L., Carnitai, P. and Forni, L., React. Kinet. Catal. Lett., **19**, 213 (1982).

13. Meshram, N.R., Hegde, S.G., Kulkarni, S.B. and Ratnasamy, P., Applied Cat., **8**, 359 (1983).

14. Edmonds, T., ' Oil Based Chemistry in Catalysis and Chemical Processes' (Ed. R. Pearce and W.R. Patterson), Blackie and Sons Ltd., Glasgow, p.90 (1981).

15. Dobres, R.M. and Baker, R.W., Catalysis, Vol. **6**, (Ed. P.H. Emmett), Reinhold, New York (1958).

16. Weisz, P.B., Adv. Catal., **13**, 137 (1962).

17. Sinfelt, J.H., Adv. Chem. Engg., **5**, 37 (1964).

18. Ciapetta, F.G. and Wallace, D.N., Catal. Rev., **5**, 67 (1971).

19. Sterba, M.J. and Haensel, V., Ind. Eng. Chem. Prod. Res. Dev., **15**, 2 (1976).

20. Sirokman, G., Sendoda, Y. and Ono, Y., Zeolite, **6(301)**, 299 (1986).

21. Bragin, O.V., Uspekhi Khim., **50**, 1994 (1981); Bragin, O.V., Russ. Chem. Rev., **50**, 1045 (1981).

22. Csicsery, S.M., J. Catal. **17**, 205; 217; 315; 322 (1970).

23. Csicsery, S.M. J. Catal. **18**, 30 (1970).

24. Kanai, J. and Kawata, N., Applied Catalysis, **55**, 115-122 (1989).

25. Ono, Y., Catal. Rev.- Sci. Eng., **34(3)**, 179-226 (1992).

26. Kanai, J. and Kawata, N., J. Catal., **114**, 284 (1988).

27. Weisz, P.B., Adv. Catal., **13**, 137 (1962).

28. Mills, G.A., Heinemann, H., Milliken, T.H. and Obald, A.G., Ind. Engg. Chem., **47**, 719 (1955).

29. Heinemann, H., Catal. Rev. Sci. Engg., 15(1), 53 (1977).

30. a : Babu, G.P., Hegde, S.G., Kulkarni, S.B. and Ratnasamy, P., J. Catal., 81, 471 (1983).

b : Babu, G.P., Ph.D.Thesis, 1983, University of Poona, Pune, India.

31. Wei., J., J. Catal. 76, 433 (1982).

32. Theodrou, D. and Wei, J., J. Catal. 83, 205 (1983).

33. Kaeding, W.W., Chu, C., Young, L.B., Weinstein, B. and Butter, S.A., J. Cat. 67, 159 (1981).

34. Derouane, E.G., `Catalysis by Zeolites" (Eds. Imelik et al.), Elsevier, Amsterdam, 5 (1980).

35. Derouane, E.G., `Molecular Shape-Selective Catalysis in Zeolite' - Selected Topics, 9th Canadian Symposium on Catalysis (1984).

36. Yashima, T., Sakaguchi, Y. and Namba, S., Proc. 7th Intl. Congr. on Catalysis, 739 (1980).

****

SUMMARY AND CONCLUSIONS

****

Pentasil (MFI) zeolite belongs to a medium pore, high silica zeolite family. Aluminosilicate framework of pentasil (MFI) has a configuration of linked tetrahedra consisting of eight five-membered rings. The three dimensional channel system is defined by ten-membered rings of tetrahedra, consisting of intersecting straight [010] and sinusoidal (zig-zag) [100] channels. The straight channel has elliptical opening of free diameter, 0.52 X 0.58 nm and the sinusoidal channel has circular openings of free diameter 0.54 X 0.58 nm. The isomorphous substitution not only alters the physico-chemical properties but also changes their catalytic behaviour. Hence in view of the above the peculiar structure and interesting characteristic properties the detailed study of synthesis and characterization of gallosilicate framework of MFI type configuration was undertaken. The physico-chemical properties of gallosilicate molecular sieve with MFI type structure were studied and compared with Al- and Fe- analogs of comparable ratio. The various factors like temperature, OH^- ion concentration, time and gross composition of the gel influencing the synthesis of Ga-ZSM-5 zeolite using triethyl-n-butylammonium bromide (TEBA-Br) template have been investigated. Crystallization data were analyzed in terms of a first order kinetic equation. The apparent activation energy for nucleation (E_n = 155.7 kJ $mole^{-1}$) and crystal growth (E_c = 94.3 kJ $mole^{-1}$) were evaluated by applying Arhenius equation. These E_n and E_c values obtained during the present studies appear to be higher than those reported

previously for the Al- and Fe- analog of pentasil (MFI) zeolite. To describe mathematically, the crystallization data obtained during the process of pentasil (MFI) gallosilicate, were fitted to the Avrami-Erofeev equation. The increase in K values (obtained from intercept) and decrease in m values (obtained from slope) with the increase in synthesis temperature corresponds to the temperature dependent on nucleation and crystallization processes. The morphology of the pentasil gallosilicate was examined by scanning electron microscope during the crystal growth. The shape of all the crystallites was found to be spherical irrespective of temperature and the composition. With increase in the concentration of gallium, the crystallite size was found to decrease without any change in shape. The crystallite size of Al- analog was found to be smaller (1.5 μm) than Ga- analog of pentasil zeolite (3.5 μm) of the same SiO_2/M_2O_3 ratio.

The synthesis of pentasil (MFI) gallosilicate with partial and total isomorphous substitution of Ga^{3+} for Al^{3+} in tetrahedral position has been attempted. The physico-chemical characterization was done by X-ray diffraction, thermal analysis, NMR, IR, XPS and sorption of different probe molecules such as water, benzene, nitrogen and hydrocarbons. X-ray diffraction patterns and IR spectra in the framework vibration region reveals structural characteristics, analogous to MFI framework alumino-silicate. XRD pattern of pentasil (MFI) gallosilicate shows slight shift in interplaner 'd' spacings towards higher values in comparison with that of the Al analog. IR spectra of

gallosilicate (MFI) shows a shift in the frequency of the main asymmetric band in the region of 1250-950 cm^{-1}. Higher shift in interplaner 'd' spacings, shift in the IR frequency in the region 1250 - 950 cm^{-1} and the FTIR spectroscopic studies of pyridine sorption revealed the presence of Ga^{3+} in the tetrahedral framework of pentasil zeolites. The increase in unit cell volume with the increase in Ga content; ^{29}Si and ^{71}Ga MASNMR; high (>80%) ion-exchange capacity confirms the occupancy of Ga^{3+} in the pentasil (MFI) framework. Thermo-analytical studies showed the stability of pentasil gallosilicate (MFI) phase upto 1253 K. XPS data showed a silicon rich surface suggesting inhomogeneous distribution of gallium.

It is observed that with the decrease in Ga content, the equilibrium sorption capacities of sorbates like water, cyclohexane, tributylamine are also decreased. However, at comparable SiO_2/M_2O_3 (M = Al^{3+} or Ga^{3+}), Al-analogs showed higher sorption capacity than for corresponding Ga analog.

The isotherms of n-butylamine (nBA) in pentasil (MFI) alumino and gallosilicates in the range (323-523 K) have been measured. The sorption data were analyzed in terms of different sorption models of sorption isotherm equations. The nBA sorption isotherm data could satisfactorily be represented by Langmuir, BET, Dubinin - Radushkevich and Freundlich sorption isotherm equations. The Sips and Koble-Corrigan equations failed to follow nBA sorption in HAl- and HGa-ZSM-5 zeolites. The amount of nBA retained during desorption at different temperatures was found to be correlated, at least qualitatively, to the strength of the

acidic centers. The decrease in chemical affinity $(-\Delta\mu)$ was found to be slower in zeolites containing increasing amounts of gallium in HGa-ZSM-5 zeolites. Isosteric heats of nBA sorption extrapolated to zero coverage were found to be in the range of 34-24 kJ $mole^{-1}$. Isosteric heat data showed that the acidic centers in HGa-ZSM-5 zeolites are much weaker than those in HAl-ZSM-5 zeolites.

Hydrocarbon conversion reactions such as aromatization of n-hexane, isomerization of o-xylene, disproportionation of toluene and methylation of toluene over Al-, Ga- and Fe- analogs of MFI zeolites and their modified forms are described and discussed.

The trend observed in the cracking as well as in the selectivity towards aromatics at the same conversion level in n-hexane aromatization reaction was HAlGa-ZSM-5 > Ga_2O_3 impregnated HAl-ZSM-5 > HGa-ZSM-5. The presence of Ga in the zeolite modifies the product distribution pattern depending upon nature of site occupancy.

The nature and concentration of the framework cation in the pentasil MFI framework is found to influence the o-xylene isomerization reaction under identical reaction conditions. The trend observed for selectivity for isomerization is HAl-ZSM-5 > HGa-ZSM-5 > HFe-ZSM-5 > Ga_2O_3 impreg. silicalite > silicalite.

The Al-, Ga- and Fe- analogs of pentasil (MFI) zeolite having same SiO_2/M_2O_3 (M = Al, Ga, Fe) were tested for disproportionation of toluene under identical conditions. The influence of temperature, space velocity and time on stream (TOS) of the feed on the product distribution was also studied. The

trend observed in the conversion for this reaction is HAl-ZSM-5 > HGa-ZSM-5 > HFe-ZSM-5 which is in accordance with the acid strength associated with the site. The p-selectivity increases with temperature and follows the order, HFe-ZSM-5 > HGa-ZSM-5 > HAl-ZSM-5. The particle size, blockage of the channels during diffusion of the products and acidity of the catalysts was found responsible for the p-selectivity. The influence of temperature, space velocity and time on stream on the methylation of toluene was also studied. Higher temperature favours the alkylation. Increase in space velocity and TOS, decreases the conversion for the reaction and increases the p-selectivity. In methylation of toluene, p-xylene was found in equilibrium values for Al and Ga analogs (MFI) while the Fe analog (MFI) showed higher (upto 40%) than the equilibrium value. The sequence observed in the % conversion is HAl-ZSM-5 > HGa-ZSM-5 > HFe-ZSM-5 which demonstrates the relationship between the conversion and the strength of the acidity of the catalyst. The order of p-selectivity is observed as HFe-ZSM-5 > HGa-ZSM-5 > HAl-ZSM-5.

LIST OF PUBLICATIONS

1. Studies in the synthesis of gallium analog of Pentasil (MFI) framework zeolite.
   S.V.Awate, P.N.Joshi, A.N.Kotasthane & V.P.Shiralkar.
   J. Incl. Phenon. & Mol. Recogn. in Chem., 13 (3), 207-218 (1992).
2. Sorption properties of ZSM-5 and its Ga isomorphs.
   S.V.Awate, P.N.Joshi, M.J.Eapen, V.P.Shiralkar.,
   J. Phys. Chem. 97, 6042-6047 (1993).
3. Thermal stability studies on the different isomorphs of pentasil zeolites.
   To be communicated
4. Catalytic reactions of aromatic hydrocarbons over pentasil (MFI) zeolites.
   To be communicated.